FORMATION AND SINTERING OF VANADIUM CARBONITRIDE

By

JAMES HENRY FERREIRA

Submitted in partial fulfilment of the requirements for the degree

Master of Science in Applied Science (Metallurgy)

In the

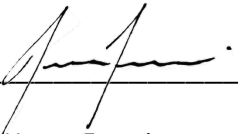Department of Materials Science and Metallurgical Engineering

Faculty of Engineering, Built Environment and Information Technology

February, 2020

Supervisor: Dr R.D. Cromarty

DECLARATION OF ORIGINALITY

I hereby declare that this project is my own unaided work and I have referenced all the sources I have used. It is being submitted in fulfilment of the requirements for the degree Master of Science in Applied Science (Metallurgy) at the University of Pretoria, Pretoria. It has not been submitted before for any degree or examination at any other university. This document represents my own opinion and interpretation of information received from research or / and interviews. I thus accept the rules of assessment of the University and the consequences of transgressing them.

_____

James Henry Ferreira
29162752
09 February 2020

UNIVERSITY OF PRETORIA
FACULTY OF ENGINEERING, BUILT ENVIRONMENT AND INFORMATION TECHNOLOGY
DEPARTMENT OF MATERIALS SCIENCE AND METALLURGICAL ENGINEERING

The Department of Materials Science and Metallurgical Engineering places great emphasis upon integrity and ethical conduct in the preparation of all written work submitted for academic evaluation. While academic staff teach you about systems of referring and how to avoid plagiarism, you too have a responsibility in this regard. If you are at any stage uncertain as to what is required, you should speak to your lecturer before any written work is submitted.

You are guilty of plagiarism if you copy something from a book, article or website without acknowledging the source and pass it off as your own. In effect, you are stealing something that belongs to someone else. This is not only the case when you copy work word-by-word (verbatim), but also when you submit someone else's work in a slightly altered form (paraphrase) or use a line of argument without acknowledging it. You are not allowed to use another student's past written work. You are also not allowed to let anybody copy your work with the intention of passing if off as his/her work.

Students who commit plagiarism will lose all credits obtained in the plagiarised work. The matter may also be referred to the Disciplinary Committee (Students) for a ruling. Plagiarism is regarded as a serious contravention of the University's rules and can lead to expulsion from the University. The declaration which follows must be appended to all written work submitted while you are a student of the Department of Materials Science and Metallurgical Engineering. No written work will be accepted unless the declaration has been completed and attached.

I, James Henry Ferreira with student number: 29162752 and topic of work: FORMATION AND SINTERING OF VANADIUM CARBONITRIDE.

Declare that:

1. I understand what plagiarism is and am aware of the University's policy in this regard.

2. This dissertation is my own original work. Where other people's work has been used (either from a printed source, internet or any other source), this has been properly acknowledged and referenced in accordance with departmental requirements.

3. I have not used another student's past written work to hand in as my own.

4. I have not allowed, and will not allow, anyone to copy my work with the intention of passing it off as his or her own work.

Signature _____

FORMATION AND SINTERING OF VANADIUM CARBONITRIDE

James Henry Ferreira

Supervisor: Dr R.D. Cromarty

Department: Materials Science and Metallurgical Engineering

University: University of Pretoria

Degree: Master of Science in Applied Science (Metallurgy)

Abstract

Vanadium carbonitride is commonly used in the steel making industry to improve the mechanical properties of steel. It is produced by the reduction reaction of vanadium trioxide (V_2O_3) or vanadium pentoxide (V_2O_5) with carbon in a nitrogen atmosphere. Vanadium carbonitride can successfully be produced in an induction heated shaft furnace.

Some briquettes have difficulty moving down the furnace during the industrial production of vanadium carbonitride in a shaft furnace. Solid plugs form in the furnaces from time to time and have a negative influence on furnace productivity.

In this study, the formation of vanadium carbonitride was investigated using a series of laboratory furnaces. In all the test work conducted, V_2O_3 and carbon were used as the basis for the starting material. The influence of factors such as temperature, retention time, pressure and feed material purity on the sintering, chemistry and agglomeration of laboratory produced pellets was determined.

It was found that, of the variables investigated, reaction temperature had the strongest single effect on the agglomeration of the pellets whereas retention time, load and insoluble impurities had an influence on the bonding strength between the agglomerated pellets.

It was concluded that during the production of vanadium carbonitride, a possible combination of factors leads to the formation of plugs in the shaft furnace. An optimal furnace operating temperature of 1200 °C with a retention time of 30 minutes was identified to reduce the occurrence of pellet agglomerations and plug formations.

Increased temperatures result in increased concentrations of vanadium and nitrogen and decreased concentrations of oxygen and carbon.

Keywords: vanadium carbonitride, sintering, shaft furnace, agglomeration, furnace bridging, plug formation.

To my late father
who ingrained the importance of knowledge in my life
and for making such a big contribution to my education.

ACKNOWLEDGEMENTS

TABLE OF CONTENTS

LIST OF FIGURES

LIST OF TABLES

ABBREVIATIONS

AMV	: Ammonium metavanadate
APV	: Ammonium polyvanadate
CAF	: Coal Ash Fusibility
CCD	: Central composite design
EDS	: Energy-dispersive X-ray spectroscopy
FCC	: Face centred cubic
HSLA	: High strength low alloy steels
LVDT	: Linear variable differential transformer
MVO	: Modified vanadium oxide (V_2O_3)
PID	: Proportional Integral Differential control
PVA	: Polyvinal acetate
SEM	: Scanning Electron Microscope
TC	: Thermocouple
XRD	: X-Ray Diffraction
XRF	: X-Ray Fluorescence
RSM	: Response surface methodology
EMF	: Electromotive force
TGA	: Thermogravimetric analysis
DTA	: Differential thermal analysis

CHAPTER 1:

INTRODUCTION

1.1.   BACKGROUND

Nitrovan is a vanadium carbonitride used in the steelmaking industry as a vanadium and nitrogen additive. It is produced by the carbothermal reduction of V_2O_3 in a nitrogen atmosphere. For this purpose, Vametco makes use of a graphite lined vertical shaft induction furnace.

Vametco experiences two problems that occur in the Nitrovan reactor:

1.   the graphite liner experiences a high wear rate and

2.   plugging in the furnace, decreasing furnace productivity and increasing costs.

Vametco contracted the Department of Materials Science and Metallurgical Engineering at the University of Pretoria to investigate mechanisms of plug formation, furnace liner wear and to find means of improving the furnace liner's life.

1.2.   PROBLEM STATEMENT

Frequent plugging and high erosion rates of the graphite furnace liner in a shaft furnace limits the throughput of the furnace during the production of Nitrovan.

1.3.   RESEARCH SIGNIFICANCE

The estimated loss in potential revenue is R1.88 million per day per furnace excluding costs of the furnace liner and maintenance. This is based on the following assumptions:

- Vametco can produce 30 drums of Nitrovan per day;

- a drum of Nitrovan has a precise weight of 200 kg;

- Vametco has the ability to distribute all the Nitrovan produced in the Nitrovan reactor;

- no production stoppages occur at any other section of the plant;

- the only problem in the production line occurs at the Nitrovan reactor due to plugging.

- Vanadium pentoxide price of 38.7 USD/kg as on September 12, 2019

- ZAR/USD exchange rate of R14.59/USD

Enhanced understanding of the physical and chemical reactions of the Nitrovan process will result in an improved understanding of the mechanisms of plug formation and furnace liner wear. Understanding the nitridation of V_xO_y will allow for a better understanding of the sintering and possible graphite liner attack that takes place during production.

1.4.   GOAL STATEMENT

A post-mortem analysis was conducted, and it was concluded that plug formation is likely caused by the fusion of pellets (conglomerate formation) and furnace liner wear.

The goal of this project is to understand:

- The chemical reactions during the production of Nitrovan.

- The dimensional changes of the feed material during the production of Nitrovan.

- Furnace liner wear mechanisms involved in the production of Nitrovan in the graphite lined tube furnace.

- The mechanism or mechanisms of plug formation.

- How to improve furnace productivity by reducing furnace liner wear and plugging.

1.5.   RESEARCH APPROACH

In this study, an experimental approach was followed. A laboratory scale induction furnace was designed and built to replicate the Nitrovan reactor at Bushveld Vametco Alloys. Pellets were produced in-house in accordance with the briquettes used in the production of Nitrovan.

This study focused on the furnace operation and the chemistry and morphology of the raw and sintered briquettes.

The research included:

- The effect of temperature on shrinkage and fusion of laboratory pellets;

- The effect of axial load on shrinkage and fusion of laboratory pellets;

- The effect of the amount of spillage added to the mixture on shrinkage and fusion of laboratory pellets;

- The effect of the amount of soluble and insoluble impurities added to the mixture on the shrinkage and fusion of laboratory pellets;

- An analysis on the physical changes of laboratory pellets under varied temperatures and exposure times.

The research excluded:

- Furnace shape;

- Physical testing of briquette shape;

- Loading and unloading operations in the furnace;

- Briquetting of the blended compounds;

- Drying of briquettes;

- Process control of the furnace operation;

- Graphite grade used for the furnace liner.

CHAPTER 2:

LITERATURE REVIEW

2.   LITERATURE REVIEW

2.1.   VANADIUM

The element vanadium (V) of the fifth group of the periodic table with the atomic number 23 has a relative atomic weight of 50.9415 g/mol. It arranges as a BCC structure with a lattice parameter of 0.30238 nm. It has an electron configuration of $[Ar]3d^3 4s^2$, which allows the vanadium compound to manifest in the oxidation states of II, III, IV or V. Due to the high melting point of vanadium, it belongs to the refractory metals group with chromium, molybdenum, niobium, tantalum and tungsten [1],[2],[3],[4].

The density of vanadium is 6.11 g/cm^3 at 25 °C and the mechanical properties are strongly dependant on the purity and the production techniques. Vanadium has a reported Young's modulus of 128 GPa, shear modulus of 47 GPa and Poisson's ratio pf 0.37. Vanadium is at 6.7 on the Mohs hardness scale and a Vickers hardness of between 628 and 640 MPa. The exact hardness is very dependent on metal purity [2], [3], [5].

Most vanadium (85%) is used as an alloying addition in the steelmaking industry. At elevated temperatures, vanadium is completely miscible in iron. Vanadium additions of between 0.1 and 5 wt% has two effects on steel: it promotes the formation of finer grains in the steel matrix and acts as a deoxidant that imparts hardness, strength and wear resistance to steel. Owing to its reactivity with carbon, vanadium is also used as a carbide stabilizer. Vanadium is a strong carbide and nitride former which causes carbide and nitride particles to precipitate in the steel. Vanadium is an austenite stabiliser with a vanadium concentration below 0.2% and a ferrite stabiliser with vanadium concentrations exceeding 1.5%. These properties are used in a large assortment of steels which include carburising steels, construction grade steels, and especially in rust and heat resistant high speed tool steels, die steels and special stainless steels [1]–[4], [6]. Vanadium in steelmaking is discussed in section 2.5.

The second most important use of vanadium is its use as an additive to provide high temperature creep resistance to titanium alloys. Vanadium is a beta-phase stabiliser for titanium alloys commonly used in automobile parts, jet-aircraft engines, and turbine motors. Vanadium foil is used as a bonding agent in cladding titanium to steel [3], [4], [7].

Vanadium is an important alloying ingredient in some commercial magnetic materials. The intermetallic V_3Ga is a useful high field (17.5T) high T_c superconductor.

Vanadium compounds are also used in the chemical industry as catalysts in several key processes including the contact process for sulfuric acid manufacturing, the production of special grades of synthetic rubber, for the synthesis of many organic intermediates and for the removal of hydrogen sulfide from the flue gases in the Stretford process. Other uses include, but are not limited to, the petrochemical industry, ceramic pigments, redox batteries and as a constituent in the red phosphors [6]–[8].

2.2. VANADIUM RESOURCES

Vanadium is not a rare element and has a relative crustal abundance of 135 ppm which is twice that of copper and almost ten time that of lead. It is the 22nd most abundant element in the Earth's crust and the 12th most common metallic element. Due to its substitutional arrangement, especially with iron, vanadium is concentrated in several lithophilic geological materials such as ultramafic and mafic igneous rocks and is more abundant in mafic than silicic rocks. As many as 80 different minerals containing vanadium are known and fall into seven broad categories: oxides, phosphates, silicates, sulfates, sulfides, titanates and vanadates [4], [7], [9].

The world resources of vanadium surpass 63 million tonnes and about 49% of these resources are located within South Africa. The vanadium reserves in South Africa are estimated to be about 3.5 million metric tonnes, 18% of the world total. Figure 2-1 gives a breakdown of the world total vanadium reserves. The world mine production figures are depicted by Figure 2-2. The primary source of vanadium occurs in deposits of titaniferous magnetite, phosphate rock, carbonaceous shale, vanadium bearing clay, uraniferous sandstone and siltstone and dolomitic shale. Substantial quantities are also present in steel converter slag, bauxite and carboniferous materials, such as crude oil, coal, tar sands and oil shale. [10], [11].
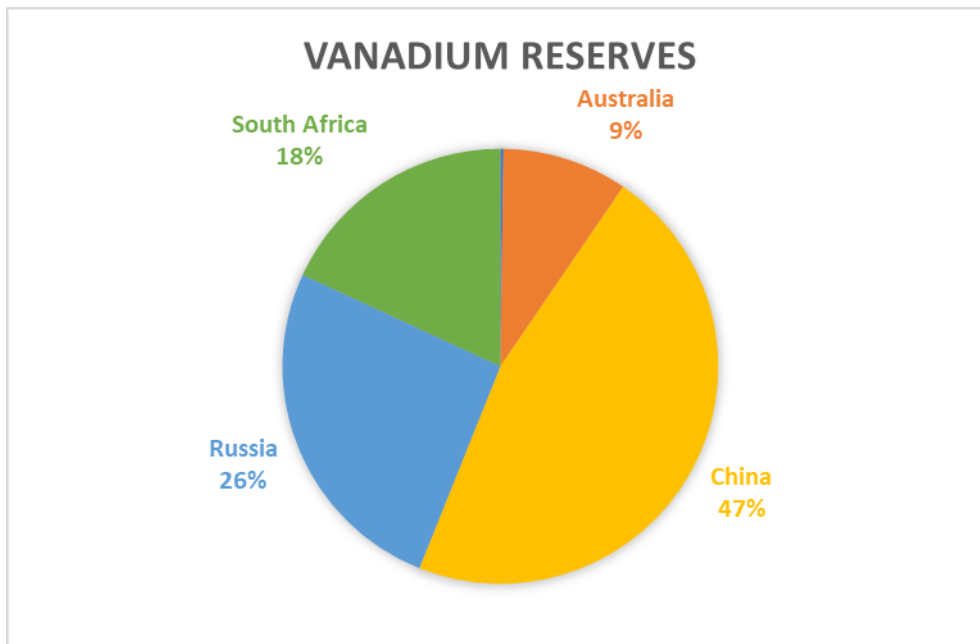
Figure 2-1: Total vanadium world reserves [11]*.*
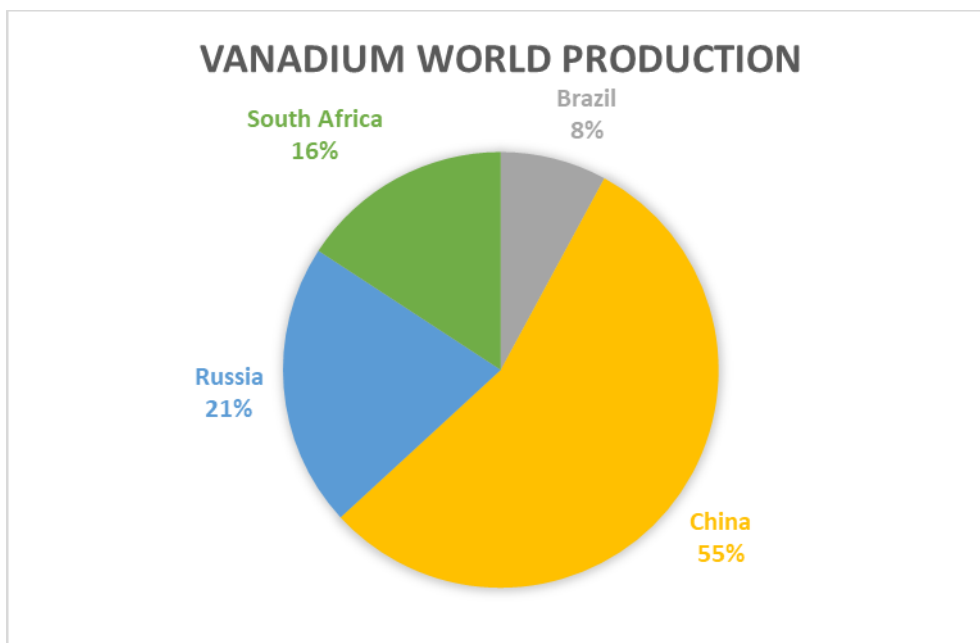
Figure 2-2: Vanadium world production [11]*.*

The largest known reserves of vanadium ore are confined within the Upper Zone of the Bushveld Complex. The vanadium-bearing ore is classified as titaniferous magnetite and is a massive, layered, mafic intrusion situated within the North West, Mpumalanga and Limpopo provinces of South Africa [10].

Titaniferous magnetite are accumulations of magnetite and ilmenite in magmatic deposits. These deposits are a major source of vanadium and commonly hold 0.2 to 1 percent V_2O_5. Titaniferous

magnetite deposits are widespread and are found in South Africa, India, China, Russia, Canada, and Australia. The major commercial deposits of economic value are found in South Africa, China and Russia, with South African ore having up to 2 percent V_2O_5 [12], [13], [14].

The South African titaniferous magnetites originate exclusively from extensive mafic intrusions in the Upper Zone of the Bushveld Complex. Figure 2-3 shows the Bushveld Complex with the vanadium bearing magnetite layers. Approximately 8 percent of magnetite is distributed in the upper 1750 m of layered basic rocks of the Bushveld Complex and a further 20 m of pure magnetite is distributed through more than 20 discrete magnetite layers. The seams and plugs of this intrusion offer a potential source of vanadium, iron, and titanium. The main seam offers a consistent vanadium pentoxide content of 1.6 percent plus or minus 0.2 percent. The main seam is hundreds of kilometres long and follows the elliptical rim of the complex. Outcrops of the orebody are seen in Figure 2-3 and can be found close to Brits, Pretoria, Roossenekal, Rustenburg, Magnet Heights, and north of the Pilanesberg [10], [14].
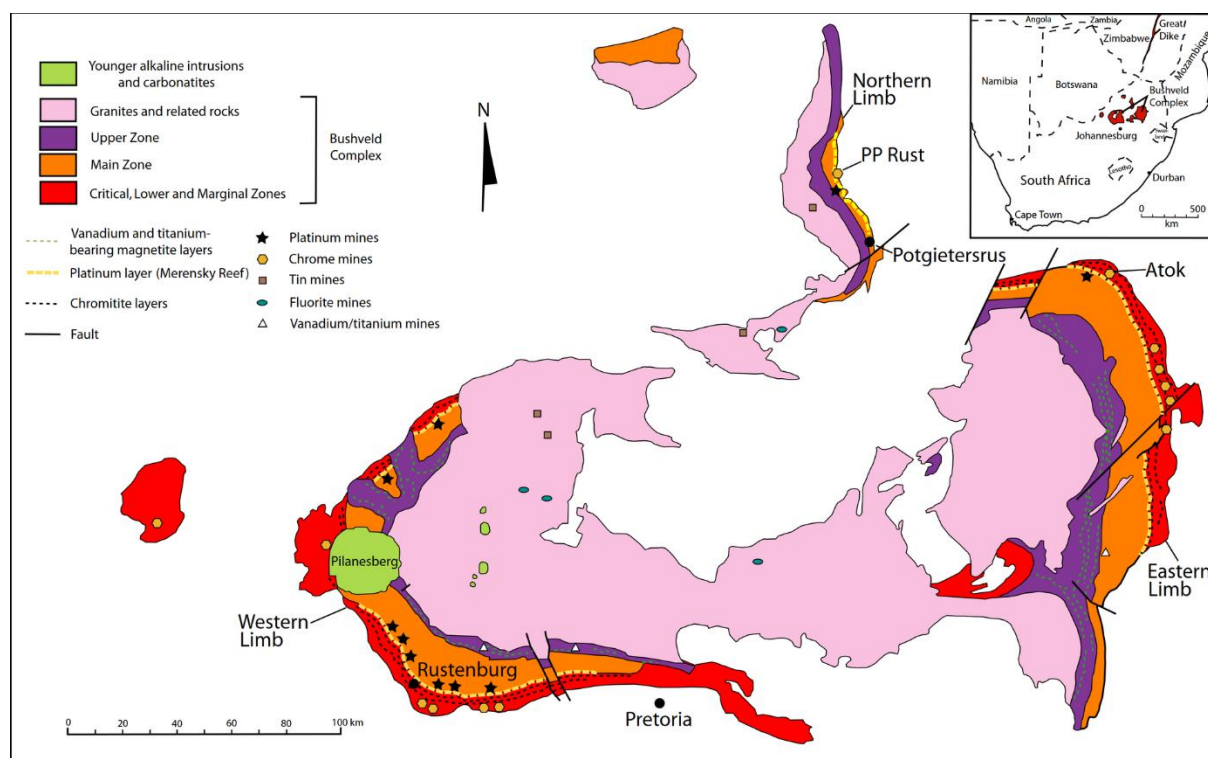
Figure 2-3: Bushveld igneous complex [15]*.*

The principal ore minerals are magnetite (Fe_3O_4) and ilmenite ($FeTiO_3$). Titanomagnetite (($FeTi)_3O_4$ or ($FeTi)_2O_3$) comprises of equant grains that are densely packed and have interstitial minor accessory silicates. Ulvöspinel (Fe_2TiO_4), is the titanium-rich spinel phase with the titanium primarily found as a solid solution. It is also found to a lesser extent as ilmenite. The ilmenite arranges itself in three

different ways: individual grains, elongated intergranular bodies, or exsolution lamellae arranged parallel to the octahedral planes of the magnetite [10], [12].

Vanadium is present as a solid solution within the magnetite-ulvöspinel series, where V^{3+} replaces Fe^{3+}. No discrete vanadium minerals are present in the ore and vanadium mostly occurs in solid solution in the magnetite (magnetic concentrate). Some vanadium occurs in ilmenite and other titanium minerals. Magnetite that is exposed to weathering can oxidise to form vanado-maghemite $((FeTi)_2O_3)$ and small concentrations of hematite, without any alteration in the texture of the ore [10], [12].

2.3.   PROCESSING OF RAW MATERIALS

The raw materials currently processed include titaniferous magnetite ores, vanadium slags derived from the ores, residues from the hydro demetallisation process of crude oil, oil combustion residues and spent petroleum catalysts. Two general processes exist to recover vanadium from titaniferous magnetite ore and can be classified into chemical and metallurgical methods. These are outlined in Figure 2-4 [2], [7].

The chemical route involves the salt roasting of the ore or concentrate to form a water-soluble sodium vanadate. The ore is crushed, milled, screened and magnetically separated. The magnetic concentrate is mixed with a sodium sulfate (Na_2SO_4) or sodium carbonate (Na_2CO_3) or both. The charge is then roasted in a rotary kiln at temperatures of between 850 to 1100 °C for two to three hours. During the roasting process, the iron and vanadium components are oxidised to the highest oxidation degree and the sodium reacts with the vanadium. This process yields a water-soluble sodium vanadate $(NaVO_3)$, which is leached using water. The leach solution is treated with $Al_2(SO_4)_3$ to remove silica and alumina. Vanadium is precipitated by adjusting the pH of the leach solution with ammonium sulfate and sulfuric acid to produce ammonium polyvanadate $(NH_4V_3O_8)$, or ammonium metavanadate (NH_4VO_3) [3], [4], [7], [12], [16].

The second process route involves the smelting of the ore to form pig iron in which the vanadium is concentrated. The ore is introduced as iron ore into a blast furnace or submerged arc furnace, which yields a vanadium-bearing pig iron with typical furnace temperatures of between 1300 to 1350 °C and a slag basicity of between 0.8 to 0.9. The vanadium in the pig iron is then oxidised to yield a vanadium-rich slag with a V_2O_5 content of between 12 to 24%. The slag is then salt-roasted, leached, and a vanadium salt precipitated as described previously in the chemical processing route. It must be mentioned that Bushveld titaniferous magnetite ores cannot be smelted in a blast furnace due to the high titania content. The formation of titanium carbo-nitrides results in the clogging of the hearth of the blast furnace. This is the reason why most companies, like Highveld and Rhovan, prefer the direct reduction route using an arc furnace or the conventional salt roast process. [3], [12], [13], [17].

Table 2-1: Typical Highveld Steel and Vanadium vanadium slag composition wt% [18].

FeO	V_2O_5	CaO	MgO	SiO_2	Al_2O_3	TiO_2	Cr_2O_3	MnO
29	24	5	4	15	5	9	5	3

Vanadium rich slag produced from the steel making route has a typical composition as shown in Table 2-1 [18]. Salt roasting results in the formation of vanadates, silicates, aluminates, chromates and ferrates of sodium. Roasting at 600 °C for 2.5 hours under oxidising conditions is sufficient for all the spinel and olivine to be decomposed. Several vanadium compounds form during the roasting, and these include $Na_5V_{12}O_{32}$, NaV_6O_{15}, $NaVO_3$, $Na_4V_2O_7$, V_nO_{2n-1} (2≤n≥8) and V_6O_{13}. Maximum vanadium recovery of approximately 90 % is achieved for a roasting temperature of 700 °C. Lower roasting temperatures result in incomplete reactions between Na_2CO_3 and vanadium compounds. Roasting at temperatures of between 800 °C and 900 °C result in the formation of a sintered water insoluble glassy phase. The soluble sodium salts dissolve in water during the leaching process, while other minerals in the leach residue remain unchanged [19].
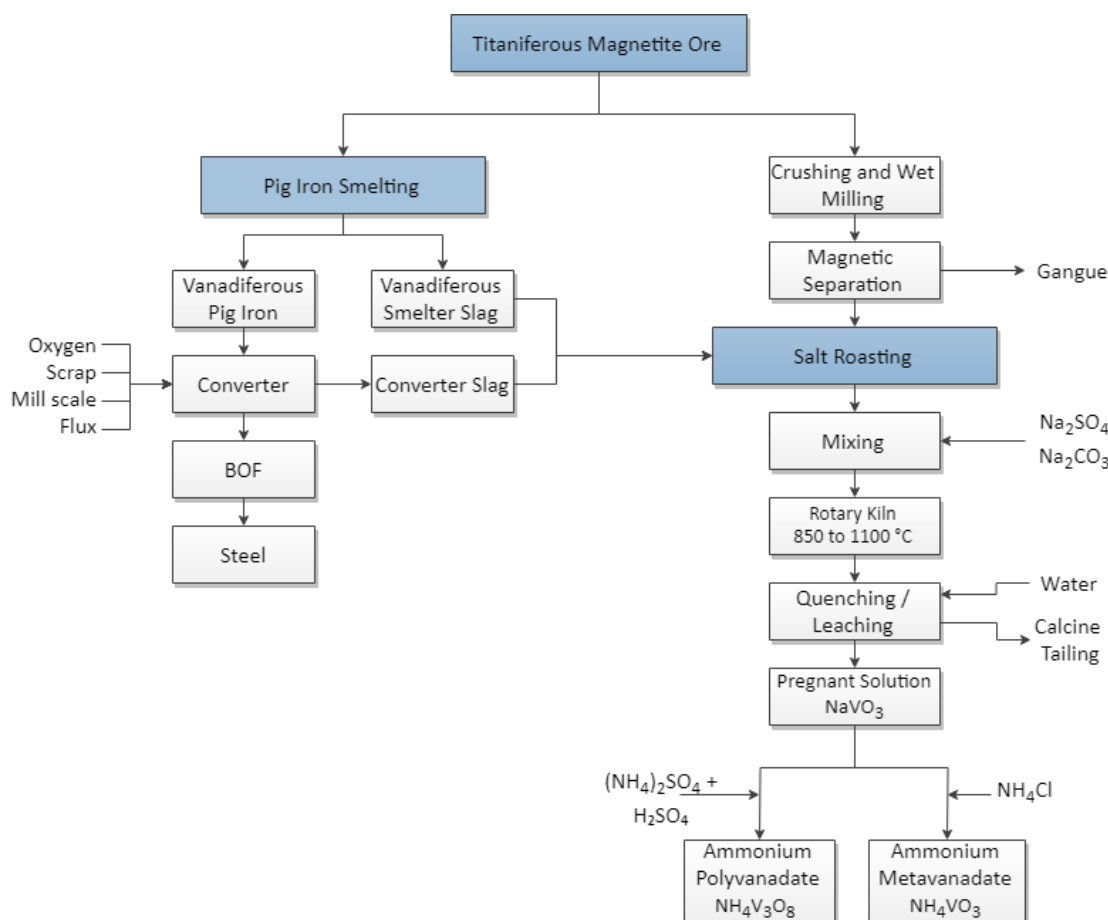
Figure 2-4: Outline of processes for vanadium recovery from vanadium bearing titaniferous magnetite.

Ammonium metavanadate (NH_4VO_3) can be thermally decomposed to form vanadium oxide, ammonia and water. The oxidation state of the vanadium compound is dependent on the temperature but most importantly, oxygen partial pressure at which the decomposition occurs. To produce V_2O_3, reducing conditions are required while for V_2O_5 oxidising conditions are required [20].

Most of the vanadium pentoxide (V_2O_5) produced is converted into ferrovanadium (FeV). Generally, two methods are used to produce ferrovanadium: reduction by aluminium and reduction by silicon.

The aluminothermic process for producing ferrovanadium is highly exothermic and allows the production of FeV with a low carbon content. The aluminothermic reduction of V_2O_5 is possible without the use of a furnace. Ferrovanadium can be prepared by the thermite reaction in magnesite lined vessels where vanadium pentoxide is reduced by aluminium granules. The charge of the aluminothermic reduction usually consists of vanadium pentoxide, aluminium, scrap iron and lime or fluorspar added as flux. Aluminium metal is converted to alumina (Al_2O_3) which reports to the slag and the V_2O_5 is reduced to vanadium metal and dissolves in the molten iron. Vanadium master alloys can be prepared by the use of this method [3], [4], [7].

The electro-aluminothermic process is efficient when V_2O_3 is used instead of V_2O_5. An electric furnace is used due to the energy balance difference between the reduction reaction of when V_2O_3 instead of V_2O_5 . The electro-aluminothermic process yields a typical vanadium recovery of between 90% to 96% in an electric furnace [3], [4], [7].

Silicon serves as a useful reducing agent for vanadium pentoxide. Ferrosilicon acts as both reducing agent and source of iron in the production of ferrovanadium. The silicothermic reaction is also exothermic, but not nearly as exothermic as that of the aluminothermic reaction, and the smelting is usually done in an electric furnace. The charge usually consists of vanadium pentoxide, ferrosilicon, lime and fluorspar as flux, and often scrap iron. This reduction process is often carried out in two or more stages and is reported to be much less efficient than the aluminothermic process with vanadium recoveries of between 75% and 80%. The reason for the lower yield of vanadium recovery in this reaction is due to the thermodynamics determining the equilibrium constant which results in a higher vanadium content in the slag due to the lower oxygen affinity for silicon in comparison to aluminium [3], [7].

Other processing routes exist but will not be discussed in this study.

2.4. VANADIUM SYSTEMS

Vanadium forms an extensive variety of compounds and alloys. The compounds and alloys of vanadium can be broadly classified into oxides, hydroxides, peroxy compounds, vanadates, sulfates and nitrates, halides and oxyhalides, interstitial compounds, and intermetallic compounds [7].

The focus of this study will be on some vanadium oxides and the interstitial compounds of vanadium carbides and vanadium nitrides.

2.4.1. VANADIUM-OXYGEN SYSTEM

As can be seen on the vanadium oxygen phase diagram [3] in Figure 2-5, vanadium forms a multitude of oxide phases. Only four oxide phases V_2O_5, V_2O_4, V_2O_3 and VO are relevant when discussing the processing and extraction of vanadium [7].

Vanadium (V) oxide, commonly known as vanadium pentoxide (V_2O_5), is usually obtained as the final product in most vanadium ore processing techniques. V_2O_5 is produced by heating vanadium compounds in air. Heating vanadium metal, vanadium nitride and sulphides, and lower vanadium oxides in air will result in the formation of vanadium pentoxide. The most common processing technique to form V_2O_5 is by calcining ammonium vanadate at 500 °C to 600 °C in an oxidising atmosphere [2], [7].

Table 2-2: Vanadium oxide summary table.

	Melting Point	Lattice
V_2O_5	678 °C	Orthorhombic
V_2O_4	1642 °C	Tetragonal
V_2O_3	1957 °C	Cubic
VO	1790 °C	Cubic

Vanadium pentoxide is a commonly used starting material for almost all important vanadium processes and products. It is used as the feed material to produce ferrovanadium, vanadium-aluminium master alloys as a starting material for vanadium compounds such as carbides, halides, nitrides, silicide, vanadates, vanadium salts and as an oxidation catalyst [2].

Vanadium pentoxide is yellowish red in powder form, has a relatively low melting point at 678 °C and belongs to the orthorhombic crystal system [7]. It is amphoteric and dissolves in strong acids, and is slightly soluble in water (0.01 to 0.08 g V_2O_5/dm³ at 25 °C) [4], [21]. At temperatures between 700 °C

and 1125 °C, vanadium pentoxide loses oxygen to form V_2O_{5-x}, where x increases with the increase in temperature. This may account for its important catalytic properties [22].

Vanadium (IV) oxide, also known as vanadium dioxide (VO_2) or divanadium tetroxide (V_2O_4) can be prepared by mild reduction of the pentoxide. Vanadium pentoxide can be reduced by vanadium (III) oxide, carbon, carbon monoxide, sulfur dioxide, oxalic acid [23] or on larger scale by reducing V_2O_5 with a hydrocarbon atmosphere at 600 °C in a rotary kiln [7].

A reversible first-order phase transformation occurs in pure vanadium (IV) oxide at 68 °C [24], making it usable in infrared modulators for missile guidance systems , optical modulators and optical shutters in cameras, data storage, and other applications [25].

Vanadium (IV) oxide has the tetragonal rutile structure at temperatures below 66 °C and a monoclinic structure at higher temperatures [26]. It is amphoteric, dissolves in non-oxidising acids and has a melting point of 1642 °C [14].
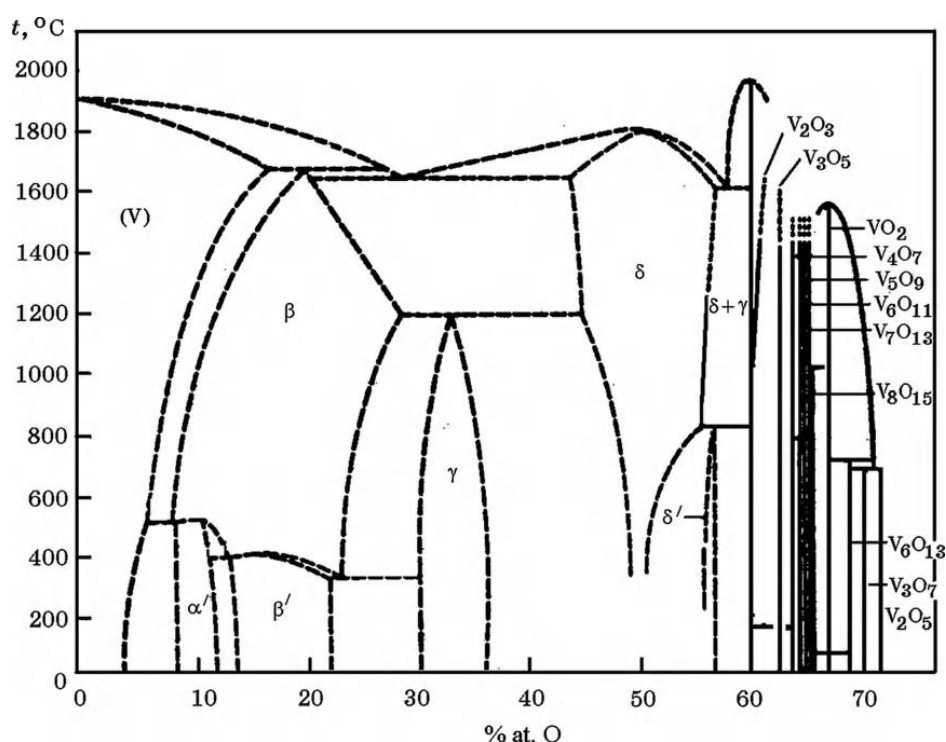
Figure 2-5: Equilibrium phase diagram for the V-O system [3].

Vanadium (III) oxide, also known as vanadium trioxide (V_2O_3) or vanadium sesquioxide, can be prepared by reducing the pentoxide with hydrogen, carbon, or several other reagents. It can also be formed by the thermal decomposition of ammonium vanadate in a reducing atmosphere at 400 °C to 900 °C [2], [7].

Vanadium trioxide is used as a substitute for vanadium pentoxide in the production of high purity vanadium metal, ferrovanadium, vanadium-aluminium master alloys, vanadium carbides and nitrides, and vanadium carbonitrides [2]. Vanadium trioxide oxidises slowly in air to form vanadium dioxide ($V_2O_{4)}$ and forms V_2O_5 at temperatures higher than 120 °C [7].

Vanadium trioxide melts at 1957 °C and crystallises with a corundum (Al_2O_3) structure [7]. It is antiferromagnetic and has a transition temperature of 160 K where a small change in temperature results in a large change of electrical resistivity [23].

Vanadium (II) oxide, also known as vanadium monoxide (VO), is prepared by the reduction of higher oxides with reducing agents such as hydrogen and carbon [23]. It can also be prepared by heating a mixture of vanadium metal and V_2O_3 in a vacuum [7].

Vanadium monoxide has a cubic defect NaCl-type crystal structure and is a nonstoichiometric compound. The homogeneity of VO_x changes with temperature and ranges between $VO_{0.9}$ and $VO_{1.30}$ at 1300 °C [27]. Vanadium monoxide is electrically conductive and paramagnetic at room temperature [23]. It has a melting point of 1790 °C. Vanadium monoxide is insoluble in water but dissolves in acids.

2.4.2. VANADIUM-CARBON SYSTEM

As can be seen in the vanadium carbon phase diagram [28] (Figure 2-6), only V_2C and VC are stable at a temperature greater than 1320 °C. The cubic vanadium monocarbide VC_y has a NaCl-type crystal structure. The lower hexagonal vanadium carbide V_2C_y (βV_2C_y) has a L'3 (W_2C) structure [29]. The two carbide phases are nonstoichiometric and have wide composition range of which the width is dependent on temperature [30].

The hexagonal vanadium carbide βV_2C_y displays a homogeneity range of $V_2C_{0.74} - V_2C_{1.0}$ for temperatures below 2210 °C [29]. Carbon atoms and unfilled interstitial sites are randomly scattered in the carbon lattice at temperatures greater than 1250 °C [31]. At lower temperatures, the non-metallic interstitial atoms and structural vacancies are redistributed and result in disorder-order phase transformations which lead to three ordered structures.

For the cubic vanadium carbide VC_y, y ranges between 0.58 and 0.875 for temperatures between 1060 °C and 2800 °C [29]. From the disordered cubic VC_y phase, a cubic ordered V_8C_7 phase forms at temperatures below 1100 °C, over the $VC_{0.87}$ - $VC_{0.875}$ range [29]. The ordered V_6C_5 phase is produced at temperatures below 1200 °C with a reported homogeneity range of $VC_{0.75}$ - $VC_{0.83}$ [32] and V_3C_2 phase with a sufficiently narrower region of homogeneity from $VC_{0.68}$ to $VC_{0.71}$ at 750 °C and from $VC_{0.665}$ to $VC_{0.721}$ at 150 °C [29].
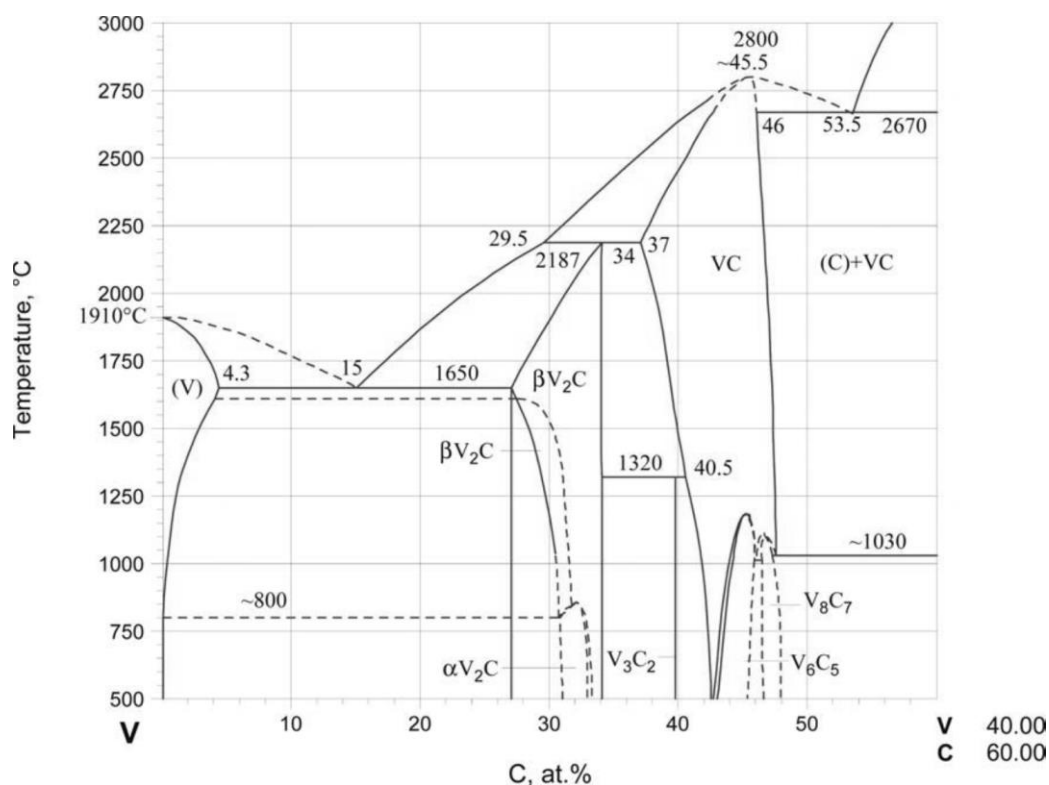
Figure 2-6: Equilibrium phase diagram for the V-C system [28]*.*

2.4.3. VANADIUM-NITROGEN SYSTEM

Vanadium reacts with nitrogen thermodynamically at all reasonable temperatures but reacts kinetically from 350 °C to form vanadium nitride and can be obtained by the direct combination of the elements [33]. Two vanadium nitride phases are known and is shown in the vanadium nitrogen phase diagram [34] given in Figure 2-7. The two intermediate vanadium nitrides are represented by formulas δVN_{1-x} and βV_2N_{1-y}. The two phases are nonstoichiometric and have wide ranges of homogeneity [7], [34]. A phase with formula $V_{32}N_{26}$ has also been reported and appears on the phase diagram as $\delta'VN_{1-x}$. Other phases with formulas $V_{16}N$, $V_{13}N$, V_9N, V_8N, V_9N_2, and V_4N have been reported [34], but are considered metastable phases, if indeed they do exist, and are therefore not shown in the phase diagram in Figure 2-7.

Vanadium mononitride VN (δVN_{1-x}) presents itself in nitrogen-rich V-N alloys and has a NaCl-type fcc cubic structure. The nitrogen atoms are arranged in the octahedral interstitial positions of the vanadium host lattice [35], [36]. VN_{1-x} is a disordered compound with a homogeneity interval ranging from $VN_{0.69}$ to $VN_{1.00}$ [37]. It was found that the lattice parameters of VN_{1-x} change as a function of composition and have a near linear relationship [35]. The melting point of δVN is given as 2340 °C ±10 °C at 1 atm N_2 pressure. [34], [37].
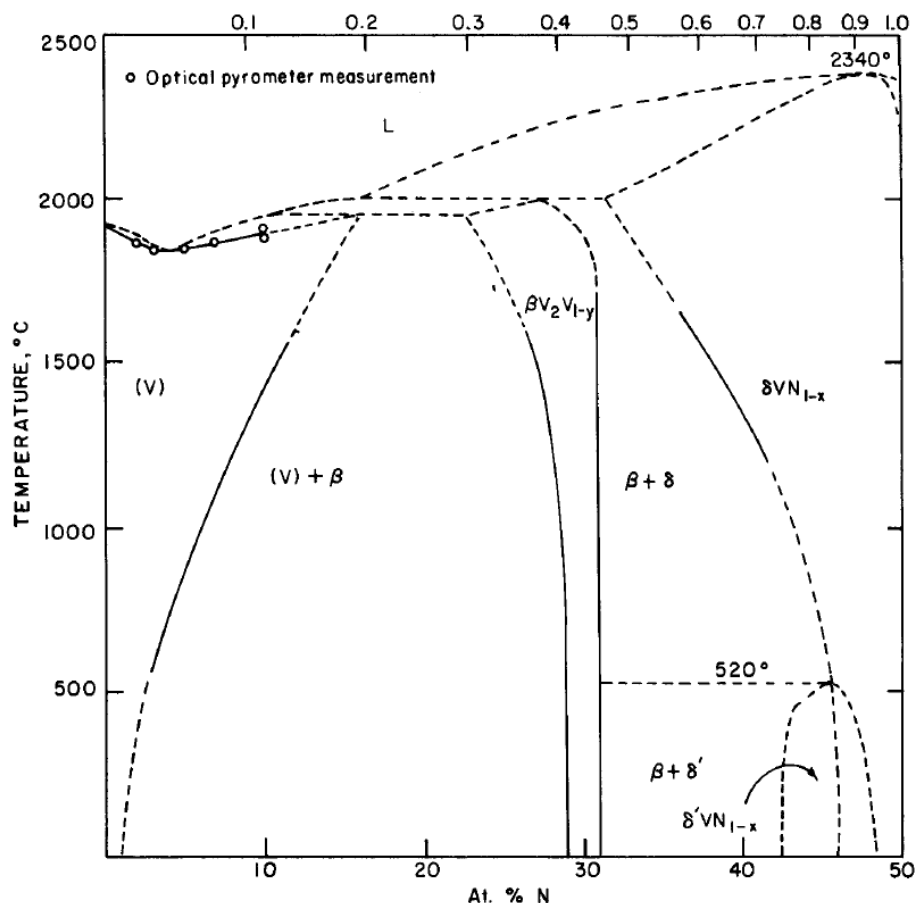
Figure 2-7: Equilibrium phase diagram for the V-N system [34].

The hexagonal closely packed vanadium subnitride V_2N (βV_2N_{1-y}) has a εFe_2N-type [37] structure and presents itself in nitrogen-deprived V-N alloys. V_2N_{1-y} is also considered a disordered compound with a homogeneity interval ranging from $VN_{0.46}$ (y = 0.08) to $VN_{0.50}$ (y = 0) [34]. The composition of V_2N_{1-y} changes linearly with nitrogen partial pressure [38]. The V_2N phase forms during the decomposition of VN followed by the formation of $(V,N)_{(ss)}$. At elevated temperatures and under vacuum, the decomposition of VN proceeds according to Equation 2.1 and 2.2 [39]:

$$2VN \ \rightarrow \ V_2N + 0.5N_2 \tag{2.1}$$

$$V_2N \ \rightarrow (V,N) + \ 0.5N_2 \tag{2.2}$$
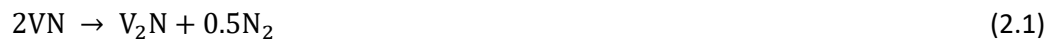
The formation of VN from V and N_2 is strongly exothermic. Gusev, Remple and Magerl [37] used experimental data to calculate the formation enthalpy $\Delta_f H°_{298}$ (Equation 2.3), entropy $\Delta_f S°_{298}$ (Equation 2.4), and Gibbs free energy $\Delta_f G°_{298}(n,T)$ (Equation 2.5) of VN_x as a function of the nitrogen stoichiometric coefficient (x):

$$\Delta_f H°_{298}(x) = -6120 - 309960x + 114800x^2 \ (\text{kJ mol}^{-1}) \tag{2.3}$$

$$\Delta_f S°_{298}(x) = -20.01 - 66.86x \ (\text{J mol}^{-1}\text{K}^{-1}) \tag{2.4}$$

$$\Delta_f G°_{298}(n, T) = 80360 - 66.8T + 229600n \ (\text{J mol}^{-1}) \tag{2.5}$$

The nitrogen concentrations of VN_x change significantly depending on temperature and nitrogen pressure. It has been reported that a stoichiometric composition of $VN_{1.0}$ can be obtained under atmospheric pressure of N_2, but later work shows that it is only possible at higher N_2 pressures [40]. Lengauer and Ettmayer [35] state that a sigmoid relationship exists between the V:N ratio and nitrogen pressure at 1450 °C.

Table 2-3: Calculated relative nitrogen content (x) and nitrogen partial pressure (P_{N2}) for cubic vanadium nitrides VN_x which evaporate correspondingly at a specified temperature T [37].

T (°C)	x	P_{N2} (x,T) (atm)
726.85	0.9512	0.000061
826.85	0.9279	0.000264
926.85	0.9034	0.000908
1026.85	0.8784	0.002609
1126.85	0.8531	0.006518
1226.85	0.8279	0.014547
1326.85	0.8028	0.029668
1426.85	0.7778	0.056137
1526.85	0.7531	0.099871
1626.85	0.7287	0.16856
1726.85	0.7046	0.27232
1826.85	0.6903	0.42414

Table 2-4: Nitrogen partial pressure P_{N2} (atm) oven cubic nitride VNx at a temperature of 1327 °C, 1527 °C and 1727 °C [37].

X	P_{N2} (atm)		
	1327 °C	1527 °C	1727 °C
0.55	-	-	0.001
0.58	-	0.000101	0.00292
0.6	-	0.00022	0.00599
0.65	0.000032	0.00157	0.0365
0.69	0.000181	0.00767	0.158
0.7	0.00028	0.0115	0.23
0.72	0.000679	0.0257	0.363
0.75	0.0026	0.0878	0.639
0.8	0.026	0.267	1.67
0.85	0.0922	0.789	4.49
0.9	0.326	2.47	12.7
0.95	1.3	8.56	39.6
0.96	1.76	11.2	50.6
0.97	2.43	14.9	65.6
0.98	3.42	20.3	86.4
0.99	5.01	28.4	117
1	8.28	43.9	172.2

The relationship between temperature and nitrogen pressure on the stoichiometric range of δ-VN_x has been studied and recorded by many researchers. At increased temperatures, the lower boundary of the homogeneity interval is displaced to $VN_{0.53}$ at 1727 °C at 1 atm N_2 pressure. Gusev, Remple and Magerl [37], calculated and summarised in Table 2-3 the relative nitrogen content (x) and nitrogen

partial pressure P_{N2} for cubic vanadium nitrides VN_x which evaporate correspondingly at a specified temperature *T*.

Gusev, Remple and Magerl compared the calculated data (Table 2-3) to experimental data (Table 2-4) that is available in literature. The tables are platted in Figure 2-8 and Figure 2-9 . The calculated results correlate well to that of the experimental data. To obtain a stoichiometric nitride $VN_{1.0}$ a nitrogen partial pressure of ≥ 40 atm is required at a temperature of 1727 °C.
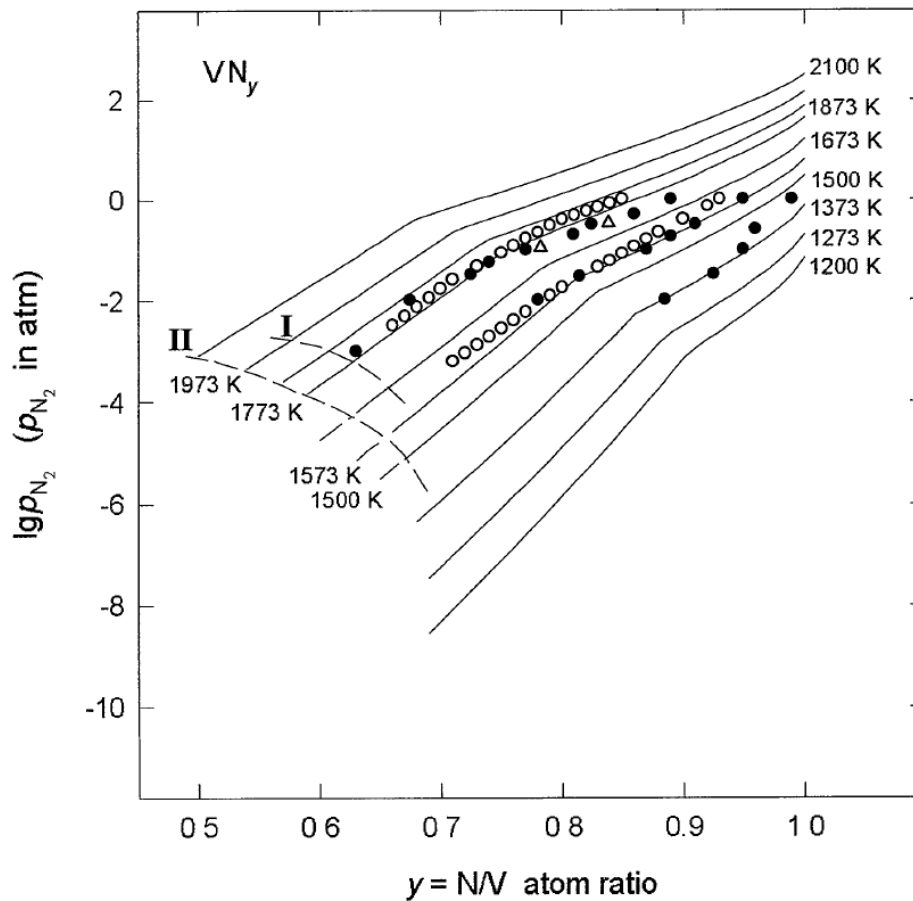
Figure 2-8: The PN2 - y isotherms for cubic vanadium nitride VNy at temperatures from 1200 to 2100 K [37].
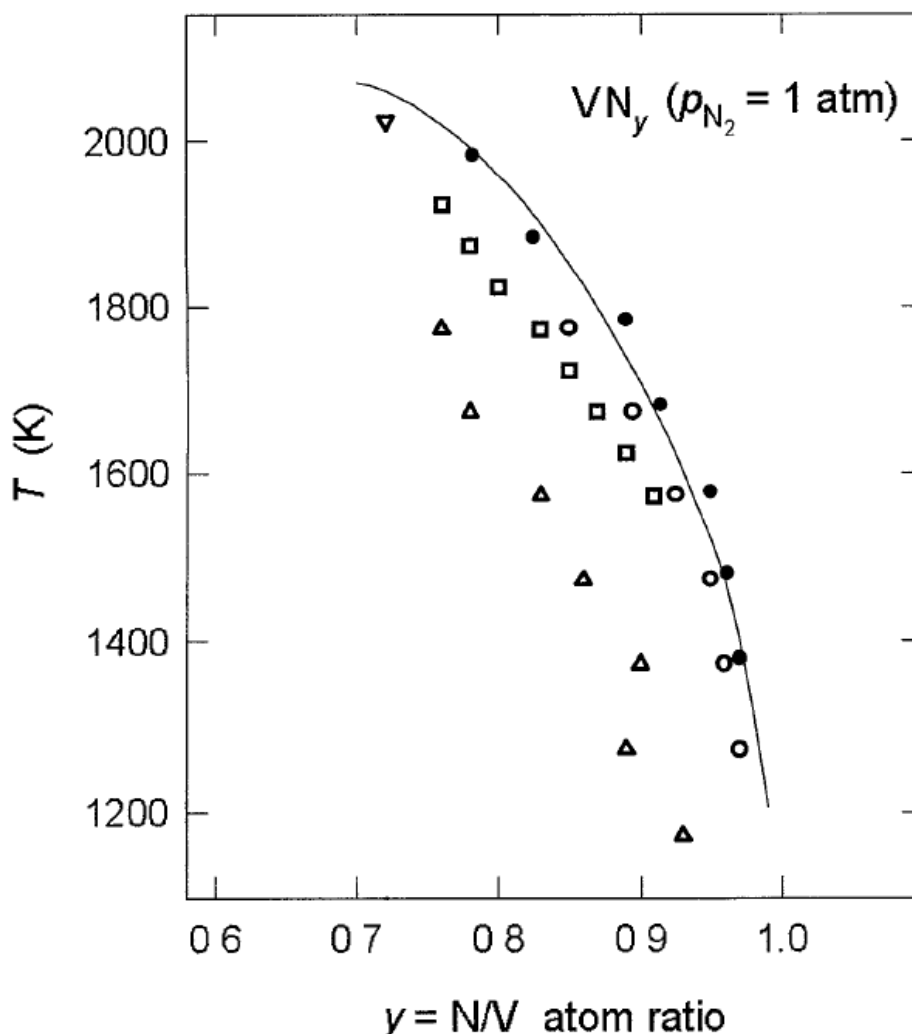
Figure 2-9: Calculated (solid line) and experimental "nitrogen content-temperature" isobars for vanadium nitride VNy under a dissociation pressure of l atm [37].

2.4.4.   VANADIUM-CARBON-NITROGEN SYSTEM

Vanadium carbonitride ($VC_{1-x}N_x$) is the solid solution of vanadium carbide and vanadium nitride which are miscible in each other [7]. Both vanadium carbide (VC) and vanadium nitride (VN) belong to the NaCl-type fcc cubic structure and their lattice parameters are very close to each other [41], [42]. Vanadium carbide and vanadium nitride are interstitial compounds with carbon or nitrogen atom vacancies resulting in unfilled nitrogen and carbon lattice sites in the vanadium carbonitride compound making it nonstoichiometric [43]. Vanadium carbonitride ($VC_{1-x}N_x$) might range from $VX_{0.75}$ to VX, where X is either nitrogen or carbon [1].

From the isotherms in Figure 2-10 to Figure 2-13 it is observed that that the γ corner of the γ + graphite + N_2 moves closer the VC side with an increase in temperature. The VN reaction is favoured at lower temperatures and the VC reactions is favoured at higher temperatures [44].
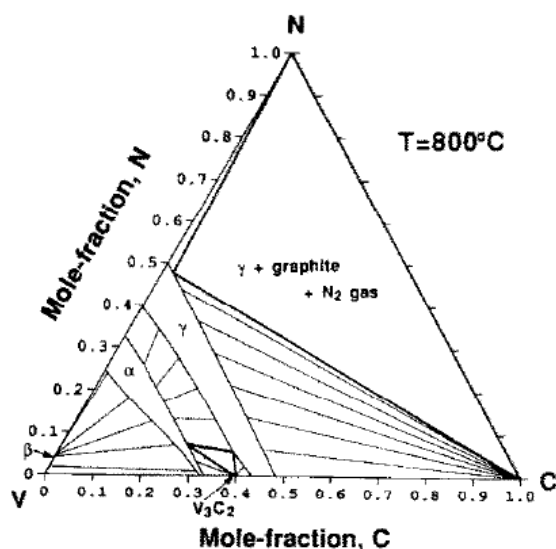
Figure 2-10: Calculated isothermal section diagram of V-C-N system at 800 °C [44].
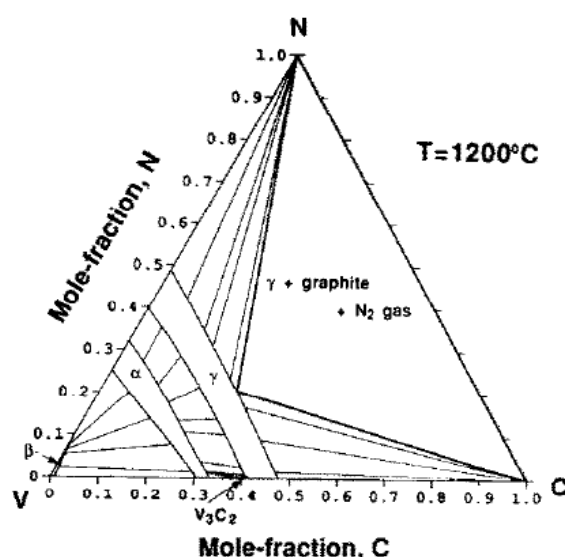
Figure 2-11: Calculated isothermal section diagram of V-C-N system at 1200 °C [44].
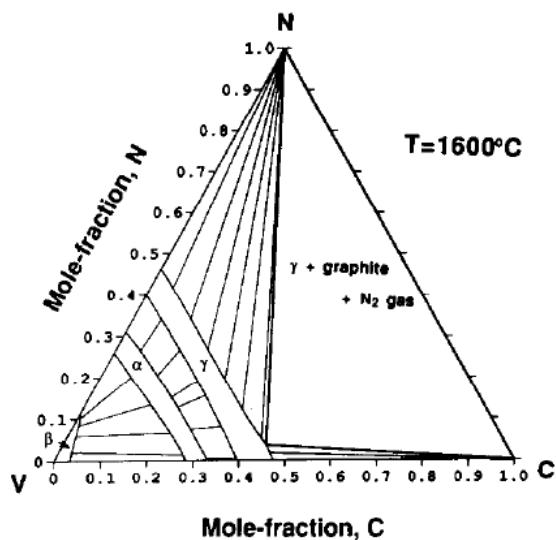
Figure 2-12: Calculated isothermal section diagram of V-C-N system at 1600 °C [44].
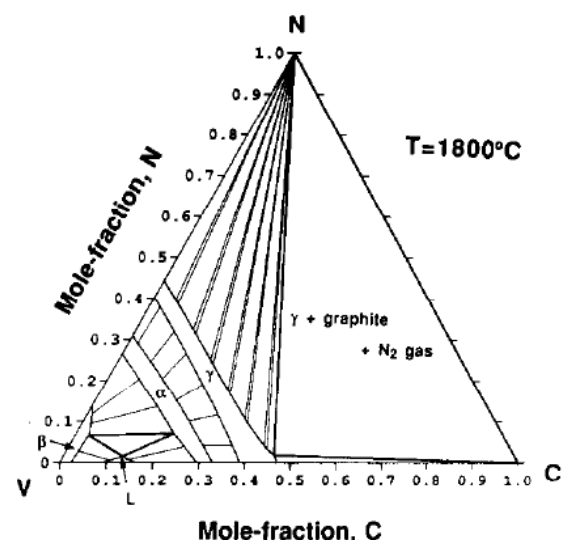
Figure 2-13: Calculated isothermal section diagram of V-C-N system at 1800 °C [44].

Nitrovan is a vanadium carbonitride and classified by Vametco as "vanadium carbide nitride" in the published materials safety data sheet (MSDS) [45] (See annexure A).

Vanadium carbonitride is produced by various methods which are discussed in detail in section 2.7.

2.5.   VANADIUM CARBONITRIDE IN STEELMAKING

It is common practice in high strength low alloy steels (HSLA), to make additions of elements such as Ti, Nb or, V to control austenite grain size. Vanadium and other elements are added to steel due to

their high chemical affinity for carbon and nitrogen which result in the formation of compounds and carbonitrides which can control austenite grain growth [46].

Vanadium can be easily added to liquid steel. It and has an affinity to form refractory carbides (VC), nitrides (VN), and carbonitrides (VCN) during reheating. As for aluminium and titanium precipitates, the vanadium compounds can act as both precipitation strengtheners and grain refiners, depending on the process temperature and the steel composition [6]. Vanadium improves the mechanical properties of HSLA steels as a microalloying element. It increases the hardenability of steel by decreasing the decomposition rate of austenite. Vanadium also increases the mechanical properties after tempering in quenched and tempered steels [46].

Nitrogen usually decreases the hardenability of steel because it decreases the content of alloying elements dissolved in austenite and delay the decomposition of austinite and form nitrides that promote the nucleation of non-martensitic phases. Alternatively, an increase of the nitrogen content in microalloyed steel increases the steel's ability for alloying elements to dissolve in austenite. The dissolved atoms segregate to the immobile austenite grain boundaries, which causes a resistance to coarsening carbonitride particles. The mechanical properties of heat-treated steels are governed by the composition of the steel, heat treatment parameters and the kinetics of austenite grain growth [46].

Due to the distorted lattice of both vanadium nitride and vanadium carbide, some nitrogen and carbon sites are unfilled leaving a stoichiometry range of $VX_{0.75}$ to VX, where x can be either nitrogen or carbon. The nitride tends to occur as the stoichiometric VX in steels and the carbide tends to the more deficient form of $VX_{0.75}$ [1].

2.6. PHYSICAL PROPERTIES

Presented in Table 2-5 are the physical properties of Nitrovan, Vanadium Nitride, Vanadium Carbide and Vanadium monoxide.

Table 2-5: Physical Properties of Nitrovan, VO, VC and VO.

Properties	Nitrovan	VN	VC	VO
Melting point	2427 °C	2320 °C	2810 °C	1790 °C
Boiling Point	Point Not available	Point Not available	3900 °C	2627 °C
Density	1.6 g/cm^3	6.13 g/cm^3	5.77 g/cm^3	5.758 g/cm3
Hardness	Unknown	12 GPa to 28 GPa	18 GPa to 31 GPa	
Source	[45]	[47]	[47]	[47]

2.7.   PRODUCTION OF VN

Vanadium nitride can be synthesized by several methods. Conventionally, VN is prepared by the carbothermal reduction of V_2O_5 in a nitrogen atmosphere at around 1500 °C [48]. Other methods to produce VN include:

1. direct reaction of pure vanadium powder under pure N_2 or NH_3 at 1650 °C [49],

2. carbothermal reduction of V_2O_3 in a nitrogen atmosphere at high temperature [50],

3. reduction of V_2O_5 with pure NH_3 and CH_4 [51],

4. reacting NH_4VO_3 with NH_3 at 900-1100 °C or with an H_2- N_2 mixture at 600-1400 °C [49],

5. reaction of vanadium VCl_4 and $VOCl_3$ with NH_3 at 1100-1600 °C and

6. by solid-state metathesis (SSM) routes at elevated temperature [43].

Vanadium nitride can also be prepared by heating a mixture of V_2O_5 and carbon under a flowing nitrogen atmosphere. The reaction becomes favourable with atmospheric nitrogen pressure and temperatures higher than 1000 °C. The initial reduction reaction from V_2O_5 to V_2O_3 takes place up to a temperature of approximately 1000 °C and the nitriding occurs between approximately 1000 °C and 1200 °C. In the presence of excess carbon, vanadium carbide occurs concurrently with vanadium nitride. The degree of the nitriding reaction is dependent on the carbon-to-oxide ratio, pelletizing pressure, particle size, nitriding temperature and time and nitrogen flow rate [52].

Tripathy, et al. [52] describe the oxide transformation during the nitriding from V_2O_5 and is given as Equation 2.6 and the sequential steps of VN formation is given by Equation 2.7 to 2.9 and the subsequent reaction is giving in Equation 2.10. Vanadium pentoxide is reduced by the carbon and moves though all the lower oxide phases to form vanadium monoxide. The monoxide forms a solid solution with the nitride and carbide and depending on the nitrogen availability, temperature and time, vanadium nitride would form [40].

$$V_2O_5 \; \rightarrow \; V_2O_4 \; \rightarrow \; V_2O_3 \; \rightarrow VO \; \rightarrow \; V(N, C, O) \rightarrow VN \tag{2.6}$$

$$V_2O_5(s) + \frac{1}{2}C(s) \rightarrow \; V_2O_4(s) + \frac{1}{2}CO_2(g) \tag{2.7}$$

$$V_2O_4(s) + \frac{1}{2}C(s) \rightarrow \; V_2O_3(s) + \frac{1}{2}CO_2(g) \tag{2.8}$$

$$V_2O_3(s) + 3C(s) + N_2(g) \rightarrow 2VN(s) + 3CO(g) \hspace{3cm} (2.9)$$

$$V_2O_5(s) + 4C(s) + N_2(g) \rightarrow 2VN(s) + CO_2(g) + 3CO(g) \hspace{2cm} (2.10)$$
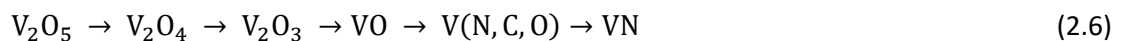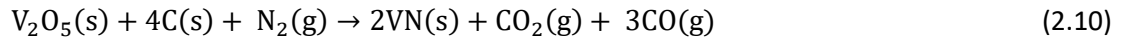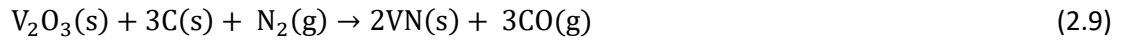
2.8. SOLID STATE SINTERING

When thermal energy is applied to a compacted powder, the powder densifies and the average grain size increases. This usually results in the shrinkage of the initial (green) volume [53][54].

The driving force of sintering is the decrease of the total surface energy. The change in surface energy is due to densification and the change in surface area is due to grain coarsening. For solid state sintering, surface energy is related to the reaction of the solid/vapour interface [54].

The different stages of sintering of two spherical particles is given in Figure 2-14. Two adjacent spherical particles will from one particle by joining at the interface. The particles will move towards each other's centres to form a single peanut-shaped particle. Depending on kinetics, one larger spherical particle will form at the final stage of sintering.

Loose powder   Early stage   Intermediate stage   Final sinter stage
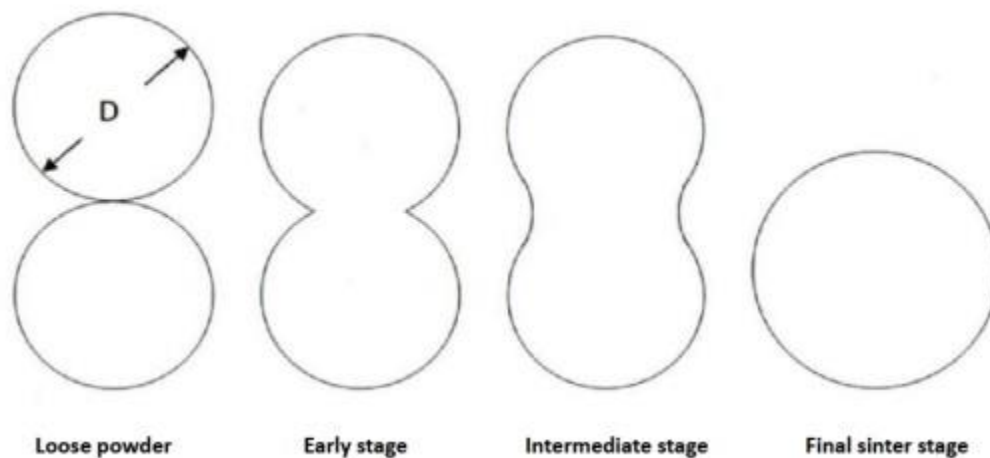
Figure 2-14: Different stages of sintering two spherical particles [55].

Zheng and Reed [56] found that shrinkage during sintering is related to green porosity. They found that during the initial sintering process, some pores grow due to nonuniform densification. A critical pore size to mean particle size ratio exist where smaller pores shrink faster than the pellet and disappear, and larger pores shrink at the same rate than the pellets. Some larger pores grow due to the elimination of the smaller pores.

During the first stagers of sintering, pellets with higher green density have lower shrinkage and a higher sintered density [56].

2.9.   EXPERIMENTAL DESIGN

Experiments are designed to describe and explain the variation of data under conditions that are expected (hypothesised) to reflect variations. Experiments usually consist of inputs, controllable factors, uncontrollable factors, and outputs. Experiments are designed to determine which variables have the most influence on a response [57].

Considering the first order model with two variables: $y = \beta_0 + \beta_1 X_1 + \beta_2 X_2 + \varepsilon$, y is the response from the system, the design factor terms are x's, the ß's are unknow parameters which is estimated from the data and Ɛ is a random <mark>error</mark> term that accounts for the experimental error in the system. This is also called the main effects model [57].

By adding interaction terms, the model changes to: $y = \beta_0 + \beta_1 X_1 + \beta_2 X_2 + \beta_{12} X_1 X_2 + \varepsilon$, where $X_1 X_2$ is the cross-product term that is represented by the two-factor interaction between the design factors [57].

In the analysis of variance (ANOVA), the sum of the squares is a measure of variation or deviation from the mean. This is calculated by the summation of the squares of the differences from the mean. The total sum of squares includes both the sum of squares from the factors and from randomness or error [57].

Reproducibly is a risk with designs that do not repeat every experiment, but centre points are repeated to determine the reproducibility of the experiments.

2.9.1.   CENTRAL COMPOSITE DESIGN

A central composite design is an experimental design useful in response surface methodology (RSM), for building a second order (quadratic) model for the response variable without needing to use a complete three-level factorial experiment [57].

The regression parameters for a second-degree polynomial regression model fit to a given response, can be estimated by a central composite design (CCD).   A polynomial, as given by Equation 2.11, describes the relationships among the measured response (y) and a number of experimental variables $(X_1...X_k)$, where k is the number of factors considered, β are regressors and ε is an error associated with the model:

$$y = \beta_0 + \beta_1 X_1 + \beta_2 X_2 + \cdots + \beta_k X_k + \beta_{11} X_1^2 + \beta_{22} X_2^2 + \cdots + \beta_{kk} X_k^2 \qquad (2.11)$$
$$+ \beta_{12} X_1 X_2 + \cdots + \beta_{k-1,k} X_{k-1} X_k + \varepsilon$$

The significance of the linear effect, curvilinear effects, interactions between factors is quantified by the regressors (β_1, β_2, β_3...) in Equation 2.11.
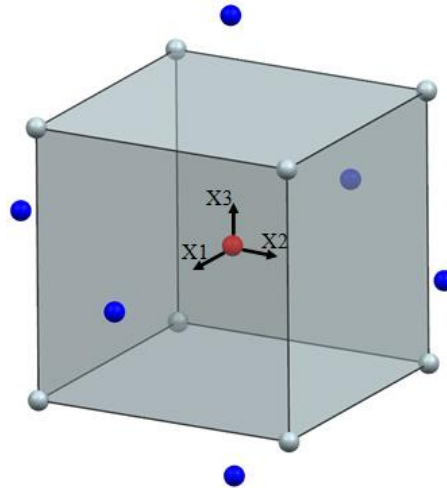
Figure 2-15: Three factor central composite design.

The values of the centre point are in the centre of the cube (red point) in Figure 2-15 and are used to detect curvature in the response. The axial points (6 blue points) are used to estimate the coefficients of quadratic terms, and the factorial points (8 grey points) are used mainly to estimate the coefficients of linear terms and two-way interactions.

2.9.2. FULL FACTORIAL DESIGN

This design is also used in RSM. The full factorial design has no alias relationships and are useful to estimate the effect of each factor and the interaction between them.

The selected design is a 2 level 4 factor design with centre points. The regression model for a factorial design is given in Equation 2.18.

$$y = \beta_0 + \beta_1 X_1 + \beta_2 X_2 + \cdots + \beta_k X_k + \beta_{11} X_1^2 + \beta_{22} X_2^2 + \cdots + \beta_{kk} X_k^2 \qquad (2.12)$$
$$+ \beta_{12} X_1 X_2 + \cdots + \beta_{k-1,k} X_{k-1} X_k + \varepsilon$$

The centre points of this design are shown in Figure 2-16 and are situated between the two cubes.
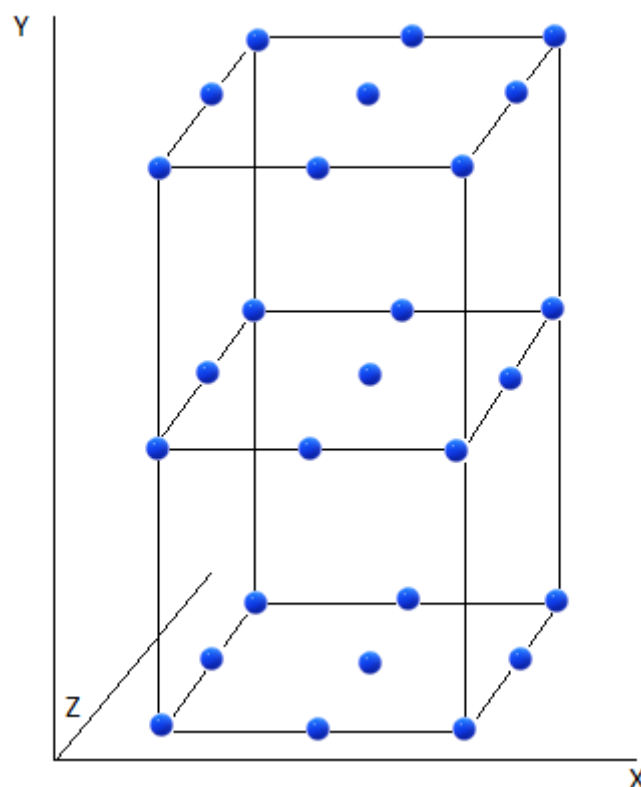
Figure 2-16: Full factorial design [57]*.*

2.9.3.   Analysis of variance

Analysis of variance (ANOVA) is a way of testing a statistical hypothesis when analysing experimental data.   A result is statistically significant if it is considered unlikely to have happened by chance, assuming the null hypothesis is true. A result is statistically significant when a probability (p-value) is less than a specified significance level and it justifies the rejection of the null hypothesis.

In this study, the null hypothesis for each experiment is that all groups are random samples from the same population.

2.10.   ANALYTICAL TECHNIQUES

2.10.1.   X-RAY DIFFRACTOMOTRY

X-ray diffractometry can be used to analyse pure vanadium nitride and carbide. The cobalt reference peak list and diffraction pattern for vanadium nitride is shown in Table 2-6 and Figure 2-17 and the cobalt reference peak list and diffraction pattern for vanadium carbide is shown in Table 2-7 and Figure 2-18. In the solid solution series, no peak data is available in commercial software, making it impossible to accurately analyse the phase.

Table 2-6: X-Ray diffraction peak list for cubic vanadium nitride (VN).

No.	h	k	l	d [Å]	2θ [°]	I [%]
1	1	1	1	2.47106	42.445	76.8
2	2	0	0	2.14000	49.416	100.0
3	2	2	0	1.51321	72.475	45.9
4	3	1	1	1.29047	87.762	18.4
5	2	2	2	1.23553	92.769	11.5

The lower 2θ peak positions of both vanadium nitride and carbide are close to each other with about 1° difference, making it almost impossible to accurately distinguish between the two. The higher 2θ peak positions are low intensity peaks, resulting in a poor quantitative analysis if both compounds are present within a specimen.
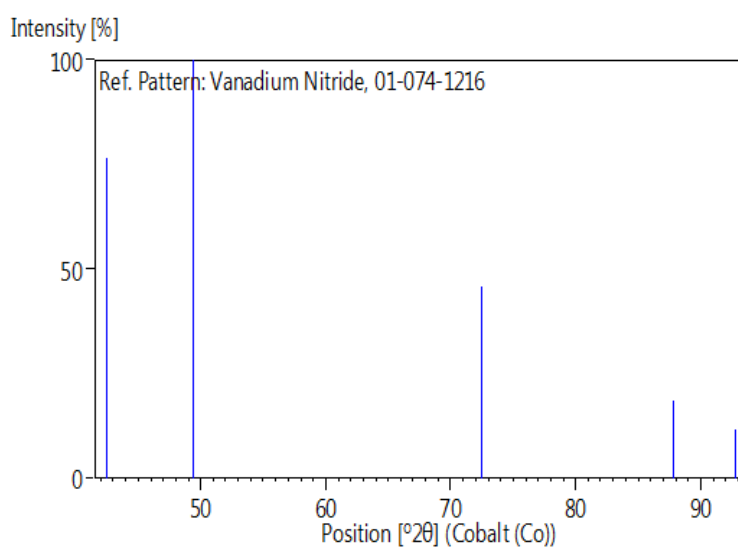
Figure 2-17: X-Ray diffraction reference pattern for cubic vanadium nitride (VN) (Calculated from ICSD using POWD-12++, (1997)).

Table 2-7: X-Ray diffraction peak list for cubic vanadium carbide (VC).

No.	h	k	l	d [Å]	2θ [°]	I [%]
1	1	1	1	2.40466	43.677	99.2
2	2	0	0	2.08250	50.876	100.0
3	2	2	0	1.47255	74.811	44.9
4	3	1	1	1.25579	90.845	21.6
5	2	2	2	1.20233	96.142	11.5
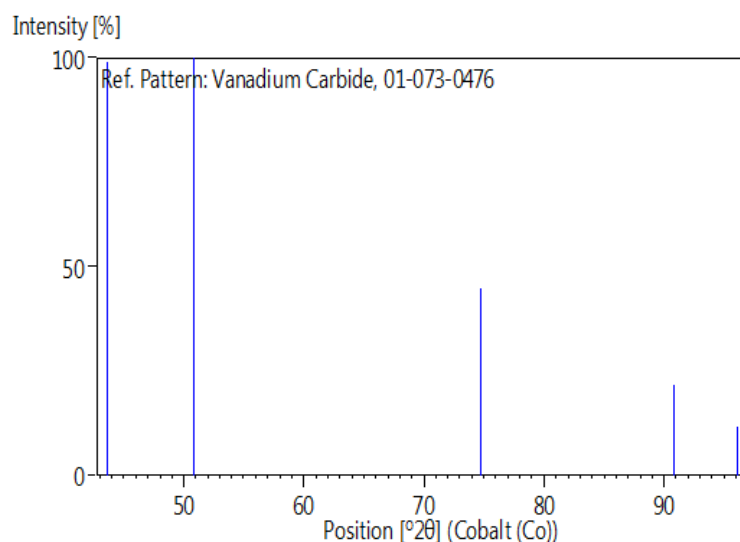
Figure 2-18: X-Ray diffraction reference pattern for cubic vanadium carbide (VC) (Calculated from ICSD using POWD-12++, (1997)).

2.10.2. ENERGY-DISPERSIVE X-RAY SPECTROSCOPY

Energy-dispersive x-ray spectrometry (EDS) can be used to perform an elemental analysis on a specimen, but the accuracy is questionable. The energies of principal K and L x-ray emission lines are listed in Table 2-8.

Table 2-8: Energies of principal K and L X-ray Emission Lines [58]*.*

Element	K	L_1	L_2	L_3
	keV	keV	keV	keV
C	0.2842			
N	0.4099			
O	0.5431	0.0416		
V	5.4650	0.6267	0.5198	0.5121

The L_2 and L_3 peak energies of vanadium at 0.5198 keV and 0.5121 keV and the K peak energy of oxygen at 0.5431 keV causes an overlap in the EDS spectrum, making it impossible to distinguish between vanadium and oxygen.

The nitrogen K peak energy at 0.4099 keV is also relatively close to that of oxygen and vanadium, causing a triple peak in the EDS spectrum. This limits the accuracy of a quantitative analysis using EDS.

2.11. VAMETCO PRODUCTION PROCESS

Bushveld Vametco Alloys sources vanadium from magnetite ore in the upper zone of the Bushveld Igneous Complex. The mineral deposit consists of a vanadium bearing titaniferous magnetite in a norite matrix. Figure 2-19 shows the typical geological layers at Vametco. The opencast mine is situated at the Vametco processing plant near the town of Brits in the North-West Province of South Africa.

The vanadium bearing titaniferous magnetite ore reserves within the lease area of Vametco form part of the Western Bushveld Complex and are estimated to be about 35 million tonnes that are mined using conventional drill, blast, load and haul mining methods. The opencast mine has a strike of 3.5 km and the ore body dips at approximately 20 degrees. Mining is executed in benches of about 10 meters in depth and accomplished with the use of excavators and haul trucks.   In full production, approximately 2.5 million tonnes of material are mined per year, of which approximately 1 million tonnes being titaniferous magnetite with the balance being waste rock.
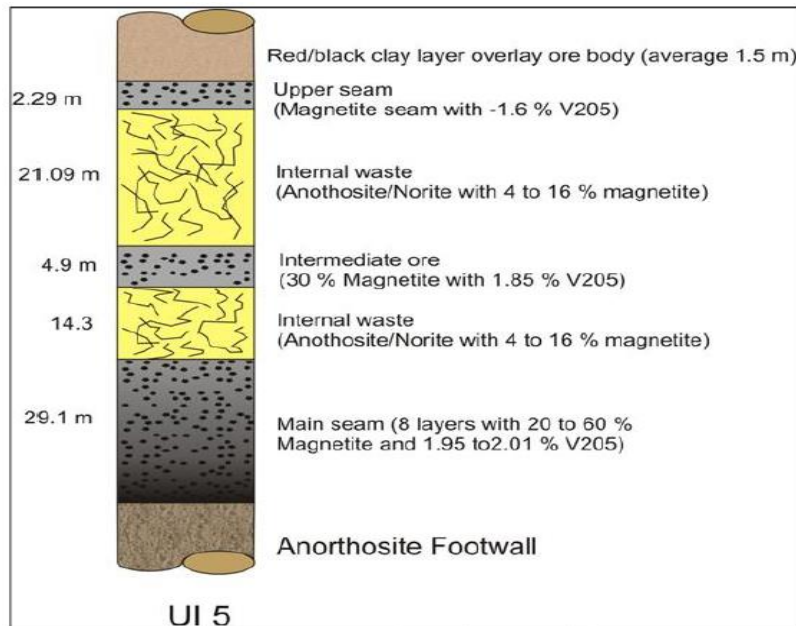
Figure 2-19: Typical geological layers at Bushveld Vametco Alloys [photo supplied by Vametco].

Primary crushers are used to reduce the size of large boulders to a maximum size of 200 mm. The ore is screened by a Grizzly screen to obtain an oversize fraction of +38 mm to -200 mm. The oversize goes to the coarse stockpile and is later fed to the secondary crusher circuit. The undersized material of the Grizzly screen and the undersized material from the secondary crushers are transported to the screen house.

The secondary crushers reduce the size of the +38 mm to -200 mm ore, fed from the coarse stockpile to a maximum size of +38 mm. The secondary crusher product is fed to the screen house where it is combined with Grizzly screen undersize. The -10 mm ore is screened out by the polydeck screens and the +10 mm to – 38 mm size is returned to the tertiary crushers. After the tertiary crusher, crushed ore is again fed to the polydeck screens in the screen house. The undersize of the polydeck screens is fed directly to the ball mill feed silos or to the -10 mm stockpile if the ball mill feed silos are full.

The -10mm ore is reduced in size to 90% -150 um in wet ball milling process. The finely ground ore is then fed to magnetic separators where the magnetic portion is separated from the gangue material. The concentrate from the first magnetic separators are fed to the secondary mill where it is further milled and again passed through a magnetic separator. The magnetite concentrate is then fed to the roasting section. Non-magnetic gangue material is deposited in slimes dams where the water is recovered and recycled in the concentrate plant.

Weighed amounts of concentrate, sodium sulphate and sodium carbonate are mixed and oxidised in a rotary kiln that is fired with pulverised coal. The mixture is roasted in oxidizing conditions at approximately 1100 °C.

The kiln off gas is scrubbed in a wet venturi scrubber and is released in the atmosphere. The solids in the scrubber liquor are settled in a thickener, dewatered over a belt filter, and returned to the kiln feed. The thickener overflow is returned to the venturi scrubbing circuit.

The solids containing sodium vanadate are wet milled, leached and washed in a counter current process over large belt filters. The tailings are disposed of on the tailings dump and aluminium sulphate and a flocculent are used to remove silica from the pregnant solution. The pregnant solution contains sodium sulphate and sodium vanadate and is pH adjusted with sulphuric acid before being pumped to the precipitation section.
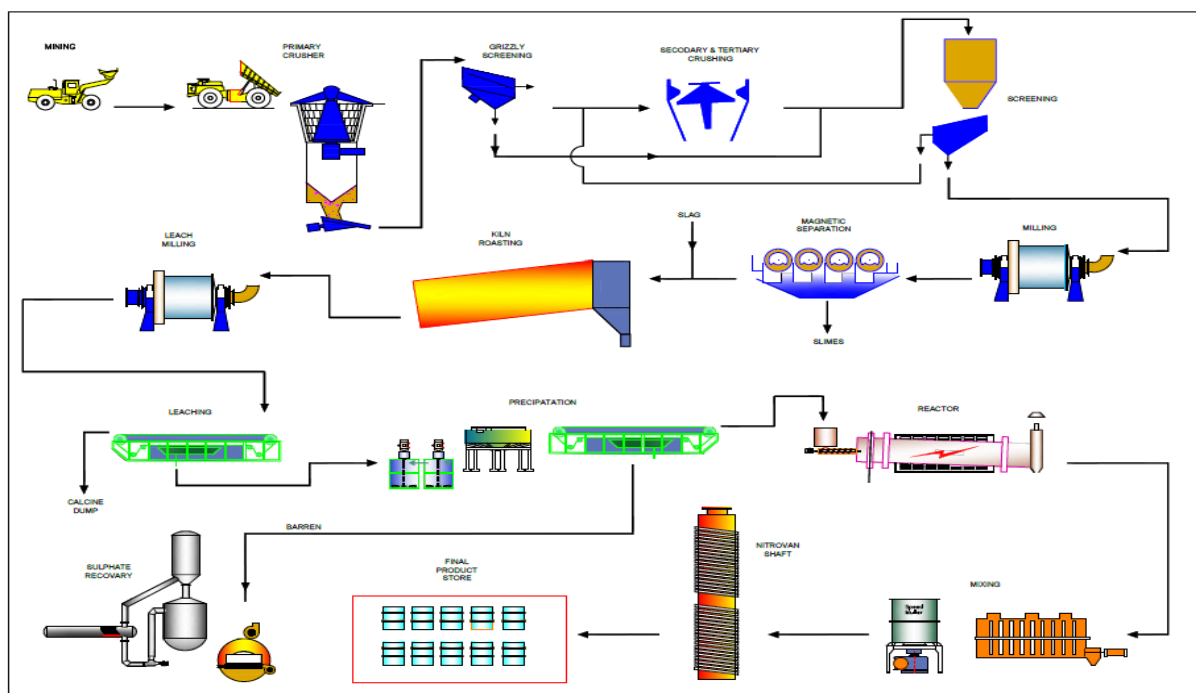
Figure 2-20: Vametco production overview [figure supplied by Vametco].

The vanadium in the pregnant solution is precipitated with ammonium sulphate to form ammonium metavanadate (NH_4VO_3) which is also known by the acronym AMV. The ammonium metavanadate is then dried in a rotary calciner at a temperature below the decomposition temperature of the AMV and fed to the converter section of the plant. The barren solution is pumped to the sulphate recovery plant (SRP).

Ammonium metavanadate is decomposed in a horizontal kiln called the "reactor". The decomposition occurs in a reducing atmosphere to produce vanadium trioxide (V_2O_3), referred to as "Modified Vanadium Oxide" (MVO). After the MVO has cooled sufficiently, it is drummed and sealed to prevent re-oxidation. The product is black in colour with some brown variations. MVO is the primary feed stock in the production of Nitrovan.

Vanadium carbonitride (Nitrovan) is produced in an induction heated shaft furnace. The estimated operating temperature is 1600 °C, but the true operating temperature is unknown. Raw materials used for Nitrovan are MVO (V_2O_3) and carbon. Recycled material from the off-gas system is often used in the mixture. This recycled material is referred to as "proven air" and the exact composition of this stream is not known.

The raw materials are precisely proportioned in accordance with the required nitrogen content, and are mixed, firstly in a horizontal paddle mixer blender and thereafter wet mixed in a muller. Two binders are added to the mixture. A starch-based product providing adequate wet and dry green strength, and a PVA base, which has been found to successfully prevent breakage in the furnace. The wet mixture is briquetted (pillow shaped rectangular ca. 30 mm x 40 mm with a ca. 20 mm thickness), and the briquettes are dried and cooled on a moving perforated plate dryer.

The raw briquettes are gravity fed through a vertical shaft induction furnace, consisting of a graphite pipe of 6m in length, ID 300 mm and wall thickness 100 mm, a set of induction coils, insulation, and water cooling. The coils are located concentrically about the graphite shaft. Electrical currents induced in the graphite generates heat, which is conducted to the shaft inner wall where heat is transferred to the slowly descending mass of briquettes. High purity nitrogen gas is introduced at the furnace discharge to firstly prevent air ingress and secondly to provide the nitrogen for reaction. An excess is called for to effectively sweep the carbon monoxide product gas to the feed hood where it is burnt to carbon dioxide. The nitrogen also acts as a coolant for the hot product.

Temperature control is crucial, as increased temperatures could result in the briquette mass to fuse, resulting in plant shut down, whereas decreased temperatures could result in an incomplete reaction and out of grade product. The reacted product passes from the furnace section through a water

jacketed cooling section before entering the discharge box. Apart from the chemical reaction taking place in the briquette, the Nitrovan undergoes a physical change in that the amorphous form of the raw briquette shrinks to a dense metallic sponge of about 40 % of the original volume. High density is desirable for optimum recovery in the steel process. The hotter the furnace, or higher the retention time, the more continuous the metallic phase becomes, with clear benefits to the user, but with an ever-increasing risk of the shaft furnace plugging.
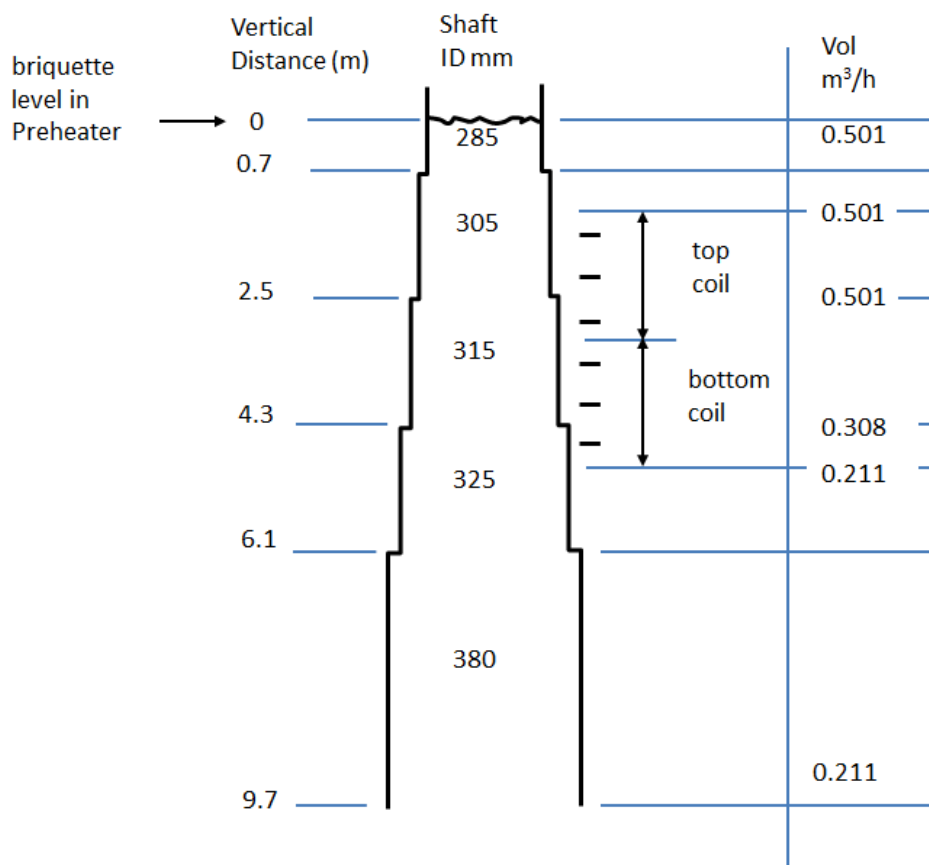
Figure 2-21: Schematic drawing of the tube furnace at Vametco [source: F. Berg-Mathiassen].

Operation output is defined by a campaign which consists of approximately a minimum of 60 drums of Nitrovan briquettes. A drum has a precise weight of 200 kg. After the completion of a campaign, the furnace is emptied to prevent the formation of plugs. A campaign lasts approximately 2 days. The liner is replaced after the furnace is drained and has cooled.

Final product drums are sent to the final products store where specific blends are made based on customer requirements. The product is packaged in paper bags and shipped in wooden boxes.

Bushveld Vametco Alloys produces two grades of Nitrovan, i.e. Nitrovan 12 vanadium and Nitrovan 16 vanadium. The different grades relate to the nitrogen content of the product. The nitrogen content

is governed by the amount of carbon added to the raw mixture. The typical analyses of the two products are shown in Table 2-9. Nitrovan has a briquette density of 3.0 – 3.5g/cm^3

2.10 TEST METHODS

Vametco makes use of a nitrogen and carbon combustion method to determine the nitrogen and oxygen content of the reacted products. The vanadium content is determined with a wet chemical analysis and other elements, such as iron and sodium, and are analysed using XRF. The oxygen content is calculated from the difference.

Table 2-9: Specification and typical analysis of Nitrovan 12 vanadium and Nitrovan 16 vanadium.

Element	Nitrovan 12 vanadium		Nitrovan 16 vanadium	
	Specification	Typical Analysis	Specification	Typical Analysis
V	76-81%	78.00%	76-81%	77.00%
N	10-14%	12.00%	14-19%	16.00%
C	10% max	7.00%	6% max	3.50%
O	1.5% max	0.75%	1.5% max	1.25%
Al		0.15%		0.15%
Si		0.35%		0.35%
Mn		0.00%		0.00%
Fe		0.40%		0.40%
S		0.15%		0.15%
Cr		0.40%		0.40%
Cu		0.00%		0.00%
P		0.03%		0.03%
Ca		0.10%		0.10%

Figure 2-22:Raw briquettes.

Figure 2-23: Nitrovan product. Source: http://www.nitrovan.co.za

CHAPTER 3:
POST-MORTEM ANALYSIS

3.   POST-MORTEM ANALYSIS

Two problems occur in the shaft furnace during operation and are most likely related. The first problem relates to high erosion of the graphite furnace liner and secondly the bridging in the furnace which may lead to plug formation. When a plug forms before the end of a campaign, the furnace needs to cool down before liner replacement can be conducted. The cooling rate of the furnace is dependent on the size of the plug formed and can take anything between 30 hours and 7 days for the furnace to cool down when plugged.

Figure 3-1: Nitrovan reactor plug at Vametco [source: F. Berg-Mathiassen (Vametco). No scale available. Liner has an original inside diameter of 315 mm].

Figure 3-2: Nitrovan reactor plug at Vametco [source: F. Berg-Mathiassen (Vametco). No scale available. Liner has an original inside diameter of 315 mm].

3.1. GRAPHITE FURNACE LINER

The graphite furnace liner experiences high erosion. The erosion can be contributed to both physical and chemical wear.

The liner experiences abrasive wear due to the movement of the briquettes down the furnace shaft. The physical wear occurs because of the progressive graphite loss from the surface of the solid graphite liner due to the relative movement of materials past the liner. The hardness and sharpness of the conveyed material contact angle and contact pressure affects the extent of abrasive wear. This local progressive diameter increase, causes a bowl effect which can be seen in Figure 3-3. A change in liner shape will influence the briquette movement down the shaft and might cause bridging inside the furnace. A contributor to this bowl effect might be due to briquette expansion which is described in section 6.4 of this document.

Figure 3-3: Bowl effect of graphite furnace liner [source: F. Berg-Mathiassen (Vametco). No scale available. Liner has an original inside diameter of 315 mm].

The chemical erosion of the furnace liner can be due to the attack of graphite with hydrogen and oxygen ions. Residual ammonia in the feed will undergo cracking in the shaft furnace which will yield free hydrogen and nitrogen. The hydrogen might react with the graphite to form hydrocarbons. Although the nitrogen gas used for the reaction is relatively pure, minor amounts of oxygen enter the furnace with the nitrogen gas. Both hydrogen and oxygen gas escapes the furnace between the liner joints to form blow holes in the joint. Figure 3-4 shows an example of a blow hole in the graphite furnace liner joint. This liner is heavily oxidised due to the removal of the liner before the furnace was completely cooled.
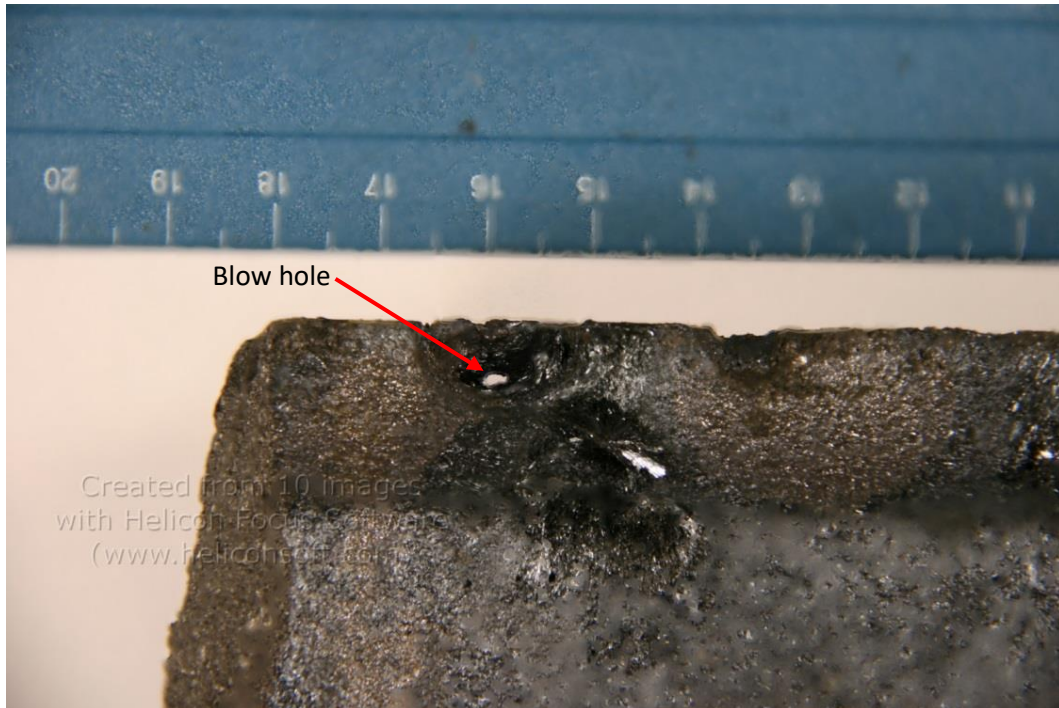
Figure 3-4: Graphite furnace liner with a blow hole in the joint.

An XRD analysis was performed on a graphite furnace liner supplied by Vametco. The sampled sections are shown in Figure 3-5. The exact history of this liner is unknown. In Table 3-1, varies vanadium oxides, which includes oxides of high oxidation states, were detected on the graphite liner. The high oxidation states of vanadium oxide are mainly due to the oxidation of the vanadium during the dismantling of the furnace at elevated temperatures.

It is well known that alkali metal catalyses the Boudouard reaction. The presence of alkalis in the shaft furnace will contribute to the chemical erosion and degradation of the graphite liner. NaV_6O_{15} was detected on the sampled liner indicating the presence of alkalis. The alkalis enter the furnace in the feed material.
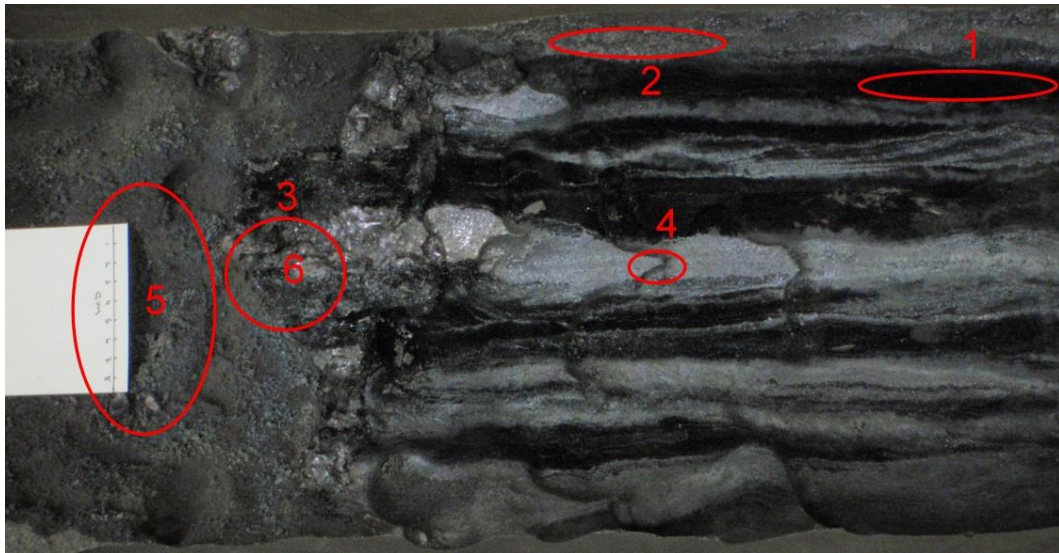
Figure 3-5: Graphite furnace liner.

High oxidation states of vanadium were detected on the graphite liner. This is mainly due to the oxidation of the vanadium compound during the dismantling of the furnace at elevated temperatures.

Table 3-1: Qualitative XRD results of incretions of a graphite furnace liner.

	C	NaV_6O_{15}	V_2O_5	VO_2	V_6O_{13}	VC	V_2CN	V_6O_5	V_2O_3	VN	V_8C_7
Site 1	X	X									
Site 2		X	X	X	X						
Site 3				X		X	X	X	X	X	
Site 4	X		X					X			
Site 5	X			X					X		
Site 6	X	X				X		X	X	X	X

A second liner was supplied by Vametco with seemingly metallic accretions as shown in Figure 3-6. The liner was removed as part of a normal furnace relining. The liner was sectioned through the accretions and it was found that briquettes were fused onto this liner under the metallic lustre layer. This is shown in Figure 3-7 and Figure 3-8.
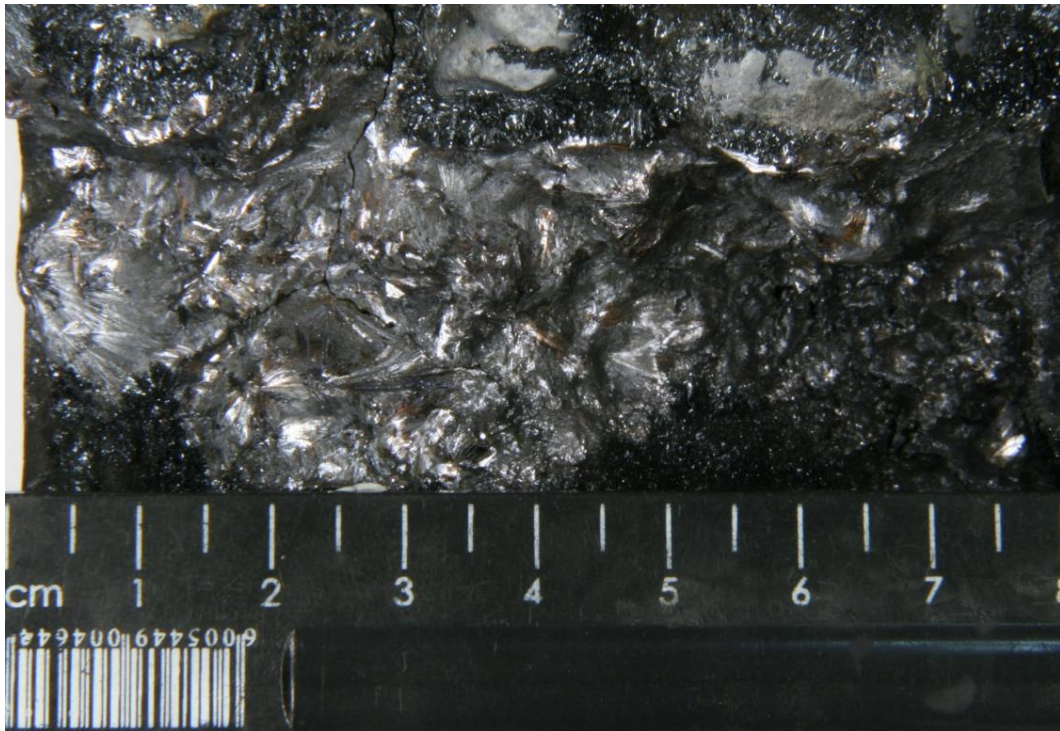
Figure 3-6: Furnace liner with metallic accretions.

Figure 3-7: Briquettes fused to furnace liner.
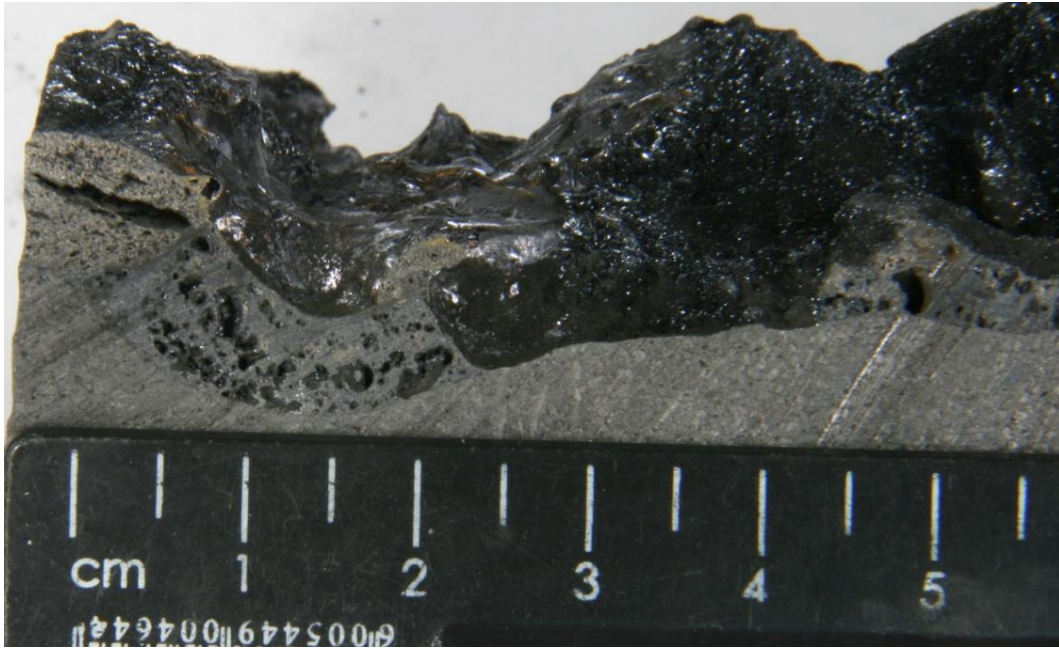
Figure 3-8: Fused pellet in a graphite liner.

3.2. BRIQUETTE-LINER INTERACTION

A polished section was prepared of the briquette and liner in Figure 3-8. From the micrograph in Figure 3-9, it can be seen that the briquette is fused onto the graphite and that different phases are present within the specimen.
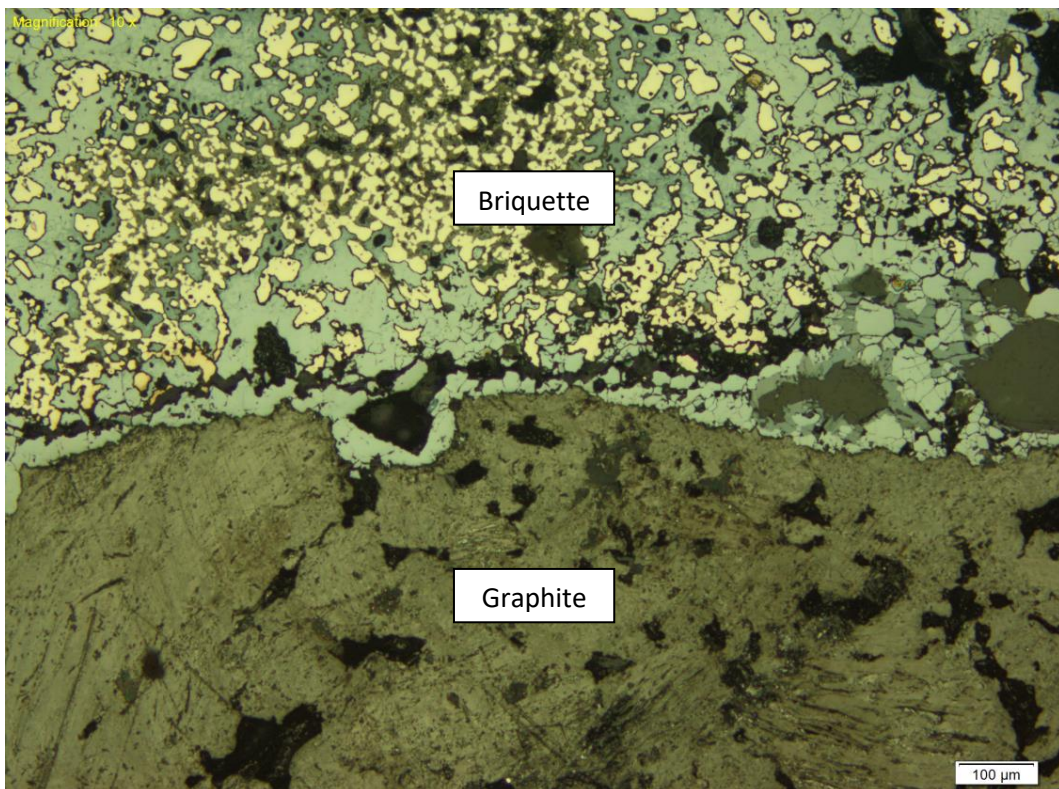
Figure 3-9: Micrograph of a Nitrovan briquette fused to a graphite liner (10 x magnifications).
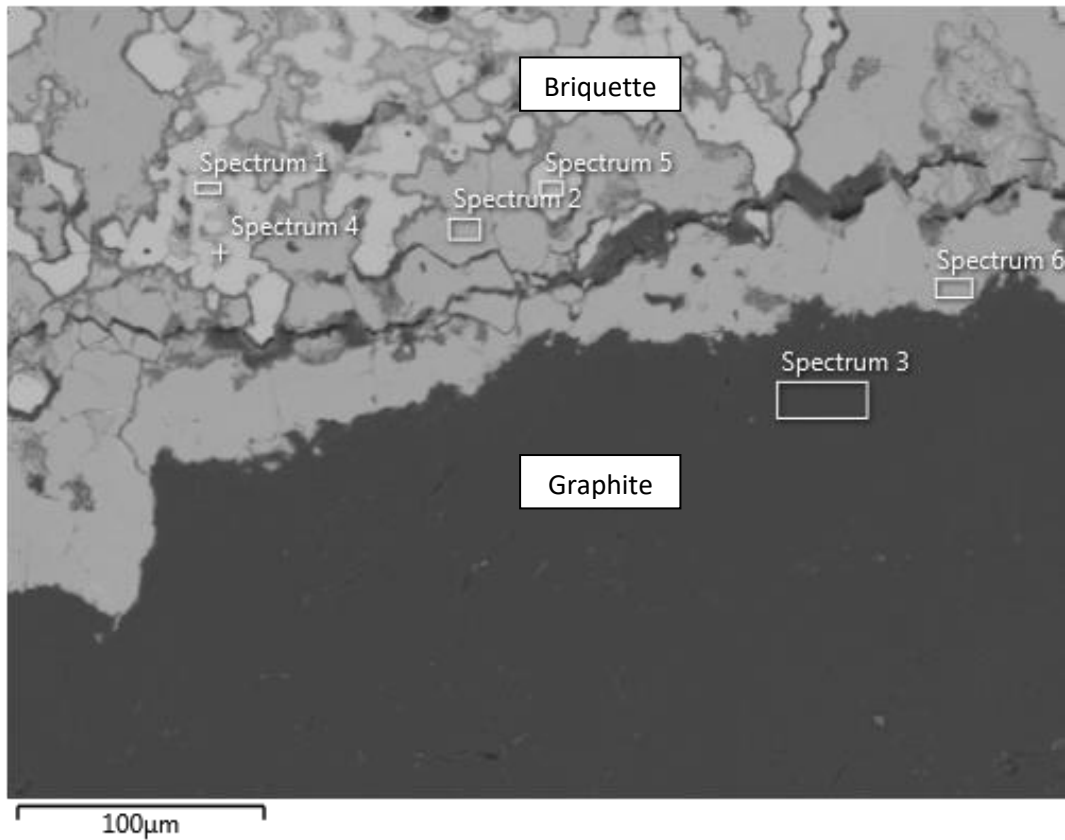
Figure 3-10: Backscatter image of a briquette fused to a graphite liner.

An EDS analysis was performed on the site to determine the chemical composition of the different phase on the interface. Refer to Table 3-2: nitrogen was not detected in any of the phases. This correspond to literature in that if vanadium carbonitride is in contact with carbon (graphite) at high temperatures, the carbide will be more stable. The oxygen content in the analysis is inaccurate due to the limitation of EDS as discussed in section 2.10.2.

Table 3-2: EDS results for backscatter image in Figure 3-10.

	C	O	V	Total	Concluded phase
Spectrum 1	45.42		54.58	100.00	VC
Spectrum 2		45.74	52.97	98.71	VO
Spectrum 3	99.85		0.15	100.00	Graphite
Spectrum 4	8.01	40.77	51.22	100.00	VO
Spectrum 5	45.84		54.16	100.00	VC
Spectrum 6	4.24	43.93	50.61	98.78	

3.3.   BRIQUETTE-BRIQUETTE INETRACTION

The reacted briquettes are often fused together when exiting the shaft furnace (Figure 3-11). This phenomenon is a regular occurrence during the day to day production of Nitrovan.

It was observed that fused briquettes are in general more frequently observed than single briquettes. Fused briquettes are broken apart on a grid below the furnace by means of force.

Figure 3-11: Fused Nitrovan briquettes.

A micrograph of the interface between two briquettes is shown in Figure 3-12. No apparent change in density, nor the fusion interface could be observed between the two briquettes.

From the backscatter image in Figure 3-13, no variable phases were observed on the fusion interface. The phases across the fusion interfaces are homogeneous in backscatter densities.

A briquette was analysed using a SEM with EDS. The backscatter image in Figure 3-14 show a different phase on the grain boundaries. The phases were analysed, and the results are tabulated in Table 3-3: EDS results for backscatter image in Figure 3-14.

Iron, carbon and phosphorous were detected on the grain boundaries of the vanadium carbonitride grains. On the triple point of the grain boundaries, a slag phase was detected. This phenomenon can be seen throughout the industry specimens.
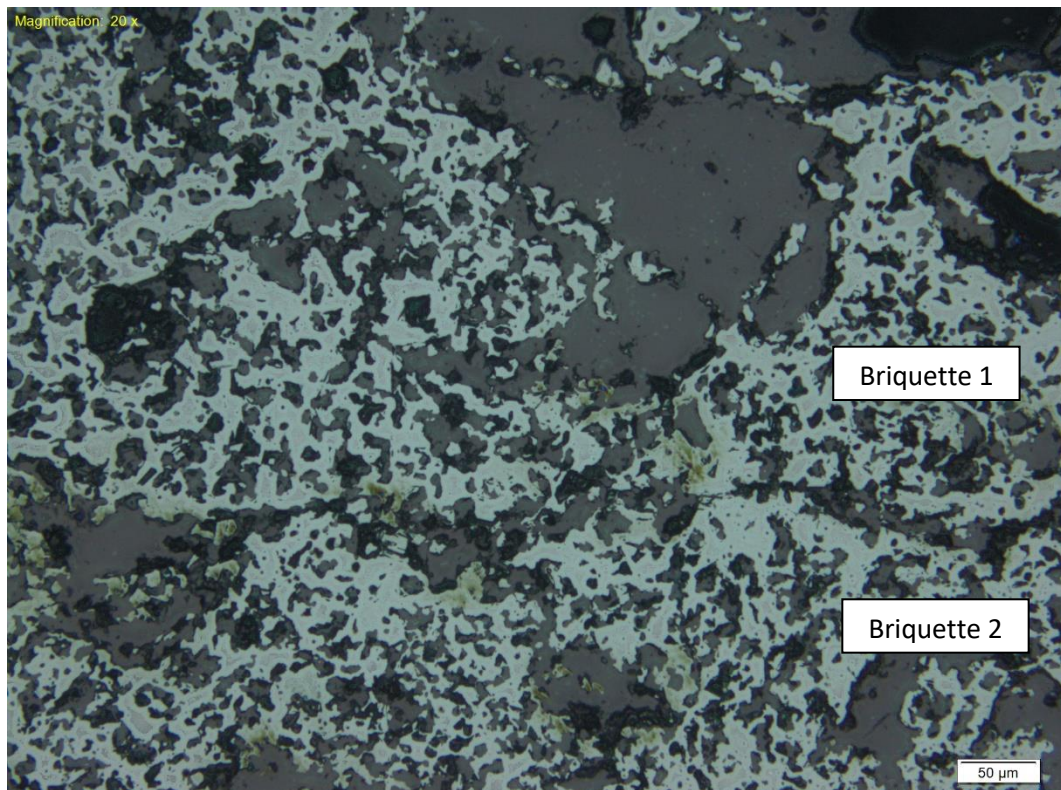
Figure 3-12: Micrograph of two fused Nitrovan briquettes.
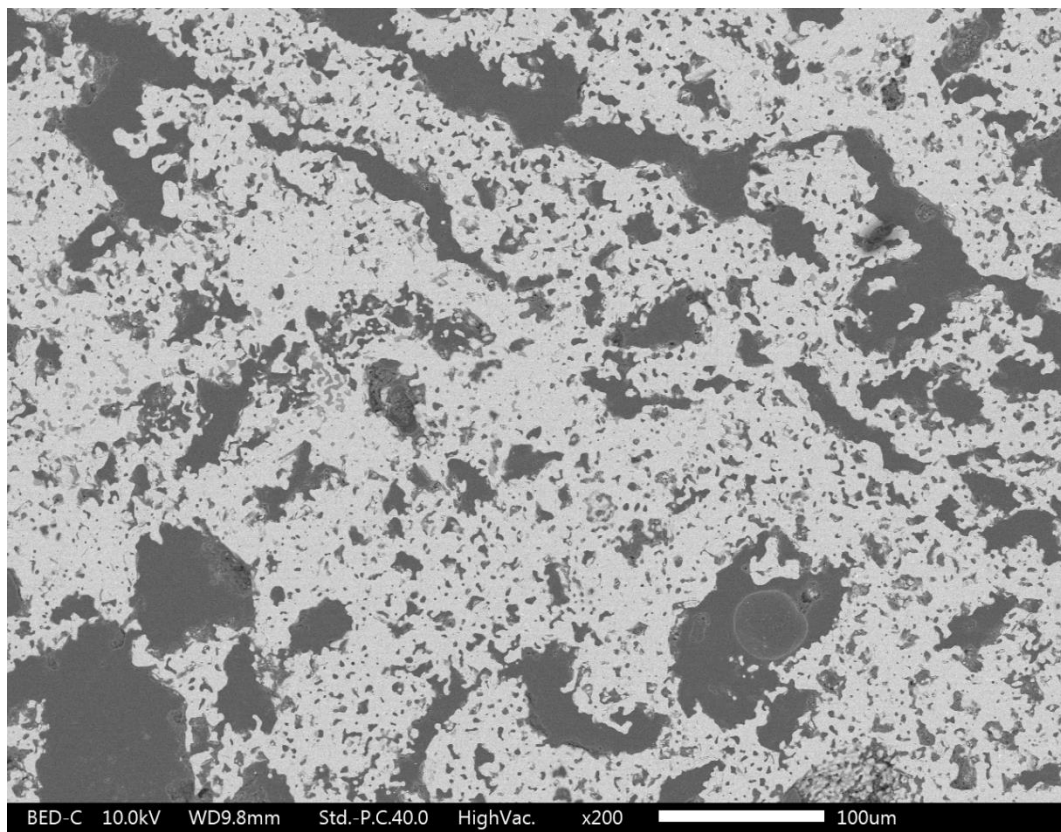
Figure 3-13: Backscatter image of fused Nitrovan briquettes.
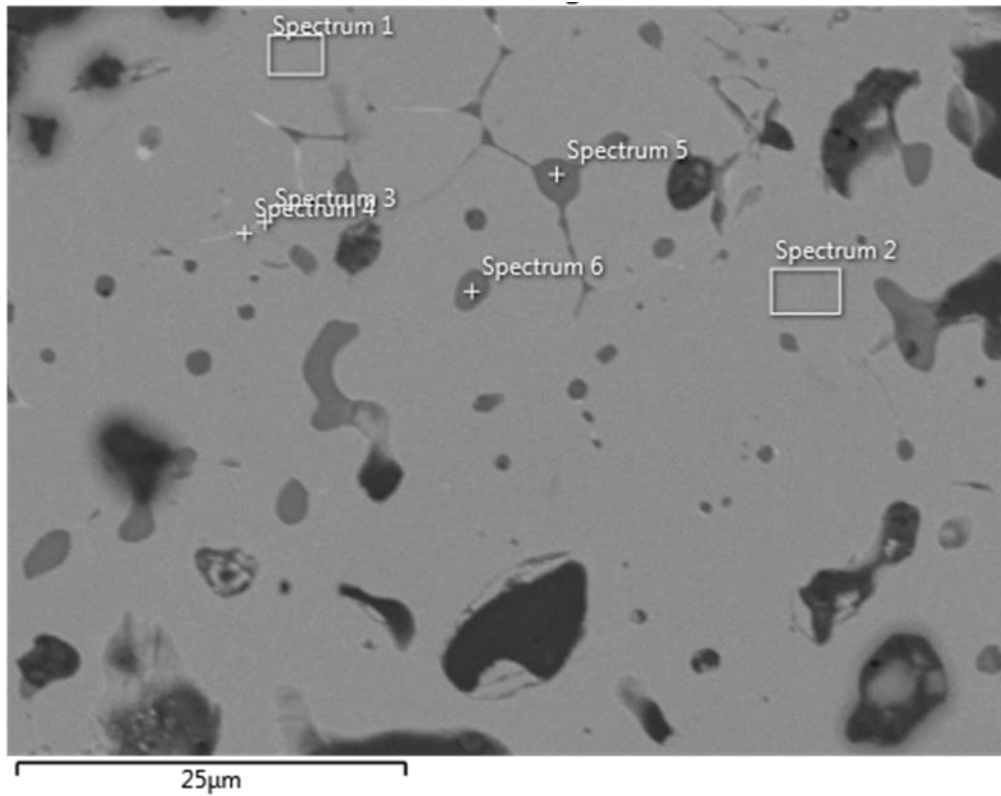
Figure 3-14: Backscatter image of Vametco Nitrovan.

Table 3-3: EDS results for backscatter image in Figure 3-14.

	Element (Atomic wt%)										
	C	**N**	**O**	**Na**	**Al**	**Si**	**Ca**	**P**	**V**	**Fe**	**Total**
Spectrum 1		33.21							66.79		100
Spectrum 2		35.00							65.00		100
Spectrum 3	60.28	15.09						2.31	15.48	6.83	100
Spectrum 4	58.26	9.02	6.67			0.78		2.74	12.27	10.27	100
Spectrum 5	47.97		34.06	0.7	8.45	4.68	4.15				100
Spectrum 6	46.13		35.61		8.8	4.75	4.73				100

CHAPTER 4:

MATERIALS

4. MATERIALS

This section describes all the raw materials used in the experiments including raw material properties.

4.1. VAMETCO MVO

A sample was supplied by Vametco to conduct experiments. The sample underwent a chemical and phase analysis.

4.1.1. CHEMICAL ANALYSIS ON VAMETCO MVO

A chemical analysis was done by the Vametco analytical laboratory on the local MVO sample and the results are tabled below.

The reported oxygen was not determined analytically but calculated from the balance.

Table 4-1: Chemical analysis on Vametco MVO.

	weight %
V	64.29
O	34.325
SiO_2	0.23
Fe	0.37
Al_2O_3	0.17
Cr	0.09
P	0.011
Mn	0.003
Cu	0.001
CaO	0.13
Na_2O	0.38

4.1.2. PHASE ANALYSIS ON VAMETCO MVO

A phase analysis was performed on the Vametco MVO sample using XRD. The diffraction pattern from Figure 4-1 shows two distinct phases with sharp peaks. The phase distribution with quantitative results is listed inTable 4-2.

The MVO provided by Vametco is a mixture of two of the vanadium oxidation states namely V_2O_3 and the more oxidised V_3O_5.

An oxidation test performed at 300 °C resulted in a mass gain of 14.91 %, suggesting that the Vametco MVO is of a higher oxidation state than pure V_2O_3 with a calculated mass gain of 17.59 % if fully oxidised to V_2O_5.
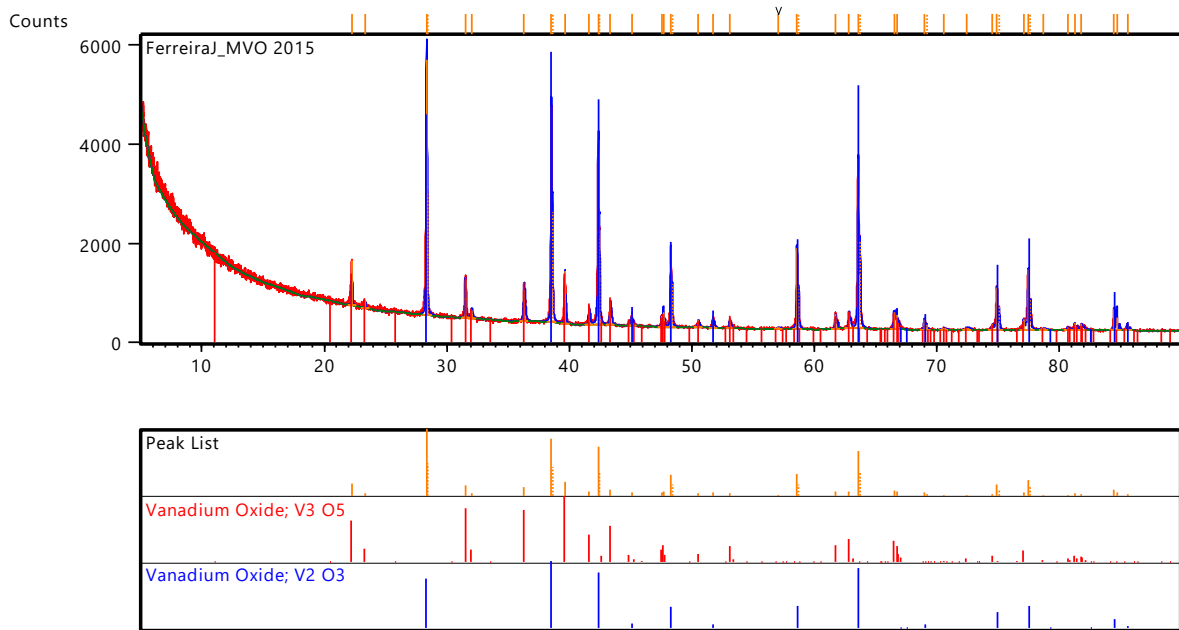
Figure 4-1: Vametco MVO diffraction pattern.

Table 4-2: Vametco MVO phase analysis.

	Weight %	3 σ error
V_2O_3	59.48	0.6
V_3O_5	40.52	0.6

4.2. PURE MVO

A MVO sample was sourced from the Stratcor facility in Hot Springs, USA. The materials and safety data sheet is attached in Appendix A.

A chemical and phase analysis was performed on this material.

4.2.1. CHEMICAL ANALYSIS ON VAMETCO MVO

A chemical analysis was done by the Vametco analytical laboratory on the local MVO sample and the results are tabled below.

The reported oxygen was not determined analytically but calculated from the balance.

Table 4-3: Chemical analysis on Vametco MVO.

	weight %
V	67.63
O	32.286
SiO_2	0.01
Fe	0.01
Al_2O_3	0.01
Cr	0.01
P	0.003
Mn	0.001
Cu	0.0001
CaO	0.01
Na_2O	0.03

4.2.2.   PHASE ANALYSIS ON MVO

A phase analysis was performed on the Stratcor MVO sample using XRD. The diffraction pattern from Figure 4-2 shows only one distinct phase with sharp peaks.

The Stratcor MVO was used with the assumption that is 100 % V_2O_3.

A standard oxidation mass gain test performed at 300 °C resulted in a mass gain of 17.43 % suggesting that the Stratcor MVO consists exclusively of V_2O_3 with a theoretical mass gain of 17.59 % if fully oxidised to V_2O_5.
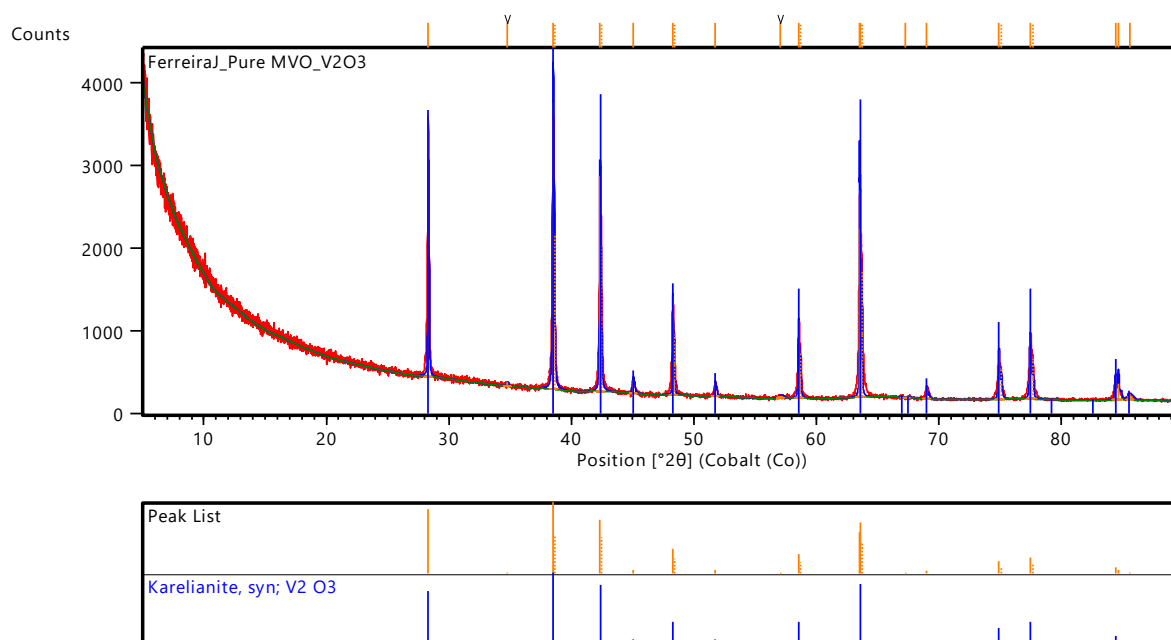
Figure 4-2: Stratcor MVO diffraction pattern.

4.3.   PROVEN AIR

Proven air refers to dust that is collected from the off-gas system of the MVO reactor at Vametco. The system was designed and produced by a company called Proven Air and Vametco uses the name of the system to refer to the off-gas dust product stream. This product is used in the Vametco briquettes when Nitrovan is produced.

A chemical and phase analysis was performed on the proven air that was provided by Vametco for experimental use.

4.3.1.   CHEMICAL ANALYSIS ON PROVEN AIR

A chemical analysis was performed by the Vametco analytical laboratory on the proven air sample and the results are tabled below.

The reported oxygen was not determined analytically but calculated from the balance.

Table 4-4: Chemical analysis on proven air.

	Weight %
V	59.41
O	37.902
SiO_2	0.06
CaO	0.11
Na_2O	0.52
S	1.389
Fe	0.24
P	0.006
Al_2O_3	0.17
Cr	0.13
C	0.063

4.3.2.   PHASE ANALYSIS ON PROVEN AIR

A phase analysis was performed on the proven air sample using XRD. The diffraction pattern from Figure 4-3 shows two distinct phases with sharp peaks. The phase distribution with quantitative results are listed in Table 4-5.
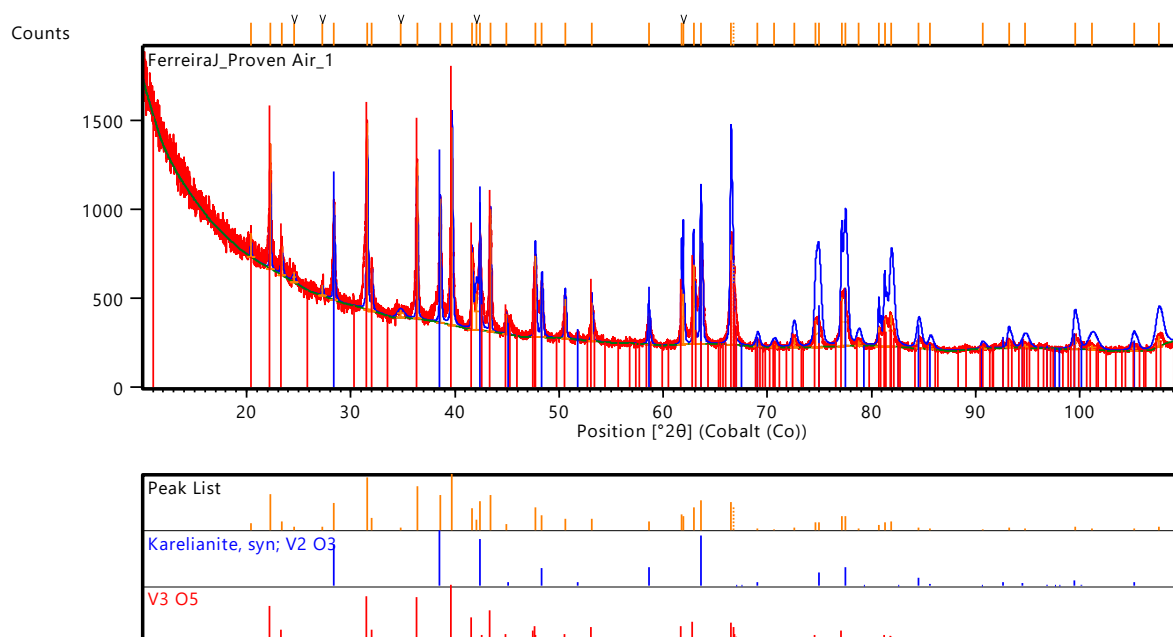
Figure 4-3: Proven air diffraction pattern.

Table 4-5: Proven air phase analysis.

	Weight %	3 σ error
V_2O_3	19.61	0.6
V_3O_5	80.39	0.6

4.4.   SPILLAGE

Spillage is recycled material from the Nitrovan reactor. Unreacted and rejected material are ground and reintroduced to the raw materials mixture.

4.4.1.   CHEMICAL ANALYSIS ON SPILLAGE

A chemical analysis was performed by the Vametco analytical laboratory on the spillage sample and the results are tabled below.

The reported oxygen was not determined analytically but calculated from the balance.

Table 4-6: Chemical analysis on spillage.

	weight %
V	51.86
O	11.3
N	9.062
C	26.553
SiO_2	0.31
Fe	0.28
Al_2O_3	0.11
Cr	0.1
P	0.013
Mn	0.001
Cu	0.001
CaO	0.12
Na_2O	0.29

4.4.2.   PHASE ANALYSIS ON SPILLAGE

A phase analysis was performed on the spillage sample using XRD. The diffraction pattern is shown in Figure 4-5. Some of the peaks are broad and overlap in certain 2Θ positions. The phase distribution with quantitative results are listed in Table 4-6. The accuracy of the quotative analysis is questionable due to the presence of poorly crystalline carbon.
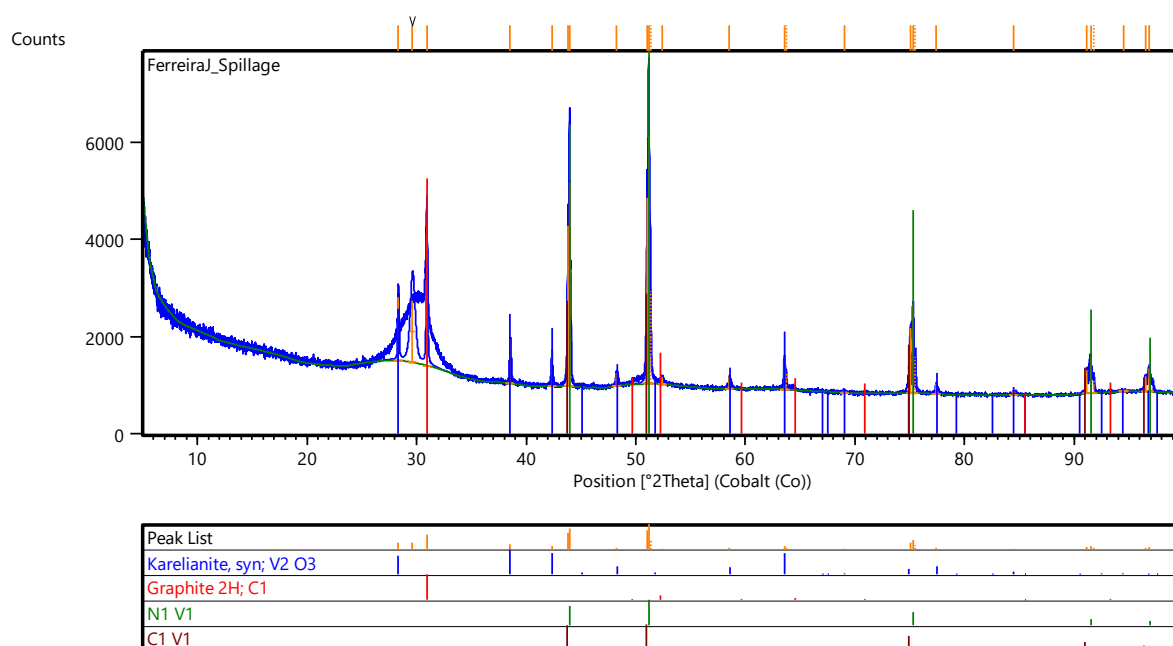
Figure 4-4: Spillage diffraction pattern.

Table 4-7: Spillage phase analysis.

	weight%	3 σ error
Graphite	35	4.2
V_2O_3	13.26	1.29
VC	27.73	2.97
VN	24.03	2.82

4.5.   CARBON

The carbon used in the experiments was supplied by Vametco. A full carbon analysis is attached as Appendix B.

A thermogravimetric analysis (TGA) in CO_2 was performed on the Vametco carbon at a heating rate of 10 °C/min and it was found that significant weight loss occurs at temperatures above 600 °C suggesting the reactivity of the carbon becomes favourable above 600 °C.
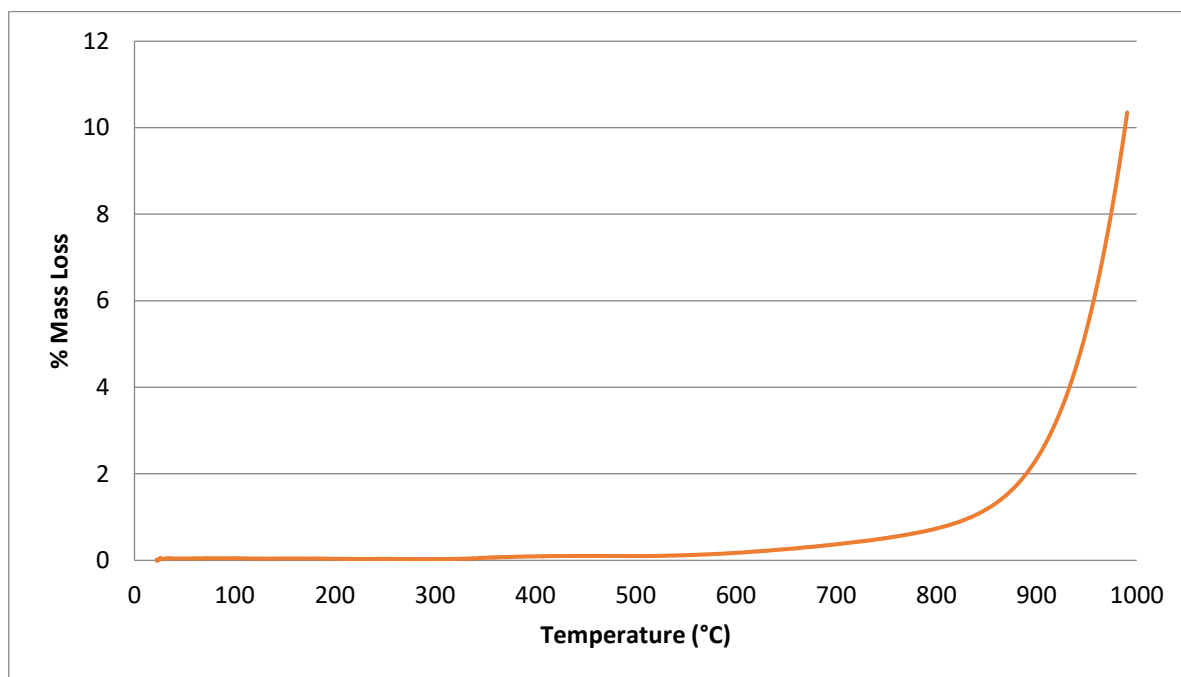
Figure 4-5: TGA of Vametco Carbon.

4.6.   SLUDGE

Sludge was collected from a thickener Vametco. The sludge was dried, and a chemical and phase analysis was performed on the sample. The dried sludge was used in experiments as an impurity addition.

4.6.1.   CHEMICAL ANALYSIS ON SLUDGE

A chemical analysis was performed on the dried sludge sample and is listed in Table 4-8.

Table 4-8: Chemical analysis on sludge.

	weight %
V	1.10
SiO_2	6.06
CaO	1.47
Fe	28.9
Ti	8.14
Al_2O_3	8.9
Cr	0.11
Mg	0.82
Mn	0.45

4.6.2. PHASE ANALYSIS ON SLUDGE
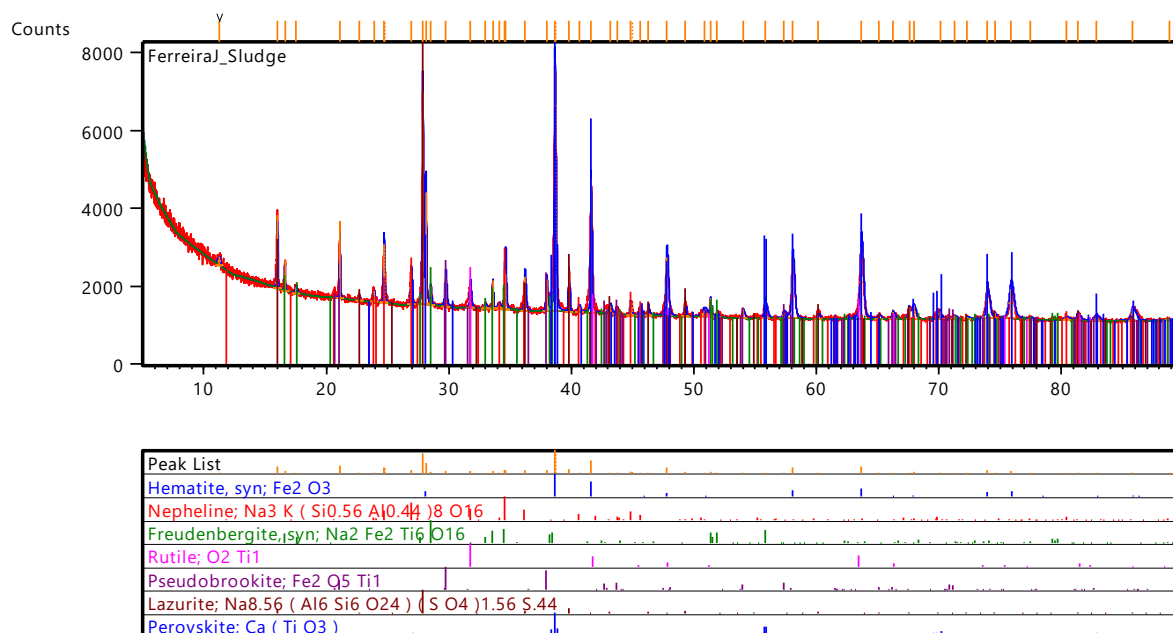
Figure 4-6: Sludge diffraction pattern.

Table 4-9: Sludge phase analysis.

	weight%
Fe_2O_3	45.23
$Na_3KAl_4Si_4O_{16}$	16.73
$Na_2Fe_2Ti_6O_{16}$	5.87
TiO_2	0.68
Fe_2TiO_5	6.03
$(Na,Ca)_8[(S,Cl,SO_4,OH)_2|(Al_6Si_6O_{24})]$	24.12
$CaTiO_3$	1.35

4.7.   BARREN SOLUTION

Barren solution was provided by Vametco and was used in the experiments as an impurity addition.

4.7.1.   CHEMICAL ANALYSIS ON BARREN

A chemical analysis was performed on the barren sample in the results as listed in Table 4-10. The residual of the analysis is H_2O.

Table 4-10: Chemical analysis on barren.

	weight %
V	0.30
SiO_2	0
CaO	0.26
Na_2O	16.42
S	17.17
Fe	0.005
Al_2O_3	0.003
Cr	0
K	0.46
Mg	0.23

4.8.   BINDERS

4.8.1.   PVA

Polyvinyl acetate is used by Vametco as a binder. PVA has a typical boiling point of 112 °C and does not take part in the reaction in the Nitrovan reactor.

4.8.2.   STARCH

Starch is used as a green strength binder. It does not take part in any reaction in the Nitrovan reaction as it decomposes at temperature below 500 °C. The starch MSDS is attached as Appendix D.

CHAPTER 5:

METHODS

5.   METHODS

The goal of the experiments is to understand the chemical reactions and dimensional changes of the feed material during the production of Nitrovan. Four main experiments were conducted to evaluate responses. This section focuses on the detailed description of how each of the experiments was executed and the precursors to the experiments.

5.1.   RAW MATERIAL DENSITY

The densities and porosities of both the laboratory and Vametco briquettes were calculated.

The samples were weighed, and the mass noted as dry mass. The samples were then impregnated under a vacuum with a fluid of known density (water = 1.0 g/cm3 and paraffin = 0.740g/cm3). The impregnated samples were weighed and noted as wet mass.

With these the void volume was calculated:

$$Void\ volume = \frac{M_{impregnated} - M_{dry}}{Density\ of\ liquid}$$

(5.13)

The percentage porosity was calculated by dividing the void volume of the sample by the volume of the sample.

$$\%\ Porosity = \frac{Void\ volume}{Sample\ volume} \times 100\%$$

(5.14)

A measuring flask was weighed, the sample inserted and weighed again. The masses were recorded and noted as the mass of flask and mass of flask and sample, respectively.

A fluid with a known density was added to the flask of known volume (i.e. 100 ml). This was noted as measured volume.

The volume of the fluid added was then calculated and noted as the volume of the fluid.

$$Volume\ of\ fluid = \frac{(A + B + C) - (A + B)}{D}$$

(5.15)

Where:
A = Flask (ml)
B = Impregnated sample (g)

C = Fluid (ml)

D = Density of fluid (g/cm³)

The volume of the sample was calculated by subtracting the volume of the fluid from the measured volume.

$$Volume\ of\ sample = Mesured\ volume - Volume\ of\ fluid \qquad (5.16)$$

The sample density was then obtained by dividing the dry mass of the sample by the volume of the sample.

$$Sample\ density = \frac{Mass_{dry}}{Volume\ of\ sample} \qquad (5.17)$$

5.2. MIXING AND PELLETISING

The laboratory pellets for all the experiment were prepared in the same way.

The typical mixture to make Nitrovan briquettes consists of primary mixture and spillage. Carbon is added at a ratio of 3.3 mole carbon per mole of V_2O_3. The composition of the primary mixture is given in Table 5-1.

Table 5-1: Primary mixture (Percentage by mass).

MVO	72.0 %
Proven Air	7.6 %
Carbon	20.4 %

Spillage is added to the primary mixture at a ratio of between 0:1 and 0.5:1 (i.e. between 0 g and 50 g per 100 g primary mixture)

$$Total\ mix = primary\ mix + spillage \qquad (5.18)$$

Starch is added at 2 % total mixture. PVA binder concentrate is added at 1.5 wt% primary mixture. PVA binder concentrate is diluted approximately 1 part to 9 parts of water (volume basis). In order to obtain a wet mixture moisture content of 14 % then requires that 17.2 ml of the diluted PVA binder be added to 100 g of the total dry mixture.

The primary mixture, spillage and binders were blended for 15 minutes in a standard kitchen mixer to obtain a homogenous mixture.

A 40 mm diameter die was used to press disc shaped pellets. The die was thoroughly cleaned with ethanol to remove possible impurities stuck on the inside of the die. Bagged samples of 30 g from each mixture were carefully poured inside the die. An Optelec hydraulic presser was used to press the pellets with a total load of 60 kN. The applied load on the samples was chosen to ensure a similar density of all pellets to maintain consistency and achieve the same density as the Vametco briquettes. The pressed pellets were dried for 24 hours at 130 °C. The moisture loss was calculated from the mass loss during drying.

For the shaft furnace experimental set, the same procedure was followed using a 10 g sample and 15 mm die at a compression force of 40 kN.

5.3. INDUCTION FURNACE

5.3.1. INTRODUCTION
The aim of these experimental sets was to simulate the reactions occurring in the Vametco shaft furnace. Two experimental sets were conducted in the laboratory scale induction furnace.

5.3.2. EXPERIMENTAL SETUP
An induction heated furnace with a graphite susceptor was used in these experiments. A single set of water-cooled copper coils are centred within the furnace with a graphite crucible inside the coils. The copper coils were cast into a refractory cement.

Power to the copper coils were supplied by a 15 kW Ambrell Ecoheat ES high frequency induction power supply.

Alumina bubbles were used as insulation between the crucible, induction coils and the outer shell of the furnace. The top of the furnace was lined with a layer of refractory fibre insulation.

Two pellets, of the same composition and diameter, were placed on top of each other inside the graphite crucible. The pellets were sandwiched between two graphite disks of the same diameter as the pellets (40 mm).

Purified nitrogen was introduced into the crucible. The nitrogen was technical grade (Nitrogen 0.5, 99.995%) gas that had been passed through a copper purifier heated to a temperature of 300 °C.

A type B thermocouple (TC) was placed next to the samples in the graphite crucible. The thermocouple was wired through a four-bore alumina sleeve in a protection sheath. The sheath was placed on a small alumina tile at the bottom of the crucible, allowing the TC hot junction to be aligned with the bottom pellet.

The thermocouple was connected to a data taker with shielded wires which was connected to a computer. The data from the thermocouple was collected and written to a text file every 5 seconds.

A PID control loop was used to control the furnace temperature.

5.3.2.1. INDUCTION FURNACE WITH VARIABLE LOAD

The experimental setup described in section 5.3.2 was used for this experimental set with a few additions.

A part graphite, part alumina pushrod was place on top of the samples and different weights were secured to the pushrod. A linear variable differential transformer (LVDT) was placed outside the furnace and the core placed on top of the pushrod to monitor any vertical movement in the furnace. Figure 5-2 is a schematic representation of this furnace.

The LVDT was connected to a data taker with shielded wire and the data was recorded every 5 seconds.

The furnace was heated at a rate of 60 °C/min to the desired temperature. When that temperature was reached, it was kept constant for 30 minutes and first cooled to 800 °C at 60 °C/min and then to room temperature at approximately the natural cooling rate of the furnace. A typical temperature profile of the furnace is shown in Figure 5-1.
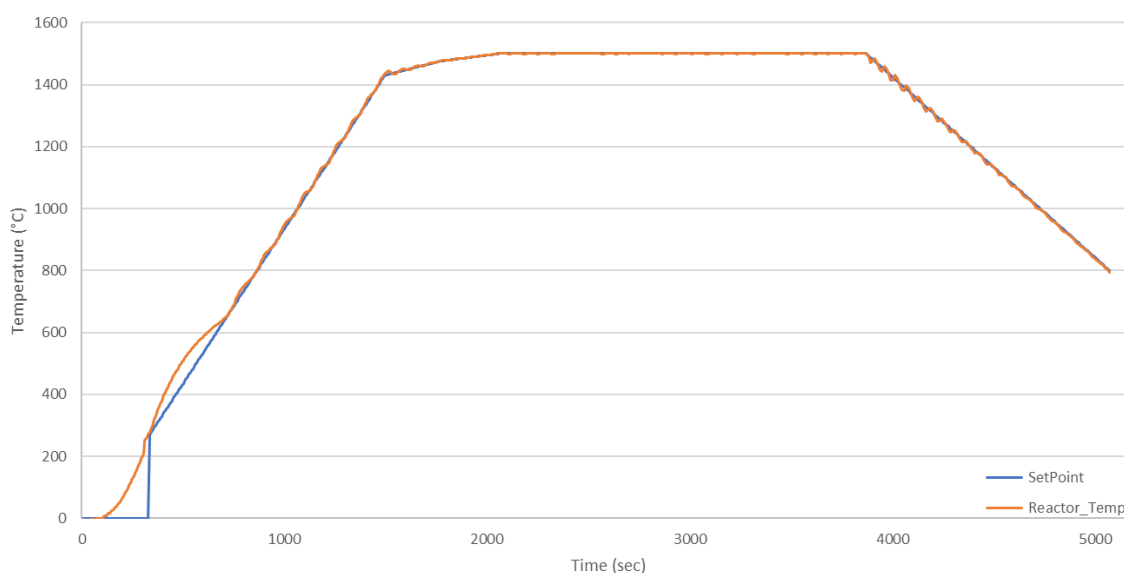
Figure 5-1: Typical temperature profile of the induction furnace used with a set point and furnace temperature.
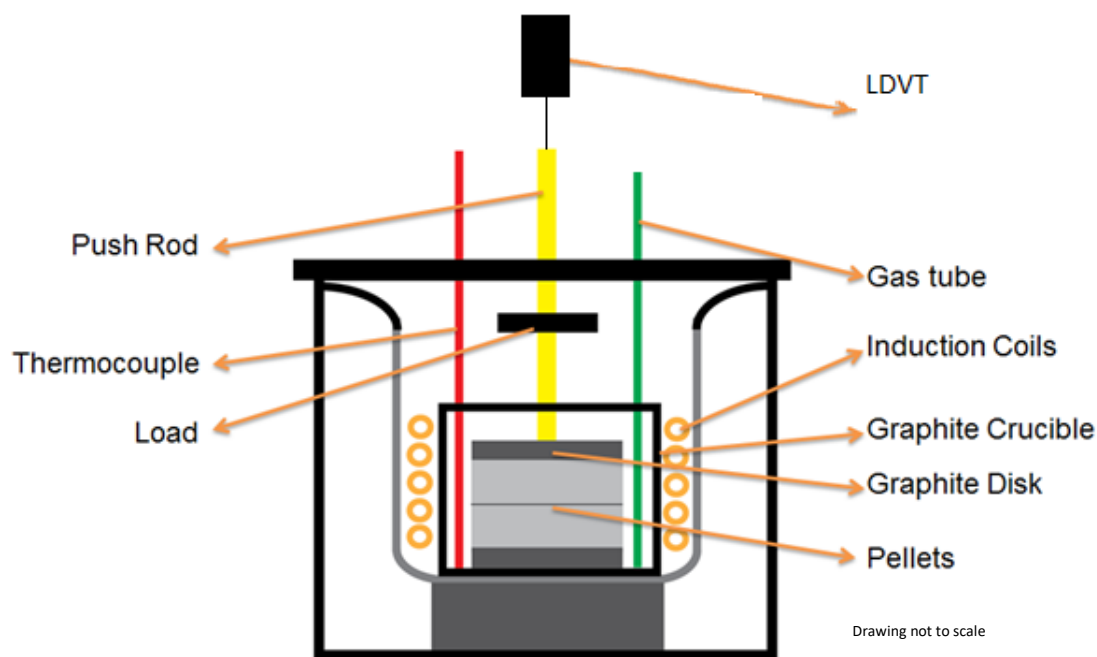
Figure 5-2: Schematic of induction furnace with variable load.

5.3.2.1.1. EXPERIMENTAL DESIGN

A three-factor central composite design (CCD) was chosen. A multiple number of input factors could be built into the design, in an appropriate combination to yield results that would in no known way be subject to bias.

Reaction temperature, amount of spillage and load were selected as variable factors and the levels are represented inTable 5-2. The respective levels are denoted as: (-*) for the lowest level, (+*) the highest level, (0) a medium level and (-) and (+) are the levels that are a factor of 0.6 away from the midpoint value.

The pellet compositions were changed by the addition of varied amounts of spillage added to the primary mixture. A ratio of between 0.3 and 0.45 to the primary mixture was added. To compensate for this, a lowest value of 0.0 and a highest value of 0.5 was chosen.

Table 5-2: Induction furnace CCD experimental levels.

	-*	-	0	+	+-
Temperature (°c)	1200	1310	1475	1640	1750
Load (Kg)	0.1	0.17	1.4	2	3
Composition (% Spillage)	0	10	25	40	50

The different component contributions in the mixtures are given in Table 5-3 in weight percentages.

Table 5-3: Mixtures with component contribution of CCD experiment.

	Spillage	MVO	P-Air	Carbon	Starch	PVA sol
Mix 1	0.00	32.80	3.46	9.29	46.46	7.99
Mix 2	4.14	29.81	3.15	8.45	46.46	7.99
Mix 3	9.11	26.24	2.77	7.43	46.46	7.99
Mix 4	13.01	23.43	2.47	6.64	46.46	7.99
Mix 5	15.18	21.86	2.31	6.19	46.46	7.99

From this setup, 18 runs were necessary to investigate every combination of the low, intermediate low, intermediate, intermediate high and high levels. The run order selection was done on a random basis. The experimental treatment combinations are given inTable 5-4.

Table 5-4: 3-Factor experiment treatment combination.

Run	Temp	Load	Comp
1	0	0	0
2	0	0	-*
3	0	0	0
4	-*	0	0
5	0	-*	0
6	+	+	-
7	+	-	-
8	-	-	-
9	0	0	+*
10	+	-	+
11	+	+	+
12	+-	0	0
13	0	0	0
14	-	+	-
15	-	+	+
16	0	+*	0
17	-	-	+
18	0	0	0

5.3.2.2. INDUCTION FURNACE WITH CONSTANT LOAD

The experimental setup described in section 5.3.2 was used for this experimental set.   The following changes were made to the setup:

1. The pushrod with the load was removed.

2. The LVDT was removed.

3. A graphite block of a known weight was placed on top of the pellets inside the crucible.

A constant load of 1 kg was applied to the pellet and graphite sandwich by placing a 1 kg graphite block on top of the sandwich inside the graphite crucible.

The mixing procedure remained the same as the previous experimental set. No spillage or Proven Air was added to the mixture. Varied amounts of barren solution and settling tank sludge were respectively added to spike the mixtures with soluble and insoluble impurities.

The furnace was heated at a rate of 60 °C/min to the desired temperature. When that temperature was reached, it was kept constant for the desired time and then cooled to room temperature at approximately the natural cooling rate of the furnace.
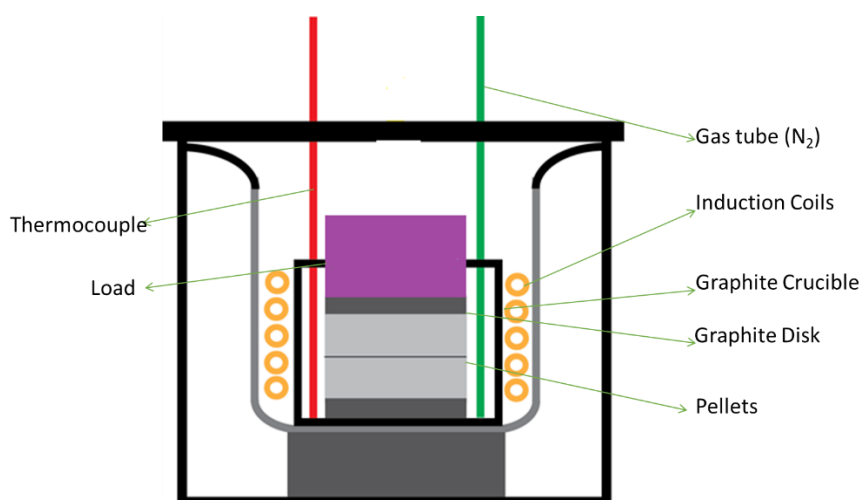
Figure 5-3:Schematic of induction furnace with constant load.

5.3.2.2.1. EXPERIMENTAL DESIGN

A full factorial with centre points design was selected for this experimental set in that it was necessary to study the main and joint effects of the factors to a response.

Reaction temperature, time at temperature, insoluble impurities and soluble impurities were selected as variable factors and the levels are represented in Table 5-5. The respected levels are denoted as: (-) for the lower level, (+) the higher level, and (0) for the centre points.

Table 5-5: Induction furnace 2 level 4 factor experimental levels with centre points.

	-	0	+
Temperature	1200 °C	1300 °C	1400 °C
Time	30 min	45 min	60 min
Insoluble impurities	0 % Fe	0.5 % Fe	1 % Fe
Soluble impurities	0 % Na_2O	0.5 % Na_2O	1 % Na_2O

Chapter 5: Methods

The soluble and insoluble impurities were added with the varied additions of barren solution and settling tank sludge. The five mixtures given in Table 5-6 are the different levels of impurities added with the weight percentage of each component in the mixtures given inTable 5-7.

Table 5-6: Mixture levels for factorial experiment.

	Insoluble	Soluble
Mix 1	-	-
Mix 2	+	-
Mix 3	-	+
Mix 4	+	+
Mix 5	0	0

Table 5-7: Mixtures with component contribution of factorial experiment.

	MVO	Carbon	Starch	PVA sol	Sludge	Barren
Mix 1	65.74	17.91	1.67	14.68	0.00	0.00
Mix 2	61.07	18.85	1.81	15.60	2.67	0.00
Mix 3	59.38	18.33	1.76	15.17	0.00	5.36
Mix 4	60.71	16.54	1.59	13.96	2.34	4.85
Mix 5	63.15	17.21	1.63	14.31	1.22	2.48

From this setup, 16 runs were necessary to evaluate the 4 factors on 2 levels. It was decided to add 5 centre points totalling the runs to 21. The run order selection was done on a random basis. The experimental treatment combinations are given in Table 5-8.

Table 5-8: Factorial experiment treatment combination.

Run	Temp	Time	Insol	Sol	Run	Temp	Time	Insol	Sol
1	0	0	0	0	12	+	-	+	+
2	-	-	-	-	13	0	0	0	0
3	-	+	-	-	14	+	+	+	+
4	+	+	-	+	15	0	0	0	0
5	-	+	+	-	16	+	-	+	-
6	-	+	+	+	17	-	-	+	+
7	+	-	-	+	18	+	+	+	-
8	-	-	+	-	19	+	-	-	-
9	0	0	0	0	20	+	+	-	-
10	-	-	-	+	21	0	0	0	0
11	-	+	-	+					

5.4.   COAL ASH FUSIBILITY FURNACE

A coal ash fusibility (CAF) furnace was used to investigate dimensional changes of Vametco briquettes and laboratory pellets. This furnace was used because of its ability to make a visual recording of the occurrence inside the furnace at specified temperatures. The furnace was limited to a maximum temperature of 1600 °C and a ramp rate of 5 °C/min.

An image of the pellet or briquette was recorded every 5 °C from 800 °C as the temperature was increased. No images were recorded after the maximum temperature was achieved. It was found that volatile components in the pellets condensed on the window during testing resulting in poor image quality.

The CAF furnace consists of an alumina tube that is heated by resistance heating on the outside of the tube. The tube was purged with nitrogen to prevent any oxidation and to supply nitrogen to the reaction. A thermocouple was placed in the centre of the furnace to obtain accurate temperature measurements. The sample was placed on an alumina stand positioned immediately in front of the thermocouple.
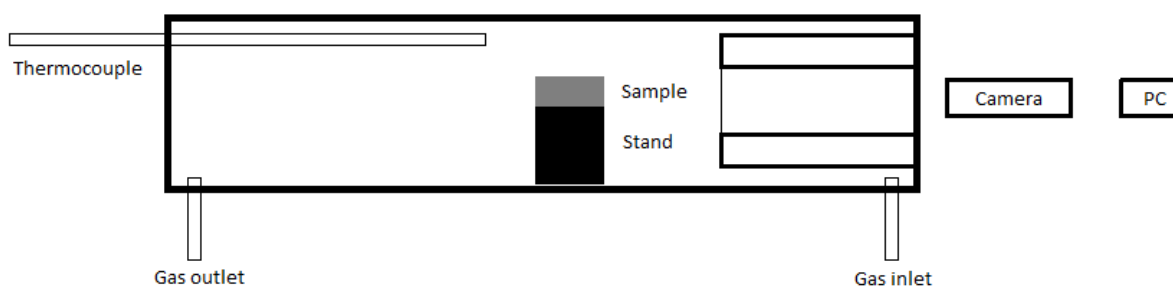
Figure 5-4: Schematic of coal ash fusibility furnace.

5.5.   TUBE FURNACE

5.5.1.   INTRODUCTION
The aim of this experiment was to evaluate the amount of sintering occurring during the production of Nitrovan.

5.5.2.   EXPERIMENTAL SETUP
A vertical tube furnace with resistance heating elements was used for this experimental set.

The sample was suspended by means of a vacuum inside a mullite working tube (see Figure 5-5). The working tube was suspended inside an alumina furnace tube surrounded by 14 heating elements.

The sample was attached to a graphite plunger with Kanthal wire. The plunger was suspended inside the furnace by means of a vacuum.

A glass quench flask, with a separate water and gas inlet, was connected to the bottom of the working tube. The top of the working tube had a glass fitting with a gas outlet on the side and a narrow neck which allowed the suspension tube to create an airtight seal.
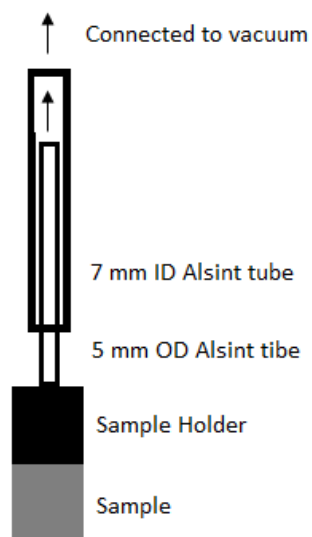
Figure 5-5: Vacuum suspended sample holder.

The inlet gas was a mixture of high purity nitrogen and carbon monoxide. The outlet gas was passed through a small horizontal tube furnace that was at approximately 800 °C. In this furnace, the gas passed over an oxygen sensor that was connected to a data taker and computer. The partial pressure of oxygen was calculated by the Nernst equation:

$$E = \left(\frac{RT}{nF}\right) \ln \left(\frac{Po_2}{Po_2{'}}\right)$$

(5.19)

Where:
E = sensor electromotive force, (mV)
R = gas constant
T = temperature, (Kelvin)
n = number of charges per reactant species
F = Faraday constant
p = partial pressure (mole fraction)

This equation describes the electromotive force (emf) developed when there are different concentrations of a reactant on each side of an electrolyte.

A zirconia sensor was used with atmospheric air used as the reference atmosphere where PO_2 = 0.209 atm. (assuming an ambient pressure of 1 atm). This simplifies the equation to:

$$Po_2 = 0.209 . e^{\left(\frac{-46.421\,E}{T}\right)}$$

(5.20)

The sample was inserted into the hot zone of the pre-heated furnace. At a specific time, the vacuum was turned off and the sample with plunger dropped into the quench cup. The sample was then quenched by adding water to the quench cup.

5.5.3. EXPERIMENTAL DESIGN

The same experimental design as described in Section 5.3.2.1.1 was used for this experimental set.

5.5.4. ANALYTICAL TECHNIQUE

The purpose of this experiment was to quantify the amount of sintering after reacting pellets. The reacted pellets were sectioned through the centre and prepared for optical analysis. The sectioned pellets were cold mounted in epoxy resin, ground and polished to a 1 µm finish. Micrographs were collected in the centre of the sample at 20 x magnification.

The micrographs were processed using ImageJ software [59] to obtain usable data from each image to determine the density and porosity of the pellets.

The following procedure was used to analyse the images:

1   Bandpass filter 40 pixels

2   Colour Threshold

3   Binary Image

4   Watershed

5   Analyse

This procedure was written as a macro in the software to ensure that the same procedure is followed with all the images. This procedure is shown Figure 5-6.

(a)   (b)

(c)

(d)

(e)
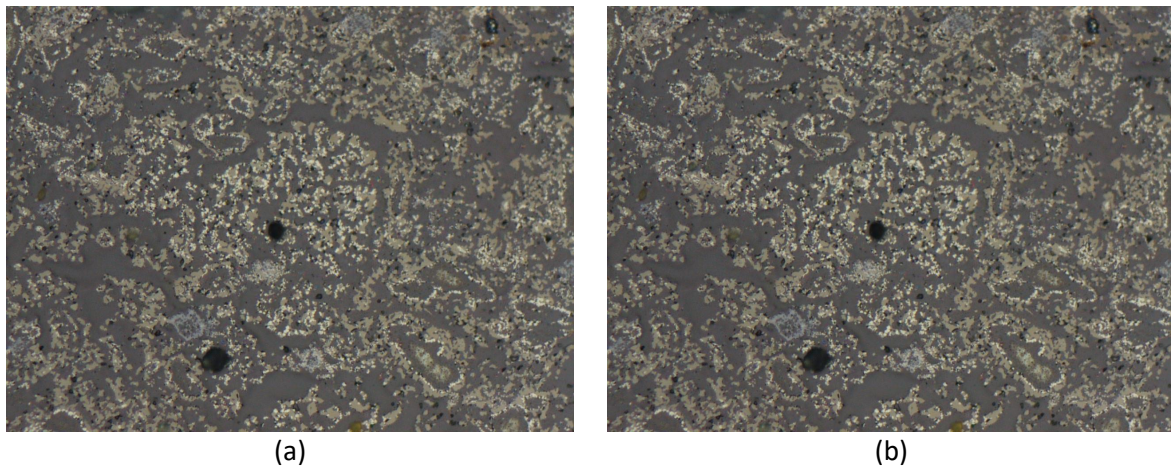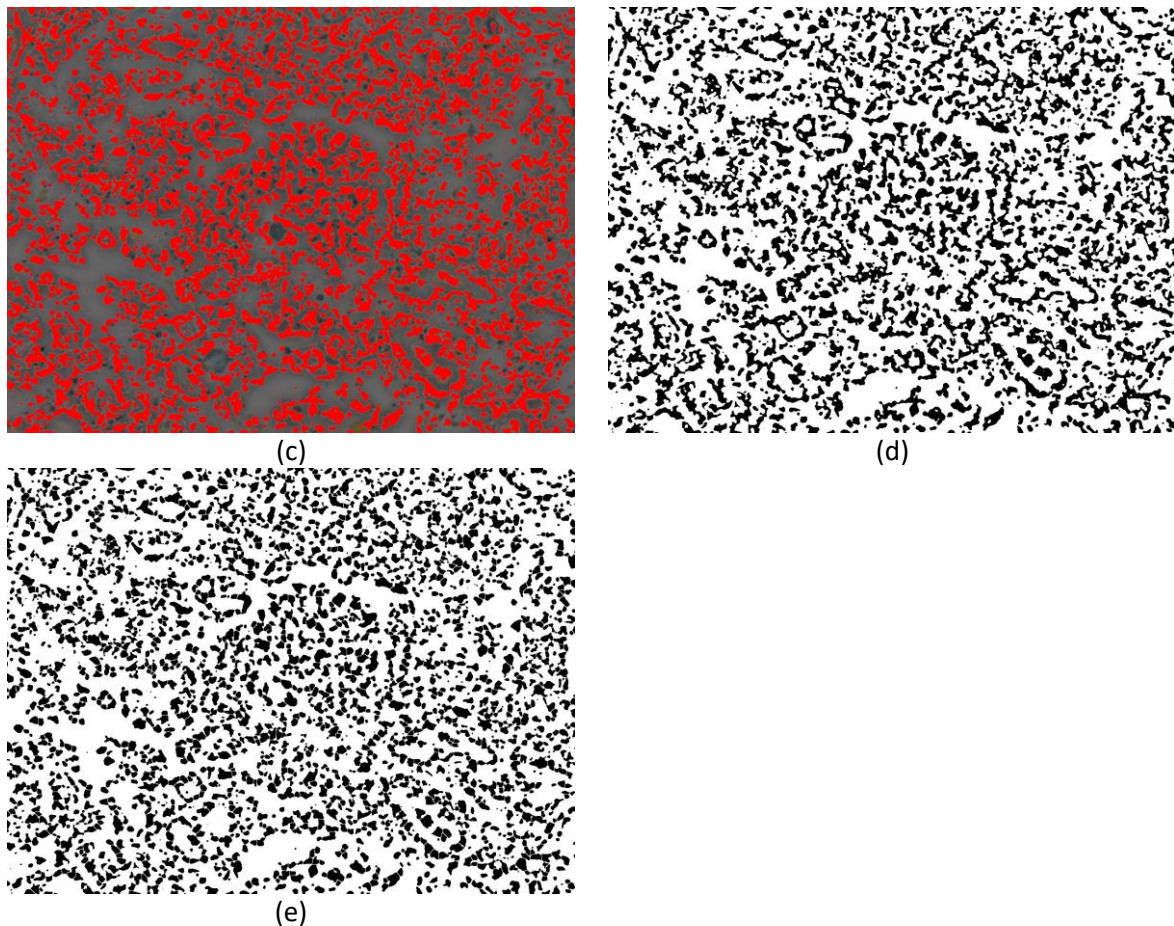
Figure 5-6: Image processing procedure:(a) Original image; (b) Bandpass filter 40 pixels; (c) Colour threshold; (d) Binary image; (e) Watershed.

5.6. REACTED PELLET DENSITY TESTING

The density of the reacted pellets that were reacted in the induction furnace factorial experimental set underwent density testing.

Due to the irregular shape of the reacted pellets, a submersion method was used to calculate the density. A dry method was necessary to avoid any dissolution or leaching of potentially critical phases. The pellets were submerged in a beaker filled with small glass beads with a known density. The volume and weight difference were used to calculate the density of the submerged pellets.

5.7. SHEAR TESTING

A shear tester was used to perform tests on the reacted laboratory pellets. The aim of the test was to calculate the amount of force necessary to break the fused pellets by means of shear.

A set of fused pellets was placed inside the test jig. The pellet position was adjusted so that the fusion plane aligned with the shear plane of the test jig

Figure 5-7 and Figure 5-8 are schematic drawings of the shear tester. The arrows marked "F" indicate the applied tension force.

For the CCD experimental set, the tester was connected to a laboratory Hounsfield tensiometer. A standard tensile test was performed. The tester was pulled apart and created a shear force between the pellets. It was noted that a more accurate instrument was needed.

The reacted pellets from the induction furnace factorial design experimental set was sheared using the same shear tester, but the tester was connected to an MTS Criterion ™ Model 45 with a 5 kN load cell. More accurate results were obtained using this equipment.

The shear stress was calculated by the equation below and the results were recorded.

$$\tau_{shear} = \frac{F}{A_0} \qquad (5.21)$$

Where:

τ_{shear} = Shear stress

F = Applied force

A_0 = Original area of pellet
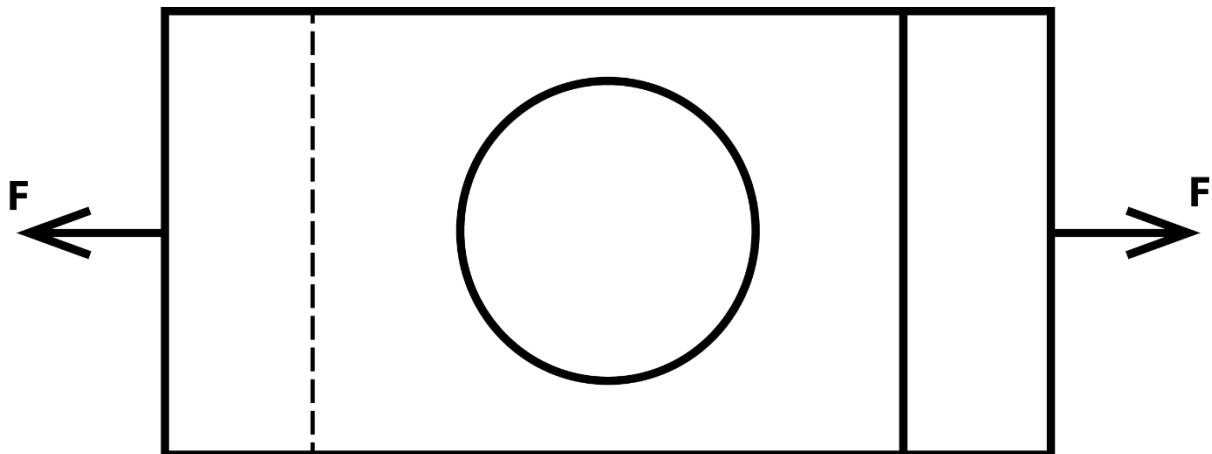
Figure 5-7: Shear tester top view.

Figure 5-8: Shear tester side view.

5.8.   STATISTICAL ANAYSIS

For this study, analysis of variance (ANOVA) was used to analysis the data. It is a collection of statistical models used to analyse the differences between groups.

5.8.1.   LOGIC

The computations of ANOVA can be defined as calculating the number of means and variances, dividing two variances and comparing the ratio to a predetermined value (handbook value) to determine statistical significance [57][60].

5.8.2.   PARTITION SUM OF THE SQUARES

Sum of squares is the sum of the square of variation, where variation is defined as the spread between each individual value and the mean. To determine the sum of squares, the distance between each data point and the line of best fit is squared and then summed up[60].

5.8.3.   F-TEST

The F-statistic is a ratio of two variances. The F-test is defined as the ration of variation between the sample means to the variations within the samples [60].

5.8.4.   P-VALUE

P values evaluate how well the sample data support the argument that the null hypothesis is true. It measures how compatible the data are with the null hypothesis. A low P value suggests that the sample provides enough evidence that null hypothesis can be rejected for the entire population [60].

5.8.5.   MAIN EFFECT

The main effect of the model refers to the primary factors of interest in the experiment. It is defined as the change in the response by the change in the level of the factors. In this study, a typical main effect would be the influence of a change in temperature in the fusing op pellets [60].

5.8.6. INTERACTION EFFECT

An interaction effect is the concurrent effect of two or more independent variables on a dependent variable in which their common effect is significantly greater (or significantly less) than the sum of the parts [60].

.

CHAPTER 6:

RESULTS

6.   RESULTS

The results obtained from the experiments will be discussed in this section. Results will largely be presented in aggregated form. The raw data is presented in Appendix F and G

6.1.   RAW BRIQUETTE DENSITY

The density and porosity of the raw Vametco briquettes were determined using a liquid with a known density. Water and paraffin were used to calculate the density and porosity of each briquette. Ten briquettes used to measure the porosity and density. The averages, standard deviations and variances are listed in Table 6-1.

Table 6-1: Average porosity and density of Vametco briquettes.

	Percentage Porosity			Density (g/cm^3)		
	Avg.	Std.	Var.	Avg.	Std.	Var.
Water	23.29	6.14	37.7	2.21	0.15	0.02
Paraffin	24.68	1.83	3.35	2.15	0.01	0.00

6.2.   INDUCTION FURNACE WITH VARIABLE LOAD

The induction furnace with a variable load experiment was executed as described in section 5.3.2.1 and the results are presented below.

Table 6-2: Factors and levels for the central composite design.

Factor	Name	Low	High
A	Temperature	1200	1750
B	Load	0.1	3
C	Spillage	0	50

The response of this experiments is measured shrinkage, LVDT shrinkage, shear, vanadium content, nitrogen content, carbon content and oxygen content.

Measured shrinkage is the difference in pellet thickness measured with a Vernier caliper before and after reaction. LVDT shrinkage is the displacement measure by the LVDT during the experiment. Shear is the force that was exerted on the pellets in order to break the two pellets apart.

The assumption has been made that the data fits a quadratic model and the response surface was analysed using this model. This model was used based on a statistical approach and not a fundamental approach.

The p-value criterion was used to reduce the model combination with factor hierarchy. The selection included the main effect and second term interactions. The selection was made on a 95 % significance.

6.2.1. RESPONSE: SHEAR

The analysis of variance for shear force as a response is given in Table 6-3. None of the factors or combination of factors have a statistically significant influence on force needed to shear the fused pellets apart.

Table 6-3: Analysis of variance with shear as response.

Source	DF	Adj SS	Adj MS	F-Value	P-Value
Model	5	0.165449	0.033090	0.83	0.554
Linear	3	0.145225	0.048408	1.21	0.348
Temperature	1	0.033385	0.033385	0.84	0.379
Load	1	0.111110	0.111110	2.78	0.121
Spillage	1	0.000730	0.000730	0.02	0.895
Square	1	0.002729	0.002729	0.07	0.798
Load*Load	1	0.002729	0.002729	0.07	0.798
2-Way Interaction	1	0.000617	0.000617	0.02	0.903
Load*Spillage	1	0.000617	0.000617	0.02	0.903
Error	12	0.479602	0.039967		
Lack-of-Fit	9	0.324613	0.036068	0.70	0.703
Pure Error	3	0.154989	0.051663		
Total	17	0.645051			

From the model summary in Table 6-4 the goodness-of-fit was determined.

Table 6-4: Model summary with shear as response.

S	R-sq	R-sq(adj)	R-sq(pred)
0.199917	25.65%	0.00%	0.00%

The regression model equation for shear is given below.

$$\text{Shear} = \quad -0.426 + 0.000301 \text{ Temperature} + 0.081 \text{ Load} + 0.00043 \text{ Spillage} \qquad (6.22)$$
$$+ 0.0161 \text{ Load*Load} - 0.00062 \text{ Load*Spillage}$$

The proposed model has a low R-sq value and indicated that the model is not a good fit to the data.

A Pareto chart was used to determine the magnitude and the importance of the effects. On the Pareto chart, bars that cross the reference line are statistically significant. The reference line for statistical significance depends on the significance level. For all the represented data $\alpha = 0.05$.
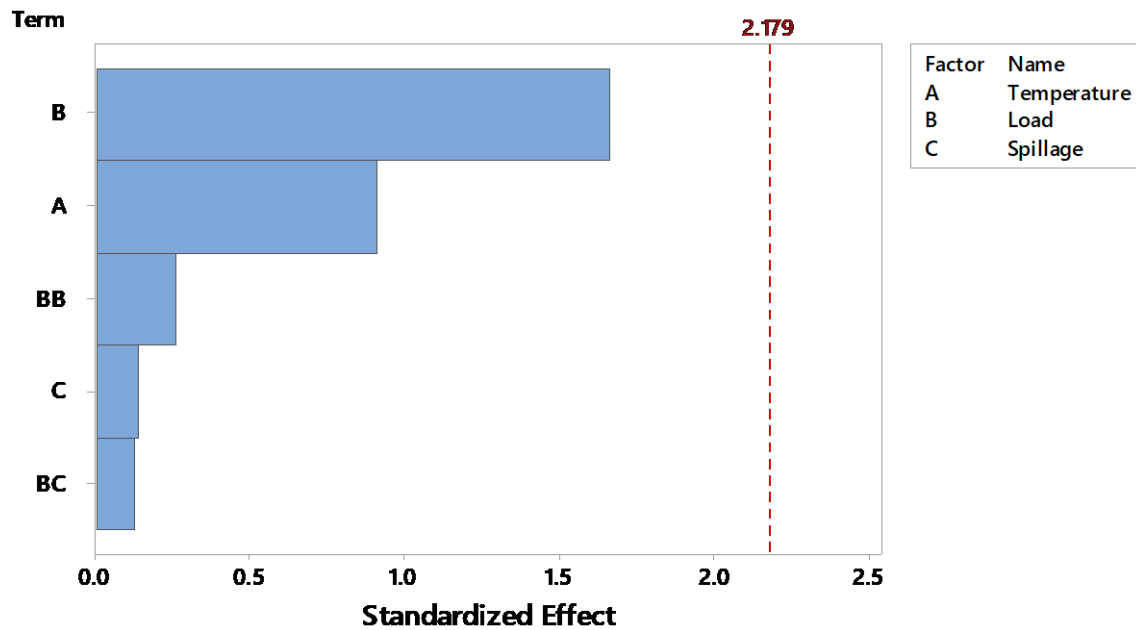
Figure 6-1: Shear Pareto chart of the standardized effect (response is shear, α = 0.05).

No effect or combination of the chosen effects has statistical significance on shear force as a response to the fusion of the pellets. The effect of load has the highest significance in this chart followed by temperature. Even though load and temperature have the most significant effect neither of these are statistically significant.
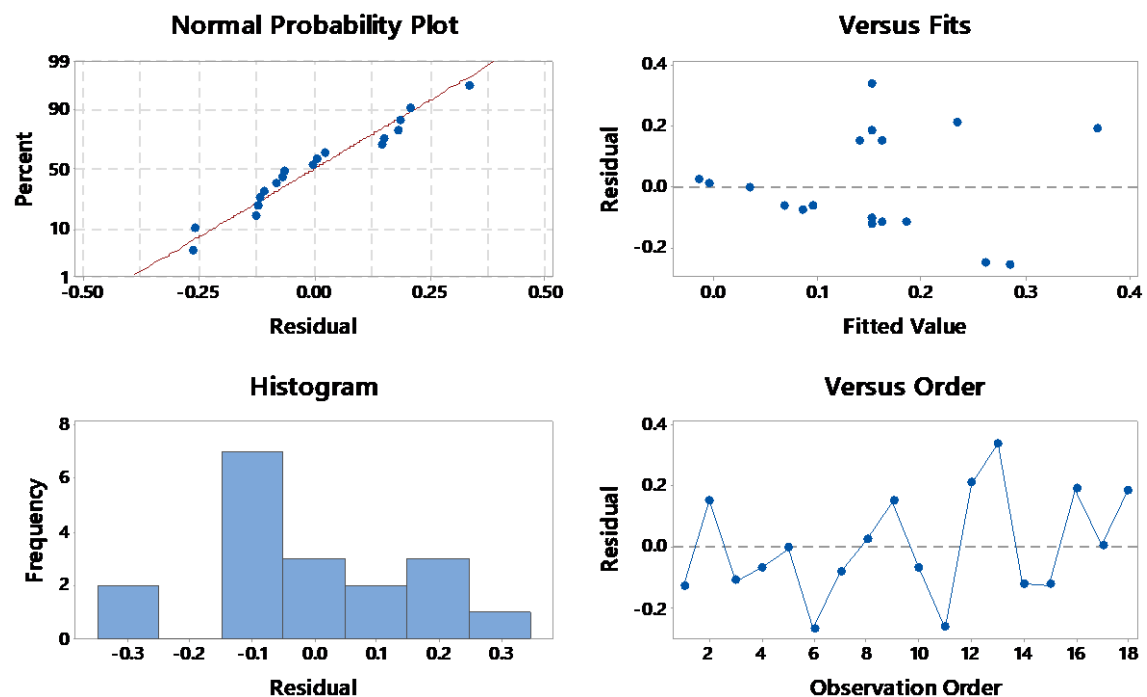
Figure 6-2: Residual plots for shear.

The normal probability plot of the residuals in Figure 6-2 shows that the residuals are normally distributed following a line on a normal probability plot.

The residual vs fitted value plot shows a downward trend which suggests a non-constant variance. The residuals appear to be normally, randomly distributed. There is a high level of confidence that the requirements (random and N(0,σ)) for the statistical fitting are met.

A larger sample size would aid in the variance of the residuals. This histogram shows a normal distribution with a tail to the right. A plot of versus order shows no apparent trend. The residuals scatter with an increase in observation order.

The shear contour plots in Figure 6-3 are based on the empirical model of section 6.2.1. It is important to note that the model is plotted and not the individual data points.

The load-temperature plot in Figure 6-3(a) shows an increase in load and temperature at a constant amount of spillage resulting in an increase in the force needed to shear the fused pellets. This correlates to the Pareto chart in Figure 6-1 where both load and temperature affects the shear force.
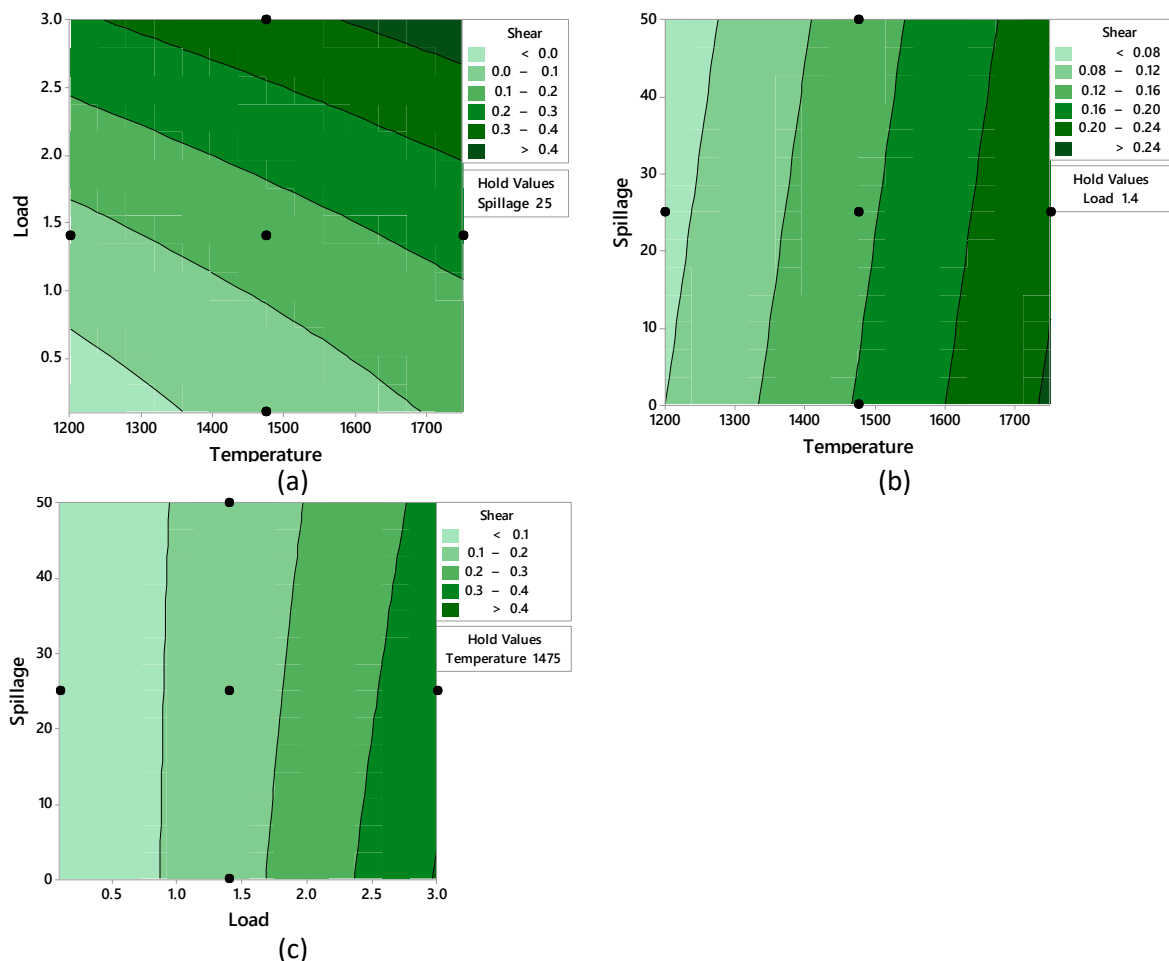
Figure 6-3: Contour plots of shear vs load, temperature (a), spillage, temperature (b) and spillage, load (c).

The Microsoft Excel pivot table of the average amount of shear with load and temperature in Table 6-5 shows the same effect, but with a deviation at 1640 °C. The average is determined by using the data obtained at specific conditions e.g. temperature and load combination. Where only one test was conducted at the specific conditions only one value is reflected in the average. Both load and

temperature have a positive effect in the fusion strength of pellets, with the influence of unknown factors.

Table 6-5: Pivot table of average shear data in response to load and temperature.

Average of Shear	Temperature					
Load	1200	1310	1475	1640	1750	Average
0.10			0.03			0.03
0.17		0.00		0.01		0.01
1.40	0.03		0.25		0.44	0.24
2.00		0.05		0.01		0.03
3.00			0.56			0.56
Average	0.00	0.03	0.26	0.01	0.44	0.15

The spillage-temperature contour plot in Figure 6-3(b) shows that with a constant load, the combination of spillage and temperature does not have a significant effect on the shear force. From the model, it is suggested that with the increase in the amount of spillage, the shear force slightly decreases.

The pivot table data in Table 6-6 is the average amount of shear with a change in the amount of spillage and temperature. At 1475 °C, the average amount of shear is higher than that at lower temperatures, but is higher than at 1640 °C. This indicates that the combination of load and spillage do not have a significant effect on shear and that unknown factors might influence fusion of the briquettes.

Table 6-6: Pivot table of average shear data in response to spillage and temperature.

Average of Shear	Temperature					
Spillage	1200	1310	1475	1640	1750	Average
0			0.31			0.31
10		0.04		0.01		0.02
25	0		0.24		0.44	0.24
40		0.02		0.01		0.02
50			0.29			0.29
Average	0.00	0.03	0.26	0.01	0.44	0.15

The spillage-load contour plot in Figure 6-3(c) shows that with a constant load, the combination of spillage and load does not have a significant effect on the shear force. Shear increases with an increase in load.

The pivot table data in Table 6-7 is the average amount of shear with a change amount of spillage and load. At 1.4 kg, the average amount of shear is higher than that at lower loads but is higher than at 2 kg. This indicates that the combination of load and spillage does not have a significant effect on shear and that unknown factors might influence the fusion strengths.

Table 6-7: Pivot table of average shear data in response to spillage and load.

Average of Shear	Load					
Spillage	**0.10**	**0.17**	**1.40**	**2.00**	**3.00**	**Average**
0			0.31			0.31
10		0.00		0.04		0.02
25	0.03		0.22		0.56	0.24
40		0.01		0.02		0.02
50			0.29			0.29
Average	**0.03**	**0.01**	**0.24**	**0.03**	**0.56**	**0.15**

6.2.2. RESPONSE: MEASURED SHRINKAGE

The analysis of variance for measured shrinkage as a response is given inTable 6-8. According to the calculated p-values and using a significance level of 0.05, temperature, spillage, load*load and load*spillage have a statistically significant effect on the measured shrinkage.

Table 6-8: Analysis of Variance with measured shrinkage as response.

Source	DF	Adj SS	Adj MS	F-Value	P-Value
Model	5	76.010	15.2020	6.16	0.005
Linear	3	48.016	16.0054	6.49	0.007
Temperature	1	23.155	23.1551	9.38	0.010
Load	1	1.396	1.3964	0.57	0.466
Spillage	1	23.465	23.4648	9.51	0.009
Square	1	13.741	13.7410	5.57	0.036
Load*Load	1	13.741	13.7410	5.57	0.036
2-Way Interaction	1	11.984	11.9837	4.86	0.048
Load*Spillage	1	11.984	11.9837	4.86	0.048
Error	12	29.609	2.4674		
Lack-of-Fit	9	27.479	3.0532	4.30	0.129
Pure Error	3	2.130	0.7100		
Total	17	105.619			

The model summary in Table 6-9 shows that the model has a relatively good fit to the data with a R^2 value of 71.97%. The predicted R^2 value is significantly less than the actual R^2 value indicating a possible over-fit suggesting that some of the term added are not important in the population.

Chapter 6: Results

Table 6-9: Model summary of measured shrinkage as response.

S	R-sq	R-sq(adj)	R-sq(pred)
1.57081	71.97%	60.29%	40.56%

The regression equation for measured shrinkage is given by equation 6.2.3.

Measured   -8.56 + 0.00792 Temperature + 6.13 Load + 0.0382 Spillage   (6.23)
Shrinkage =   - 1.143 Load*Load - 0.0871 Load*Spillage

The Pareto chart in Figure 6-4 shows the effects and combination of effects on the measured shrinkage of the pellets.   The spillage, temperature, load*load and load*spillage effects are statistically significant in the measured shrinkage of the pellets.
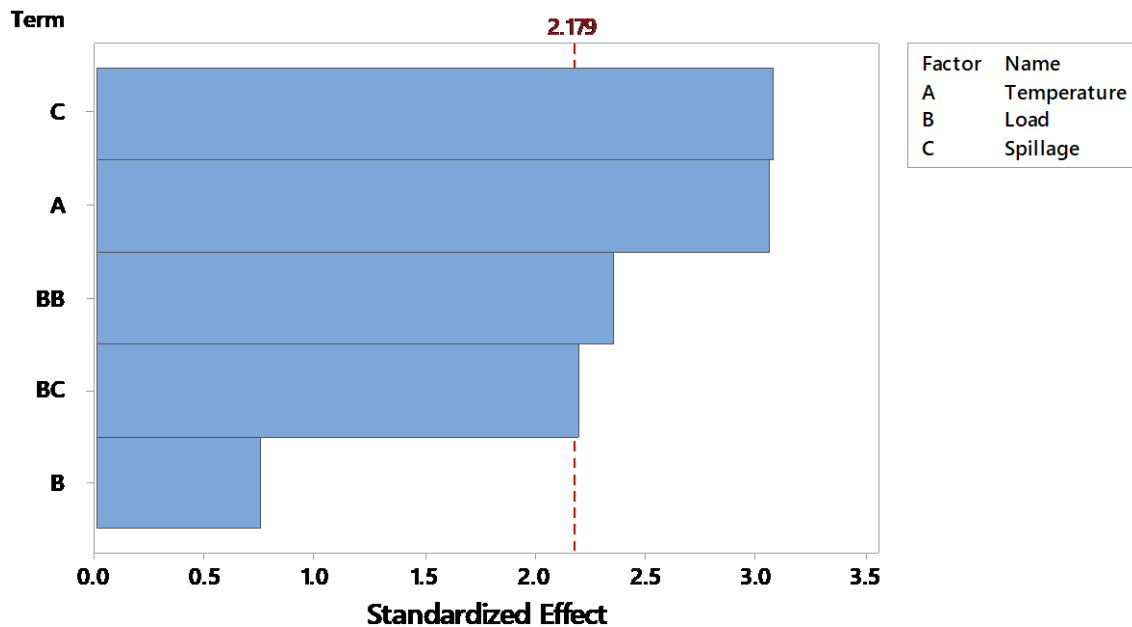
Figure 6-4: Measured Shrinkage Pareto chart of the standardized effect (response is measured shrinkage, α = 0.05).

The normal probability plot of the residuals in Figure 6-5 shows that the residuals are normally distributed following a line on a normal probability plot.

The residual vs fitted value plot shows a scattering of the residuals with no apparent trend suggesting a constant variance.

A plot of versus order shows no apparent trend. The residuals scatter with an increase in observation order.
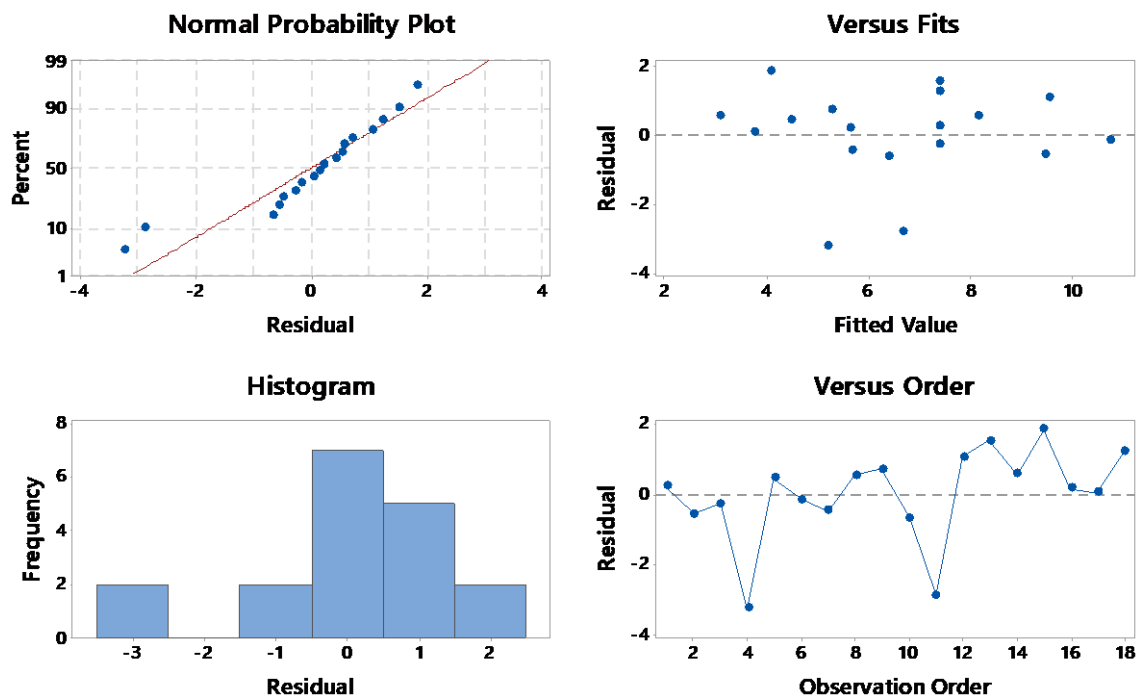
Figure 6-5: Residual plots for measured shrinkage.

6.2.3. RESPONSE: LVDT SHRINKAGE

The plotted data in Figure 6-6 shows the vertical shrinkage determined by the LDV of the pellets to a change in load. It must be noted that the plot also represents a change in temperature, load and pellet composition due to the experimental design parameters.

It is evident that the load exerted on the pellets is not the only or even the main driving factor for the shrinkage of the pellets.

A similar plot in Figure 6-7 shows the vertical shrinkage determined by the LDV of the pellets to a change in load.

Keeping in mind that other factors influence the shrinkage of the pellets, it is evident that temperature is indeed more a significant driver of the vertical shrinkage.

To interpret the data, it is necessary to investigate the interaction of all the variable factors.
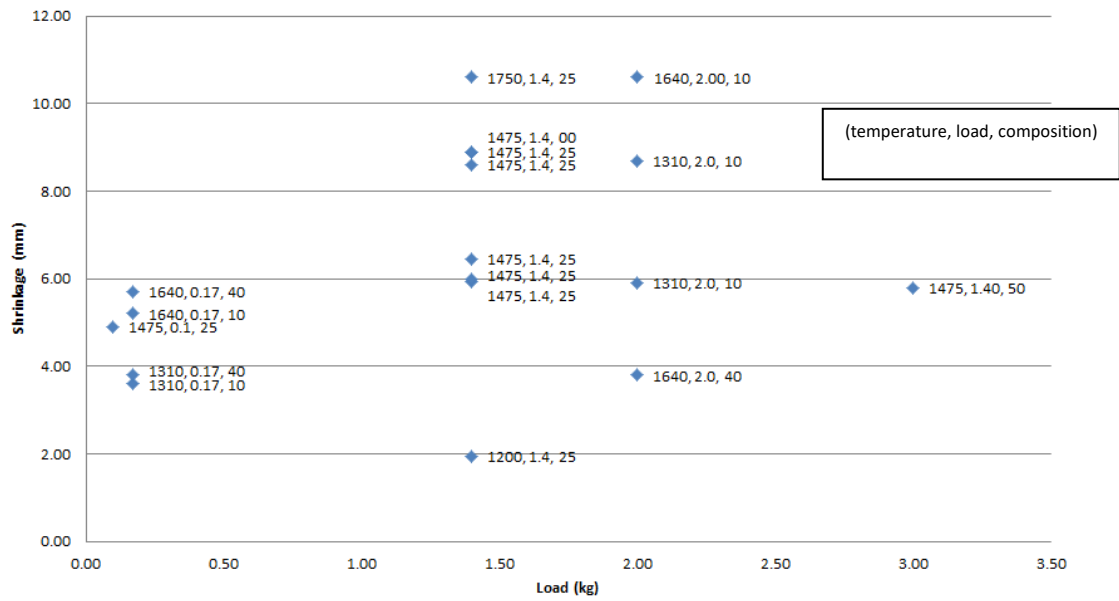
Figure 6-6: Shrinkage with variable load.
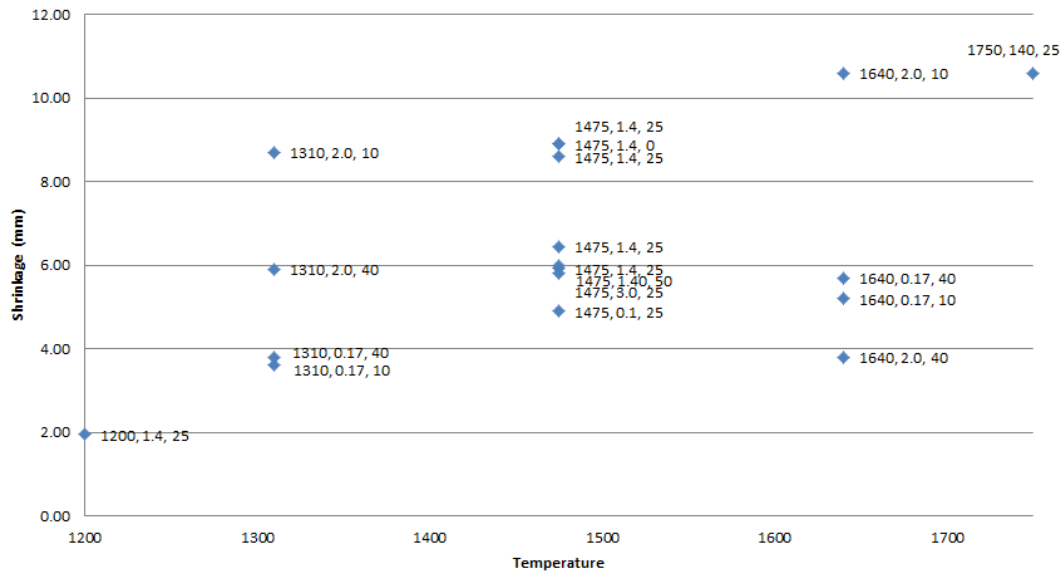
Figure 6-7: Shrinkage with variable temperature.

The analysis of variance for LVDT shrinkage as a response is given in Table 6-10. According to the calculated p-values and using a significance level of 0.05, temperature, spillage, load*load and load*spillage have a statistically significant effect on the measured shrinkage.

Table 6-10: Analysis of variance with LVDT shrinkage as response.

Source	DF	Adj SS	Adj MS	F-Value	P-Value
Model	5	70.911	14.1822	4.69	0.013
Linear	3	29.590	9.8632	3.26	0.059
Temperature	1	13.517	13.5167	4.47	0.056
Load	1	2.429	2.4292	0.80	0.388
Spillage	1	13.644	13.6437	4.51	0.055
Square	1	17.994	17.9944	5.95	0.031
Load*Load	1	17.994	17.9944	5.95	0.031
2-Way Interaction	1	14.831	14.8313	4.90	0.047
Load*Spillage	1	14.831	14.8313	4.90	0.047
Error	12	36.311	3.0259		
Lack-of-Fit	9	33.727	3.7474	4.35	0.127
Pure Error	3	2.584	0.8615		
Total	17	107.222			

The model summary in Table 6-9 shows that the model has a relatively good fit to the data with a R^2 value of 66.13%. The predicted R^2 value is significantly less than the R^2 value indicating a possible over-fit suggesting that some of the terms added are not important in the population.

Table 6-11: Model summary of LVDT shrinkage as response.

S	R-sq	R-sq(adj)	R-sq(pred)
1.73952	66.13%	52.02%	22.48%

The regression equation for measured shrinkage is given by equation 6.24.

LVDT Shrinkage =	-7.80 + 0.00605 Temperature + 7.02 Load + 0.0764 Spillage - 1.308 Load*Load - 0.0969 Load*Spillage	(6.24)

The Pareto chart of standardized effect on the LVDT shrinkage as a response is LVDT shrinkage in Figure 6-8 showing the load*load and load*spillage effects are statistically significant in the measured shrinkage of the pellets. This is significantly different from that of the measure shrinkage in Figure 6-4.
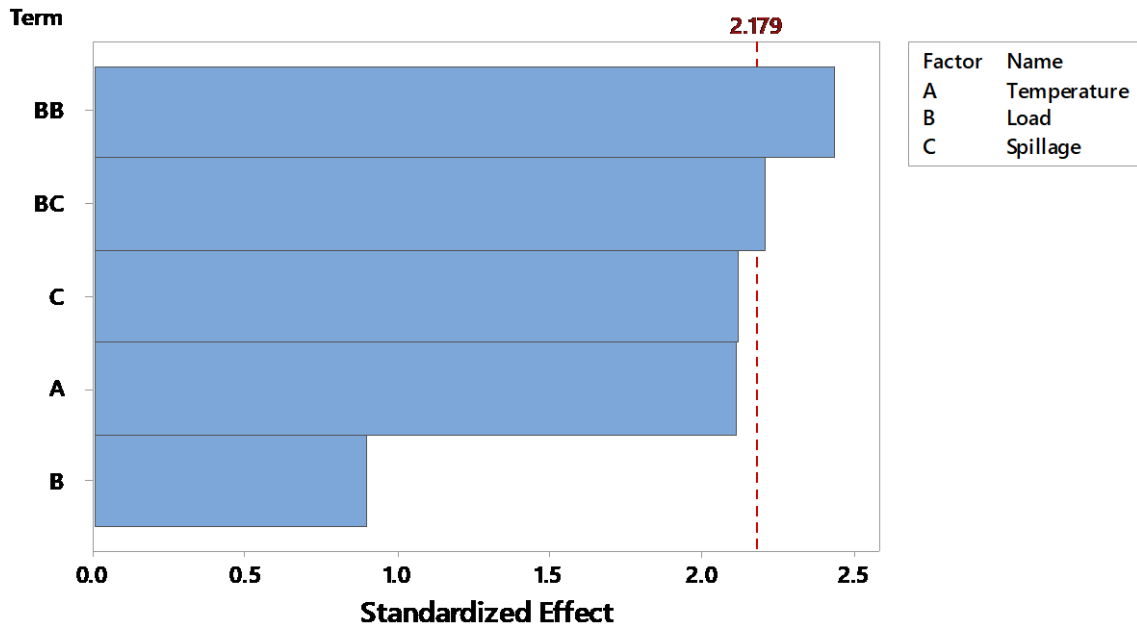
Figure 6-8: LDVT Shrinkage Pareto chart of the standardized effect (response is LVDT shrinkage, α = 0.05).

The normal probability plot of the residuals in Figure 6-9 shows that the residuals are normally distributed following a line on a normal probability plot with two possible outliers to the left.

The residual vs fitted value plot shows a scattering of the residuals with no apparent trend suggesting a constant variance.

A plot of versus order shows no apparent trend. The residuals scatter with an increase in observation order.
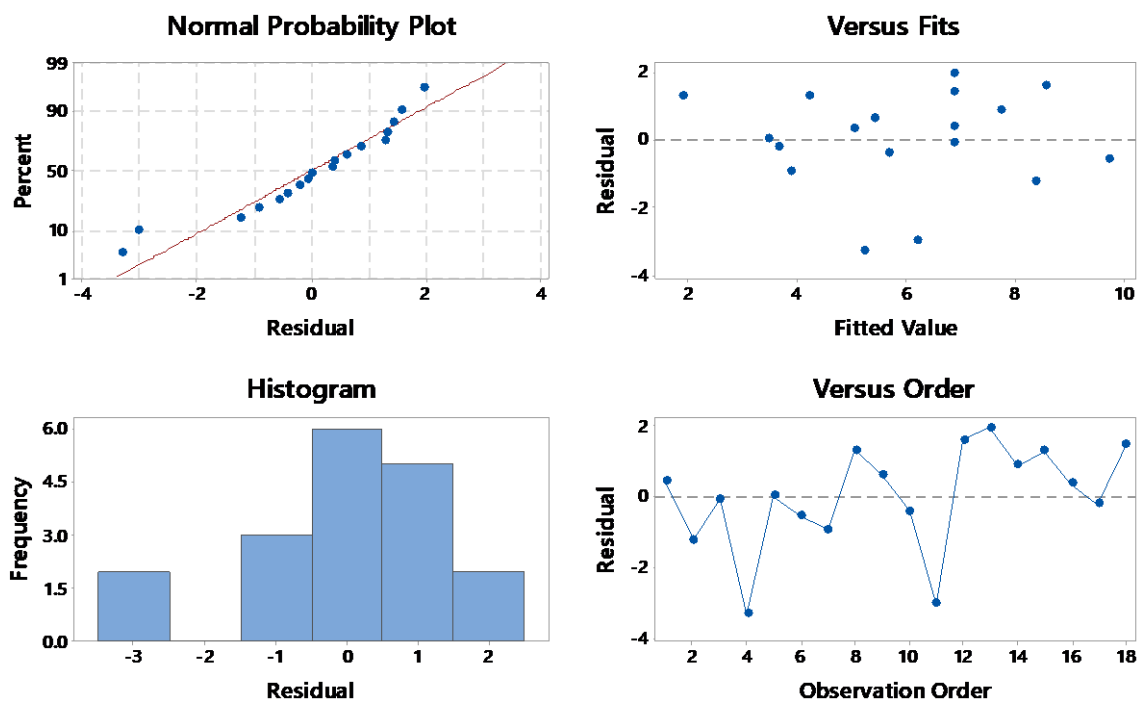
Figure 6-9: Residual plots for LVDT shrinkage.

The measured shrinkage model as described in section 6.2.2 was plotted as contour plots in Figure 6-10. Plot (a) shows an increase in measured shrinkage with an increase in temperature. Load has a peculiar effect on the measured shrinkage in that the shrinkage increases with an increase in load up to the centre point and decreases with a further increase in load.

The phenomenon in the model as seen in Figure 6-10(a) is skewed by the data obtained from the furnace run at 1475 °C with an applied load of 3 kg. The pellets shrank with only a measured amount of 5.8 mm in a vertical direction. The same phenomenon can be seen in Figure 6-11 where the amount of shrinkage was measured electronically with a LDVT during the test. From Table 6-12 and Table 6-16, a clear trend in the data can be observed: pellets will undergo an increased amount of shrinkage with an increased applied load and furnace temperature.

This furnace run yielded the highest force required to shear the pellets from each other which is consistent with amount of load applied to the pellets. Excluding this data point from the statistical analysis is thus not good practice and this data point will remain in the above-mentioned model.
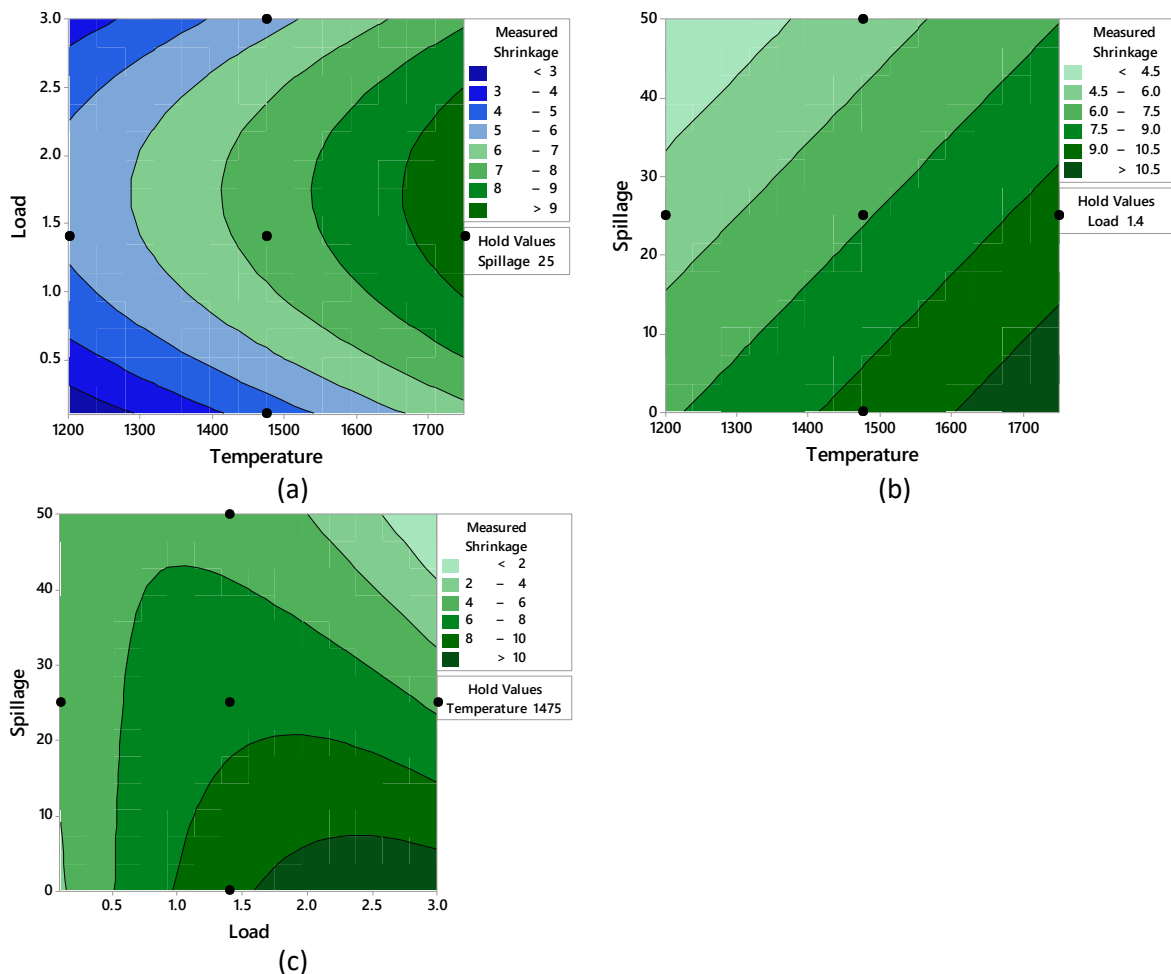
Figure 6-10: Contour plots of measured shrinkage vs load, temperature (a), spillage, temperature (b) and spillage, load (c).

Table 6-12: Pivot table of average measured shrinkage data in response to load and temperature.

Average of Measured Shrinkage	Temperature					
Load	1200	1310	1475	1640	1750	Average
0.10			4.90			4.90
0.17		3.70		5.45		4.58
1.40	1.95		7.85		10.60	7.46
2.00		7.30		7.20		7.25
3.00			5.80			5.80
Average	1.95	5.50	7.23	6.33	10.60	6.54

Figure 6-10 (b) is the contour plot of spillage and temperature with a constant load. As the amount of spillage increases with temperature, the amount of measured shrinkage decreases. The pivot table of average measured shrinkage in response to the amount of spillage and temperature, in Table 6-13, corresponds to the contour plot.

This can be explained by the composition of the spillage. Spillage contains already reacted products. With the addition of spillage, the concentration of reacted products increases. This leads to a decrease in the amount of non-reacted material that can potentially react and shrink.

Table 6-13: Pivot table of average measured shrinkage data in response to spillage and temperature.

Average of Measured Shrinkage	Temperature					
Spillage	1200	1310	1475	1640	1750	Average
0			8.90			8.90
10		6.15		7.90		7.03
25	1.95		7.15		10.60	6.93
40		4.85		4.75		4.80
50			6.00			6.00
Average	1.95	5.50	7.23	6.33	10.60	6.54

From the Pareto chart in Figure 6-4, spillage and load have a statistically significant effect on the measured shrinkage. The contour plot of spillage and load with a constant temperature in Figure 6-10 (c) shows an increase in shrinkage with an increase in load. With the addition of spillage, the measured shrinkage decreases. The combination of spillage and load shows that the maximum shrinkage was obtained with a higher load and no spillage.

Table 6-14: Pivot table of average measured shrinkage data in response to spillage and load.

Average of Measured Shrinkage	Load					
Spillage	0.10	0.17	1.40	2.00	3.00	Average
0			8.90			8.90
10		4.40		9.65		7.03
25	4.90		7.46		5.80	6.93
40		4.75		4.85		4.80
50			6.00			6.00
Average	4.90	4.58	7.46	7.25	5.80	6.54

The contour plots of LVDT shrinkage in Figure 6-11 correspond to the contour plots of measured shrinkage in Figure 6-10. The same trends are visible when comparing the different plots to each other.

The pivot tables of LVDT shrinkage in response to the variables are given in Table 6-15, Table 6-16 and Table 6-17. The data is similar to that of the measured shrinkage with a small difference in values.

(a)

(b)

(c)
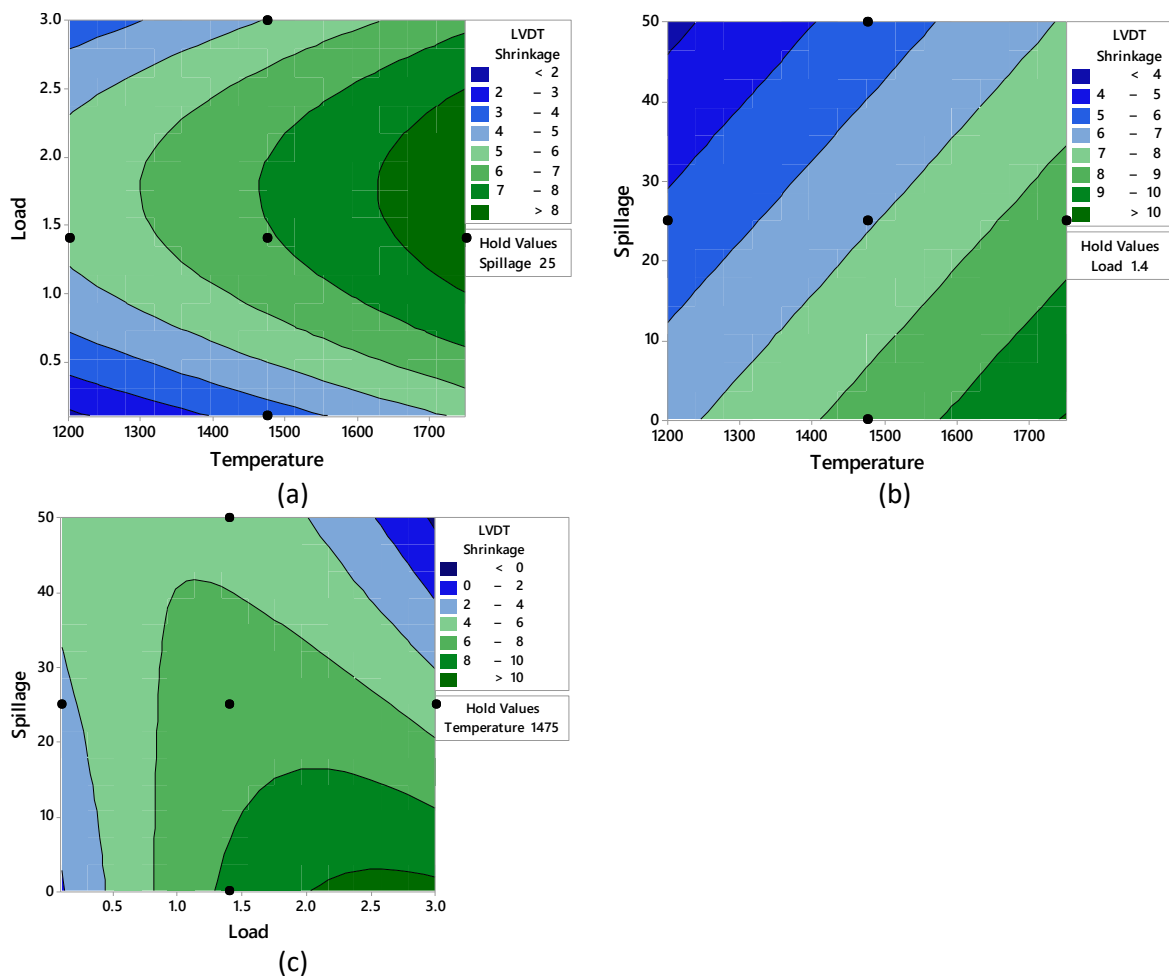
Figure 6-11: Contour plots on shrinkage measured by LVDT vs load, temperature (a), spillage, temperature (b) and spillage, load (c).

Table 6-15: Pivot table of average LVDT shrinkage data in response to load and temperature.

Average of LVDT Shrinkage	Temperature					
Load	1200	1310	1475	1640	1750	Average
0.10			3.50			3.50
0.17		3.33		4.10		3.71
1.40	1.91		7.42		10.15	7.07
2.00		7.06		6.20		6.63
3.00			5.40			5.40
Average	1.91	5.20	6.68	5.15	10.15	5.94

Table 6-16: Pivot table of average LVDT shrinkage data in response to spillage and temperature.

Average of LVDT Shrinkage	Temperature					
Spillage	1200	1310	1475	1640	1750	Average
0			7.15			7.15
10		5.91		6.07		5.99
25	1.91		6.71		10.15	6.54
40		4.48		4.23		4.36
50			6.04			6.04
Average	1.91	5.20	6.68	5.15	10.15	5.94

Table 6-17: Pivot table of average LVDT shrinkage data in response to spillage and load.

Average of LVDT Shrinkage	Load					
Spillage	0.10	0.17	1.40	2.00	3.00	Average
0			7.15			7.15
10		3.07		8.91		5.99
25	3.50		7.23		5.40	6.54
40		4.36		4.35		4.36
50			6.04			6.04
Average	3.50	3.71	7.07	6.63	5.40	5.94

6.2.4. CHEMICAL

A chemical analysis was done by Vametco on all the reacted laboratory pellets that formed part of the CCD experiments. The pellets were divided into an outer and an inner part. The average elemental weight percentage of the inner and outer parts was calculated and plotted against the reaction temperature.

The surface plots presented in Figure 6-12 are based on the same empirical model as discussed in section 6.2. Plot (a) shows the effect of temperature and spillage on the amount of vanadium. The

vanadium concentration increased with an increase in temperature. An increase in the amount of spillage caused a slight decrease in the vanadium concentration.

The nitrogen vs temperature and spillage plot in Figure 6-12(b) shows the nitrogen content initially increased to a maximum and then decreased with increasing temperature. As nitrogen concentration decreased, the carbon content increased.
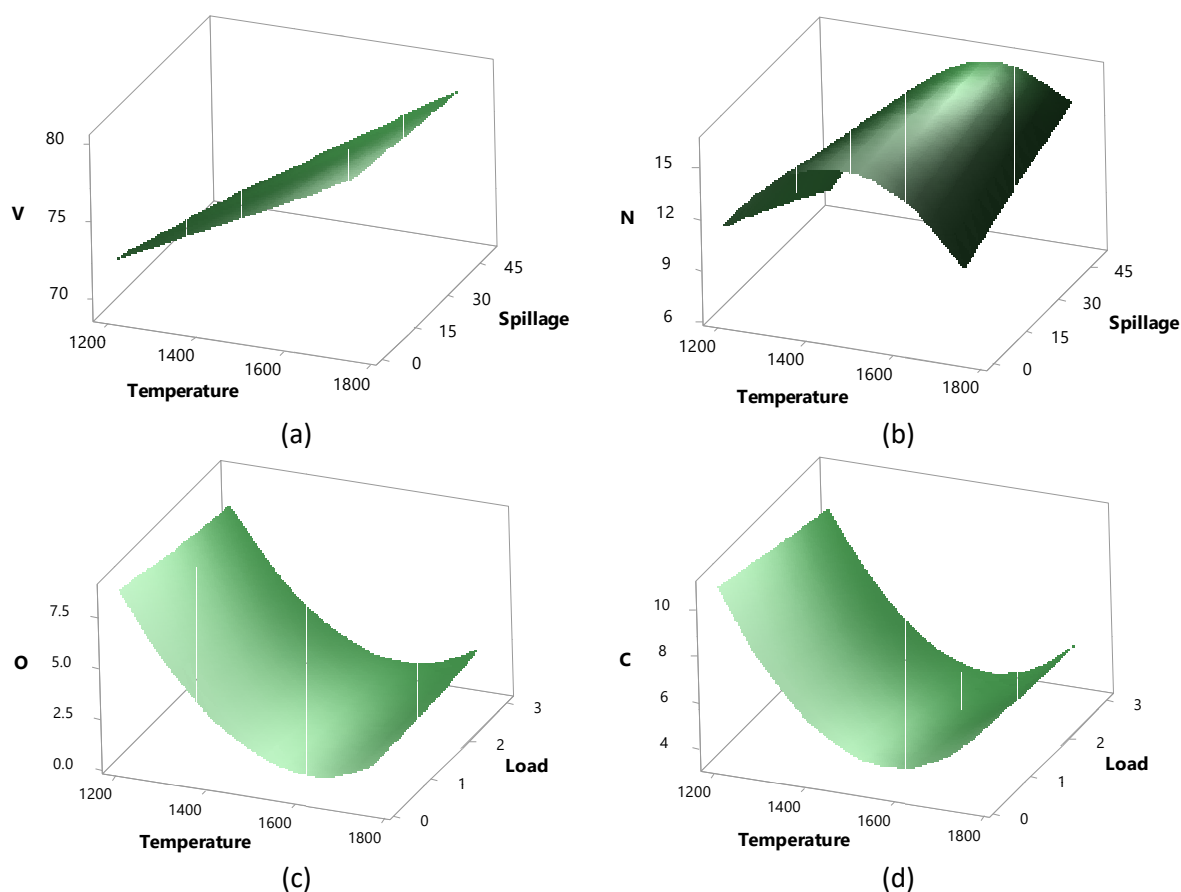
Figure 6-12: Surface plots of vanadium (a), nitrogen (b), oxygen (c) and carbon (d) vs Load, Temperature.

The mass percentage of nitrogen versus temperature is plotted in Figure 6-14. The average nitrogen content was calculated for each temperature range and a trendline fitted to the calculated averages. The trendline indicates an increase in nitrogen content with an increase in temperature. Note that the equation displayed on this graph is not the actual empirical equation describing the reaction, but rather the general trend of the reaction. The elemental increase with temperature is asymptotic and dependent on other chemical components in the system.
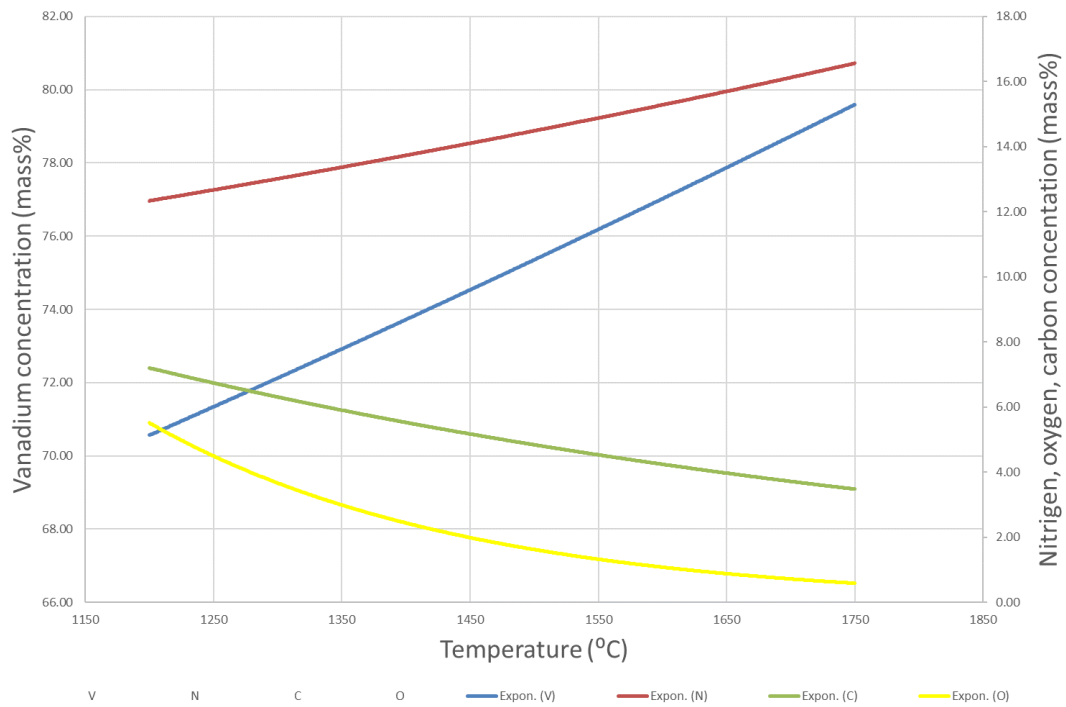
Figure 6-13: Chemical concentration vs temperature .
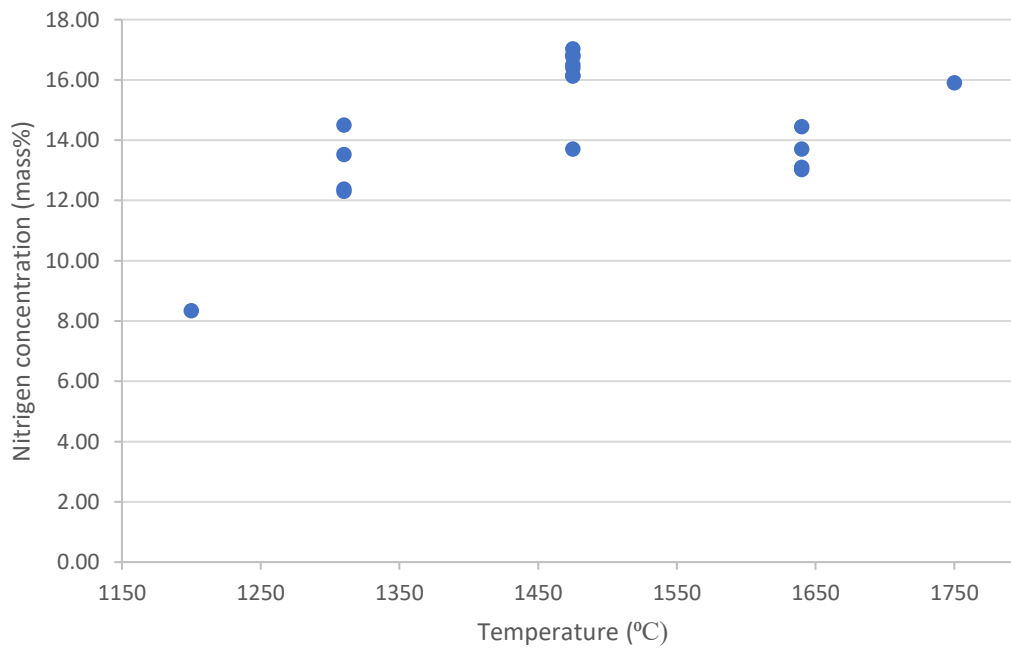
Figure 6-14: Plot of Nitrogen content versus. temperature

As the temperature increased in the system, the amount of carbon decreased in the final product.

The carbon in the raw pellets acted as reducing agent for the oxides in the system. The carbon reacted

with the available oxygen and formed CO at elevated temperatures. The asymptotic decrease of carbon in the products was dependent on the available oxygen in the system Figure 6-15.

The vanadium content in the product will increase with a decrease in both carbon and oxygen with an increase in reaction temperature. According to the reduction reaction, carbon reacts with the oxide to form CO resulting in a decrease in both carbon and oxygen. Assuming that no other oxides are present in the system, the sum of the carbon and oxygen decrease must add up to the vanadium increase as can be seen in Figure 6-17. This increase is asymptomatic and is limited by the availability of oxygen and carbon.
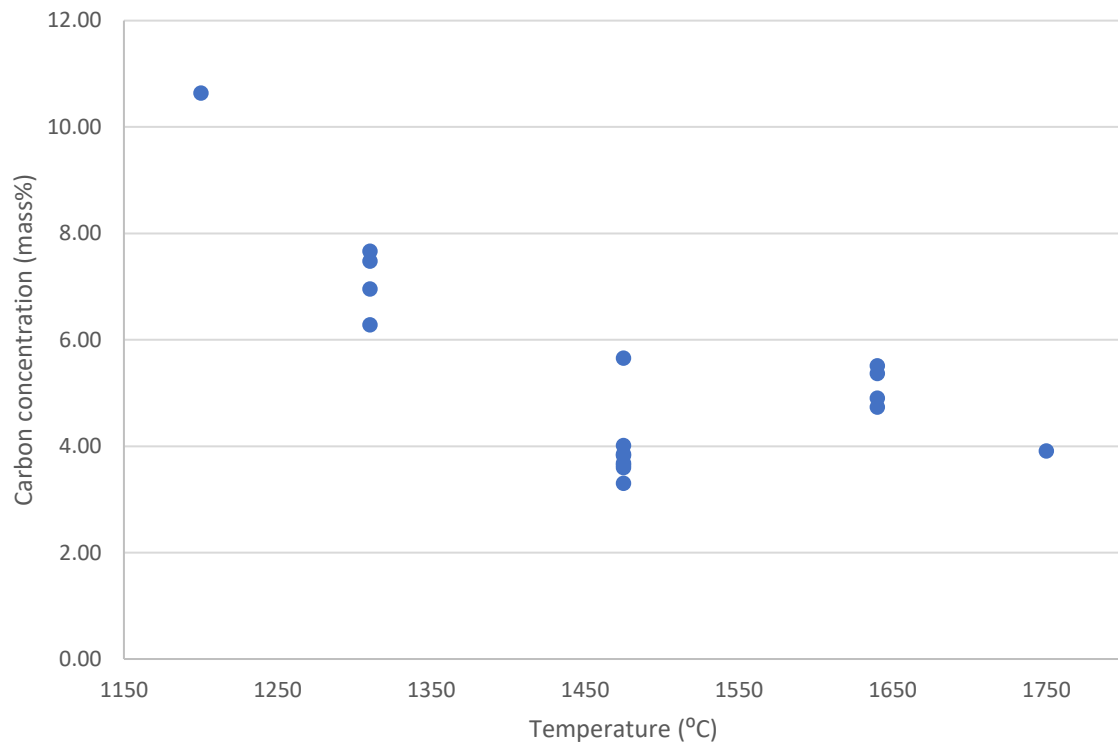
Figure 6-15: Plot of carbon content versus temperature.
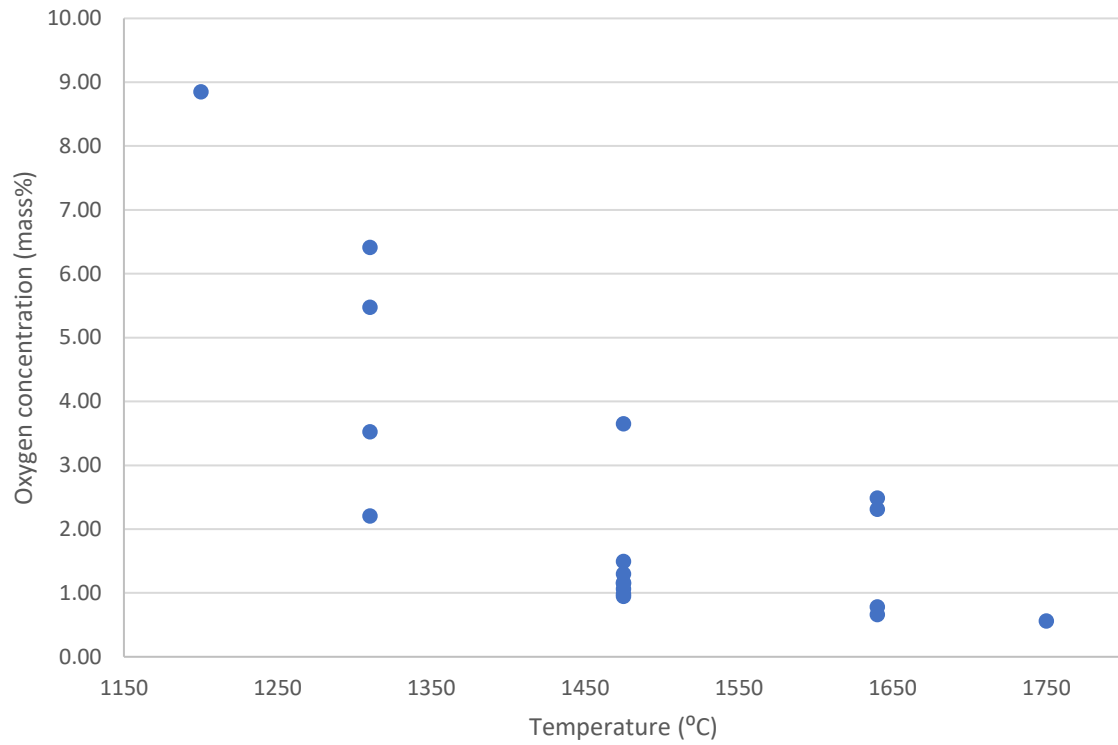
Figure 6-16: Plot of Oxygen content versus temperature.
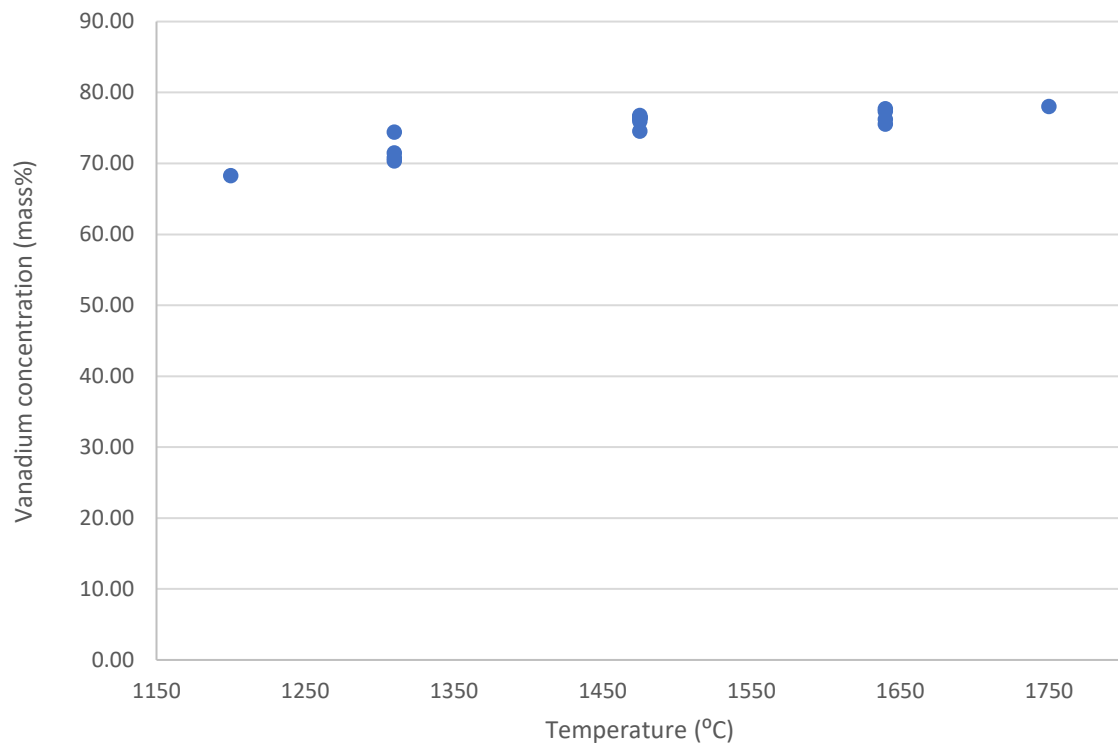
Figure 6-17: Plot of vanadium content versus temperature.

The plots in the above-mentioned figures are an indication of the kinetics that drive the reaction. From a thermodynamic point of view, the reactions are feasible at all reasonable temperatures. Kinetically, the reaction rate is faster elevated temperatures.

6.3. INDUCTION FURNACE WITH CONSTANT LOAD

The induction furnace with constant load experiment was executed as described in section 5.3.2.2 and the results are presented below. The aim of this experiment was to determine to what extent the impurities influence the fusion of the briquettes to each other.

The factors for this experiment are listed in Table 6-18. The measured response for these experiments was the shear force needed to separate the pellets and a chemical analysis on the reacted pellets.

Table 6-18: Factors and levels for the induction furnace factorial design.

Factor	Name	Low	High
A	Temperature	1200 ^{0}C	1400 ^{0}C
B	Time	30 min	60 min
C	Insoluble Impurities	0 wt% Fe	1 wt% Fe
D	Soluble Impurities	0 wt% NaO	1 wt% NaO

6.3.1. SHEAR

The shear force was determined as described in section5.7. The analysis of variance in Table 6-19 show a statistical significance for all the linear factors excluding soluble impurities.

Table 6-19: Analysis of variance with shear as response.

Source	DF	Adj SS	Adj MS	F-Value	P-Value
Model	16	29.4974	1.8436	37.71	0.002
Linear	4	19.0505	4.7626	97.41	0.000
Temp	1	13.7357	13.7357	280.93	0.000
Time	1	0.5402	0.5402	11.05	0.029
Insol	1	4.7745	4.7745	97.65	0.001
Sol	1	0.0000	0.0000	0.00	0.982
2-Way Interactions	6	8.0489	1.3415	27.44	0.003
Temp*Time	1	0.1633	0.1633	3.34	0.142
Temp*Insol	1	0.8871	0.8871	18.14	0.013
Temp*Sol	1	1.8985	1.8985	38.83	0.003
Time*Insol	1	0.3326	0.3326	6.80	0.060
Time*Sol	1	0.4907	0.4907	10.04	0.034

Insol*Sol	1	4.2768	4.2768	87.47	0.001
3-Way Interactions	4	1.7755	0.4439	9.08	0.028
Temp*Time*Insol	1	0.1875	0.1875	3.84	0.122
Temp*Time*Sol	1	0.1924	0.1924	3.93	0.118
Temp*Insol*Sol	1	0.6803	0.6803	13.91	0.020
Time*Insol*Sol	1	0.7153	0.7153	14.63	0.019
4-Way Interactions	1	0.0269	0.0269	0.55	0.499
Temp*Time*Insol*Sol	1	0.0269	0.0269	0.55	0.499
Curvature	1	0.5956	0.5956	12.18	0.025
Error	4	0.1956	0.0489		
Total	20	29.6930			

From the model summary in Table 6-20 the goodness-of-fit was determined. The proposed model has a high R-sq value and indicated that the model is a good fit to the data.

Table 6-20: Model summary with shear as response.

S	R-sq	R-sq(adj)	R-sq(pred)
0.221119	99.34%	96.71%	*

The regression equation for shear is given below.

Shear = -12.17 + 0.01014 Temp - 0.0607 Time - 5.55 Insol + 8.14 Sol   (6.25)
+ 0.000051 Temp*Time + 0.00462 Temp*Insol - 0.00689 Temp*Sol
+ 0.108 Time*Insol + 0.114 Time*Sol - 17.59 Insol*Sol
- 0.000090 Temp*Time*Insol - 0.000092 Temp*Time*Sol
+ 0.01317 Temp*Insol*Sol + 0.199 Time*Insol*Sol
- 0.000109 Temp*Time*Insol*Sol - 0.395 Ct Pt

A Pareto chart was used to determine the magnitude and the importance of the effects. On the Pareto chart, bars that cross the reference line are statistically significant. The reference line for statistical significance depends on the significance level. For all the represented data α = 0.05t.
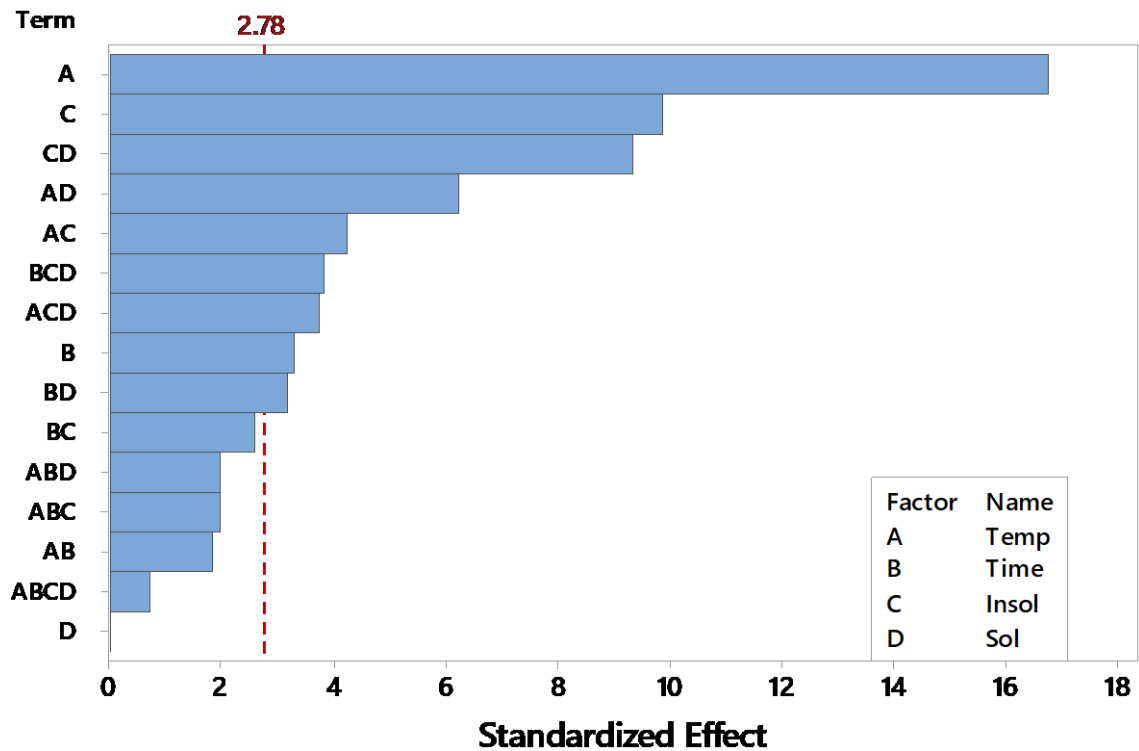
Figure 6-18: Shear Pareto chart of the standardized effect (response is shear, α = 0.05).

The Pareto chart in Figure 6-18 shows all the factors and combination of factors that are statistically significant on the shear force needed to separate the pellets after reaction. Temperature has the principal effect on shear followed by insoluble impurities. It was determined that the factor of time also shows a statistically significant effect.

The main effects plots of shear in Figure 6-19 confirms that temperature and insoluble impurities had a significant influence.
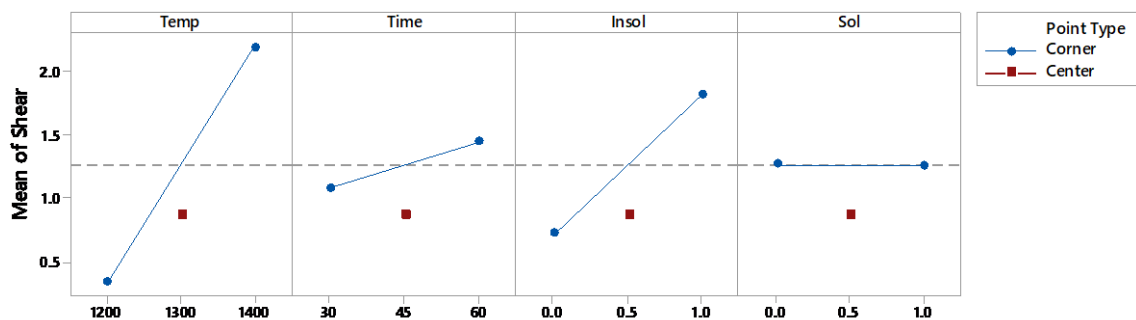
Figure 6-19: Main effects plot for shear - fitted means.

The interaction plots for shear in Figure 6-20 shows that all the factors interact with one another to some extent. Nonparallel lines indicate that an interaction occurred. The more nonparallel the lines are, the greater the strength of the interaction.
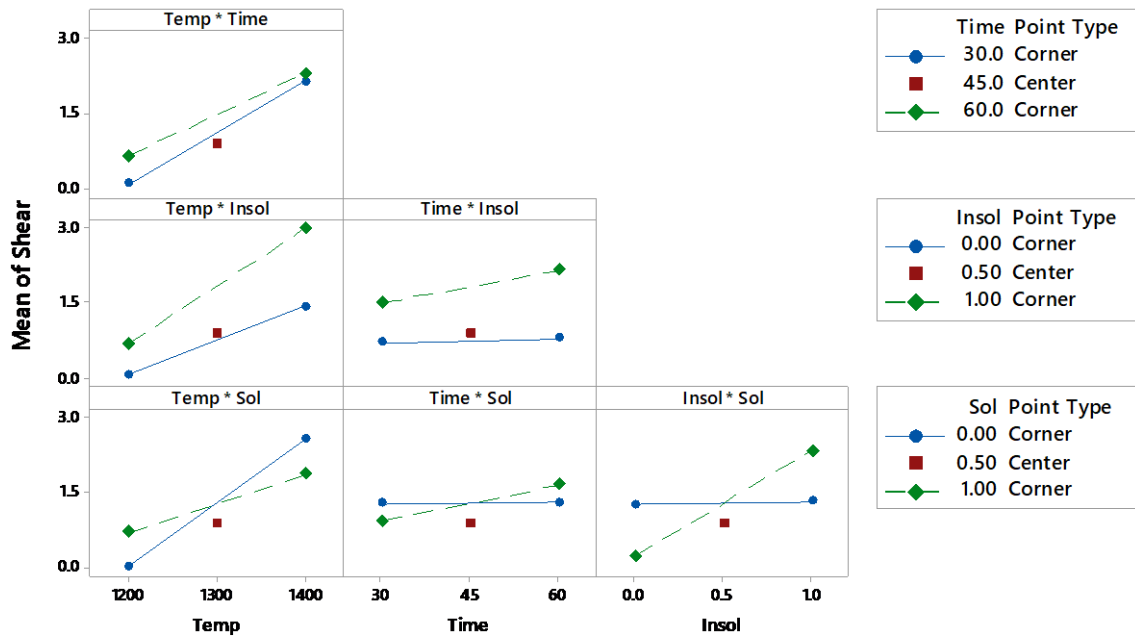
Figure 6-20: Interaction plot for shear - fitted means.

From Figure 6-21, with increased temperature, the shear force also increased. Time had little effect on shear.
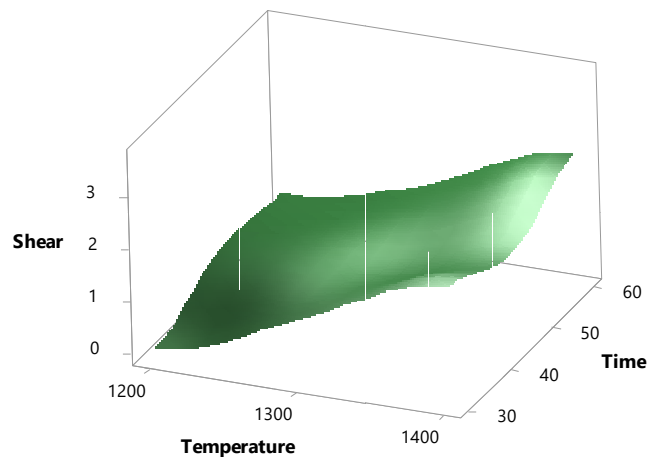
Figure 6-21: Surface plot of shear vs time, temperature.

The surface plot of shear versus temperature and insoluble impurities in Figure 6-22 shows that with increased temperature and insoluble impurities, the shear also increased.
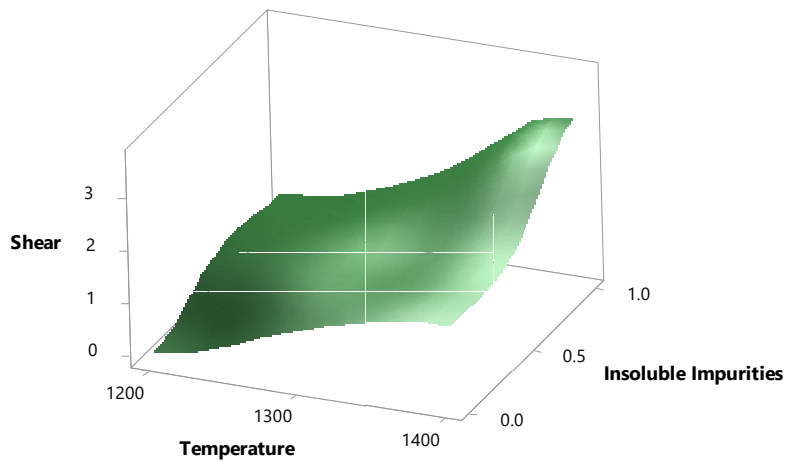
Figure 6-22: Surface plot of shear vs insoluble impurities, temperature.

6.3.2. CHEMICAL

The chemical data represented in Figure 6-23 shows that with an increase in temperature, both vanadium and nitrogen contents increased. Oxygen and carbon concentrations decreased with increased temperature.

Retention time had little influence on the chemical compositions at high temperatures, but at low temperature the retention time had a notable influence. At 1200 °C, a longer retention time caused an increase in vanadium and nitrogen concentrations and a decrease in carbon and oxygen concentrations.

(a)　　　　　　　　　　(b)

(c)   (d)
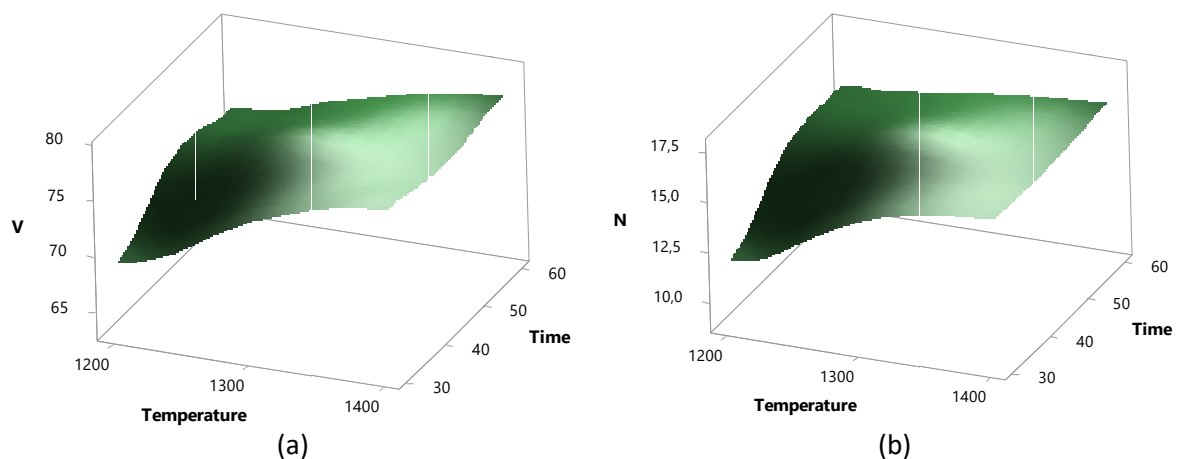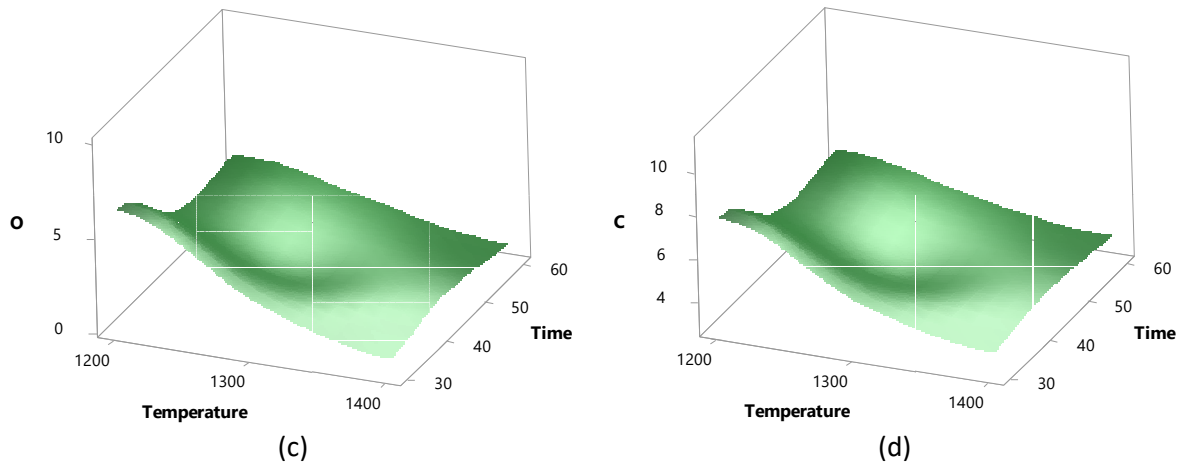
Figure 6-23: Surface plots of vanadium (a), nitrogen (b), oxygen (c) and carbon (d) vs Load, Temperature.

6.4.   COAL ASH FUSIBILITY FURNACE

A laboratory pellet was placed inside the furnace and heated to 1600 °C. From the images taken, it is known that no visible changes take place before 1200 °C. From this temperature, the pellet showed evidence of expansion. The maximum expansion was noted to be at a temperature of 1370 °C. Thereafter the pellets shrank until the last image taken at 1600 °C. Figure 6-25 and Figure 6-26 shows the expansion and shrinkage of the laboratory pellets. A video link of this experiment is available at:

https://youtu.be/a-ng2RTPxI4

 (Scan this QR code for a direct link the video)

(a)   (b)   (c)
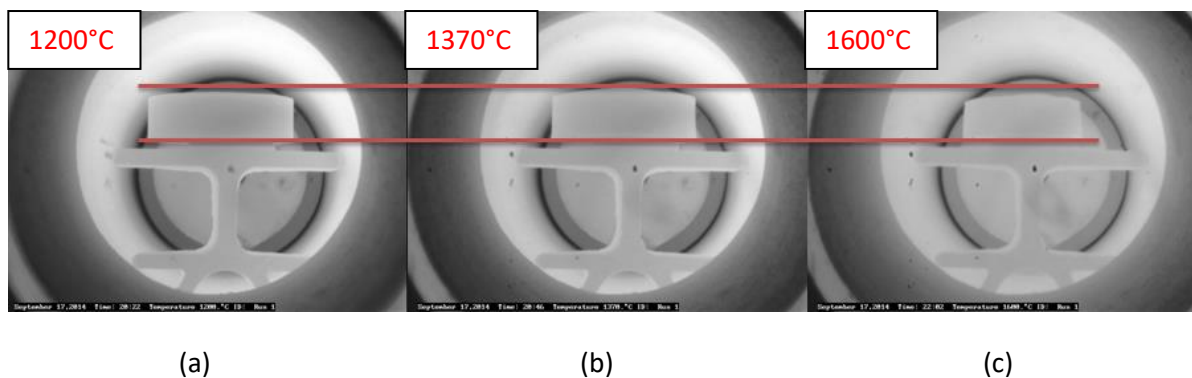
Figure 6-24: Axial shrinkage of laboratory pellets.
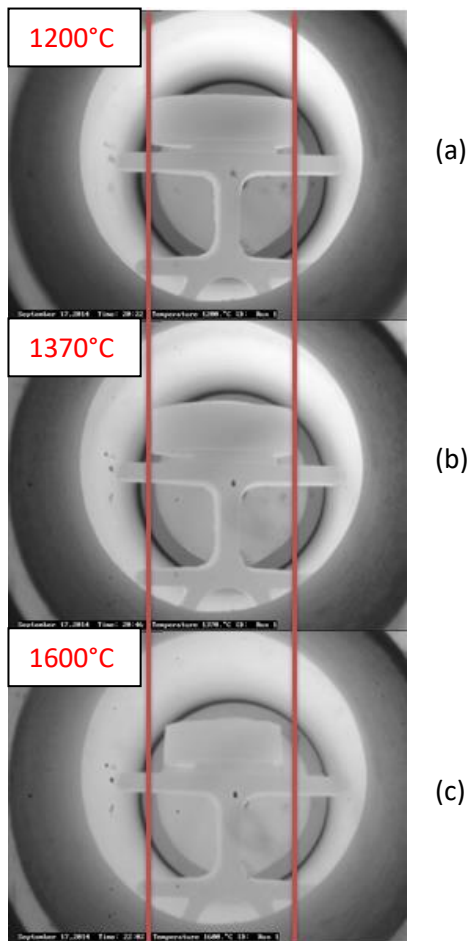
Figure 6-25: Radial shrinkage of laboratory pellets.

The same test was done on a briquette supplied by Vametco. The same expansion and shrinkage pattern were observed during the reaction of this briquette. Maximum expansion was noted at a temperature of 1370 °C and thereafter the briquette shrank until the maximum temperature of 1600 °C. .   A video link of this experiment is available at: https://youtu.be/69xPPznvXWQ

(Scan this QR code for a direct link the video)
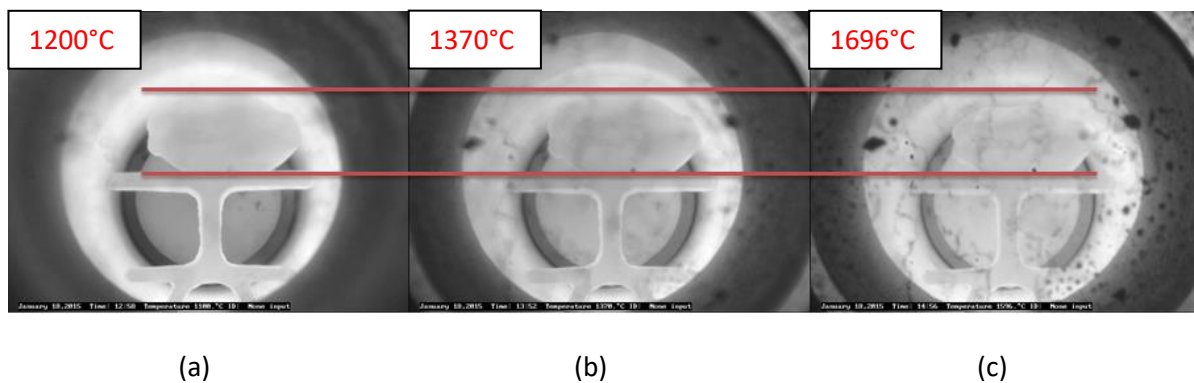
Figure 6-26: Axial shrinkage of laboratory pellets.
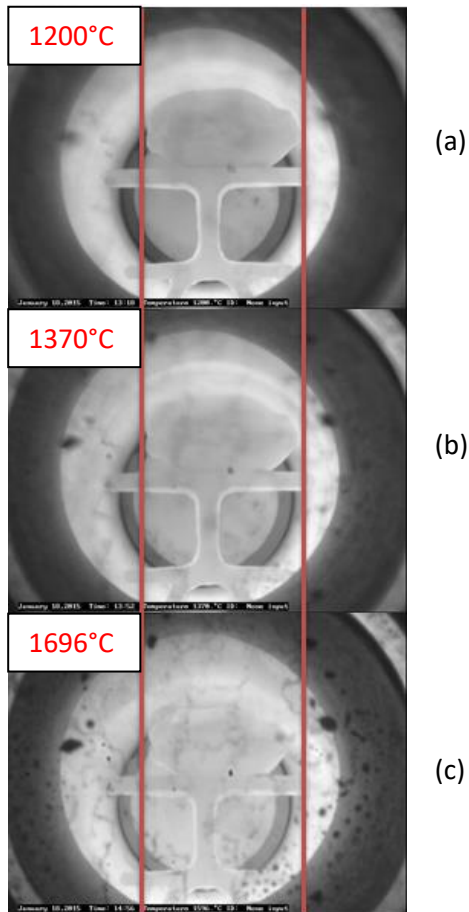
Figure 6-27: Radial shrinkage of Vametco briquettes.

At high reaction rates, gas may cause the pellet/briquette to expand. The exact mechanism of the expansion is unknown. This expansion will cause a reduction in the already limited space at the start of the reaction zone. Before the reaction zone, the briquettes experience a significant axial load exerted from the briquettes above. A combination of the axial forces from above and the radial forces from the expanding neighbouring briquettes may possibly force the mass into an effective bridge and potential plug.

It is worth mentioning that it was noted during test with the briquettes from Vametco that an accumulation formed on the window of the furnace. This can be seen in Figure 6-27. This is indicative of a higher impurity level in the production briquettes than in the lab produced pellets.

6.5. TUBE FURNACE

The tube furnace experiment was executed as described in section 5.5.3 and the results are presented below. The aim of the experiment was the evaluate to sintering of the pellets.

The factors for this experiment are listed in Table 6-21. The response to this experiment was the amount of sintering as determined by image analysis.

The percentage area calculated is the area occupied by product in the micrographs. This percentage was determined as described in section 5.5.4.

Table 6-21: Factors and levels for the tube furnace factorial design.

Factor	Name	Low	High
A	Temperature	1200 ⁰C	1400 ⁰C
B	Time	30 min	60 min
C	Insoluble Impurities	0 wt% Fe	1 wt% Fe
D	Soluble Impurities	0 wt% NaO	1 wt% NaO

The Analysis of variance in Table 6-22 show that temperature, time and insoluble impurities had a statistically significant influence on the amount of sintering.

Table 6-22: Analysis of variance with %Area as response.

Source	DF	Adj SS	Adj MS	F-Value
Model	15	1164.45	77.630	35.56
Linear	4	571.66	142.916	65.47
Temperature	1	237.48	237.479	108.79
Time	1	96.92	96.919	44.40
Insoluble Impurities	1	21.26	21.262	9.74
Soluble Impurities	1	14.88	14.876	6.81
2-Way Interactions	6	15.49	2.581	1.18
Temperature*Time	1	7.35	7.354	3.37
Temperature*Insoluble Impurities	1	4.14	4.143	1.90
Temperature*Soluble Impurities	1	5.40	5.396	2.47
Time*Insoluble Impurities	1	3.99	3.989	1.83
Time*Soluble Impurities	1	2.79	2.788	1.28
Insoluble Impurities*Soluble Impurities	1	0.24	0.238	0.11
3-Way Interactions	3	15.34	5.112	2.34
Temperature*Time*Insoluble Impurities	1	0.06	0.056	0.03
Temperature*Time*Soluble Impurities	1	1.13	1.132	0.52
Time*Insoluble Impurities*Soluble Impurities	1	9.22	9.225	4.23
4-Way Interactions	1	9.79	9.789	4.48
Temperature*Time*Insoluble Impurities*Soluble Impurities	1	9.79	9.789	4.48
Curvature	1	0.20	0.198	0.09
Error	3	6.55	2.183	

Source		P-Value
Total	18	1171.00
Model		0.007
Linear		0.003
Temperature		0.002
Time		0.007
Insoluble Impurities		0.052
Soluble Impurities		0.080
2-Way Interactions		0.483
Temperature*Time		0.164
Temperature*Insoluble Impurities		0.262
Temperature*Soluble Impurities		0.214
Time*Insoluble Impurities		0.269
Time*Soluble Impurities		0.341
Insoluble Impurities*Soluble Impurities		0.763
3-Way Interactions		0.251
Temperature*Time*Insoluble Impurities		0.883
Temperature*Time*Soluble Impurities		0.523
Time*Insoluble Impurities*Soluble Impurities		0.132
4-Way Interactions		0.124
Temperature*Time*Insoluble Impurities*Soluble Impurities		0.124
Curvature		0.783
Error		
Total		

The model summary in Table 6-23 indicates that the model is a good fit with a r-squared value of 99.44%.

Table 6-23: Model summary with %Area as response.

S	R-sq	R-sq(adj)	R-sq(pred)
1.47750	99.44%	96.64%	*

The regression equation for %Area is given below. The %Area refers to the area covered by material over the whole area of the pellet exposes to the lens. The greater the area covered, the larger the

amount of sintering that took place. i.e. for solid material the %Area would tend to 100% and will decrease as the porosity of the material increases.

%Area = 27.149 + 9.035 Temperature + 4.143 Time + 2.703 Insoluble Impurities (6.26)
+ 1.364 Soluble Impurities - 0.959 Temperature*Time
+ 1.38 Temperature*Insoluble Impurities
+ 0.821 Temperature*Soluble Impurities
- 0.706 Time*Insoluble Impurities - 0.979 Time*Soluble Impurities
+ 0.173 Insoluble Impurities*Soluble Impurities
+ 0.100 Temperature*Time*Insoluble Impurities

The Pareto chart in Figure 6-28 indicates that temperature and time had a statistically significant influence on sintering with the 95% confidence interval plotted as the 3.18 line.
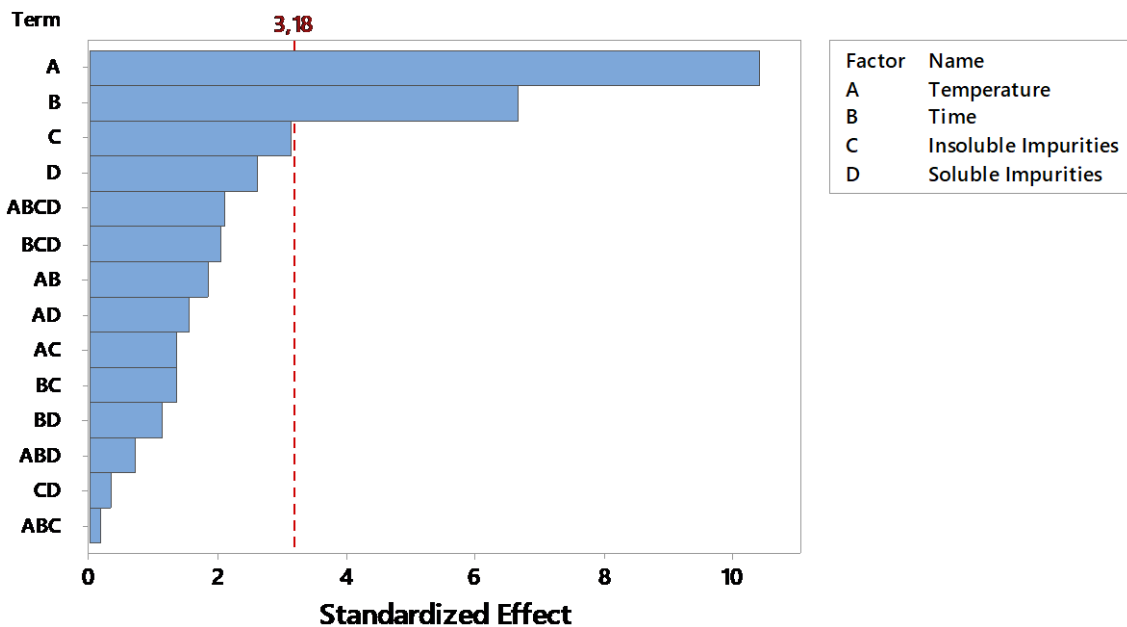
Figure 6-28: Percentage Area Pareto chart of the standardized effect (response is % Area, α = 0.05).

Temperature, time, insoluble impurities and soluble impurities had an influence on the amount of sintering, with temperature as the leading influencer. Only temperature and time had a statistically significant influence. This is evident in the main effects plotted in Figure 6-29 .
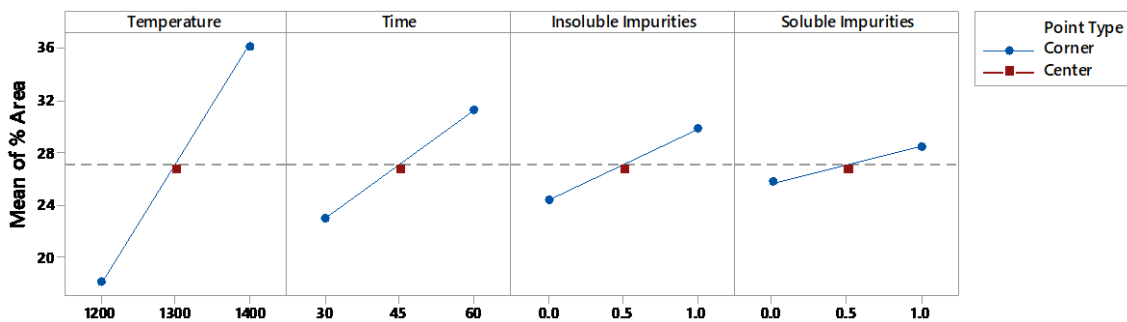
Figure 6-29: Main effects plot for % Area - fitted means.

From the surface plot in Figure 6-30, the % area increased with an increase in temperature and time. It can be concluded that the amount of sintering is directly related to temperate and residence time at temperature
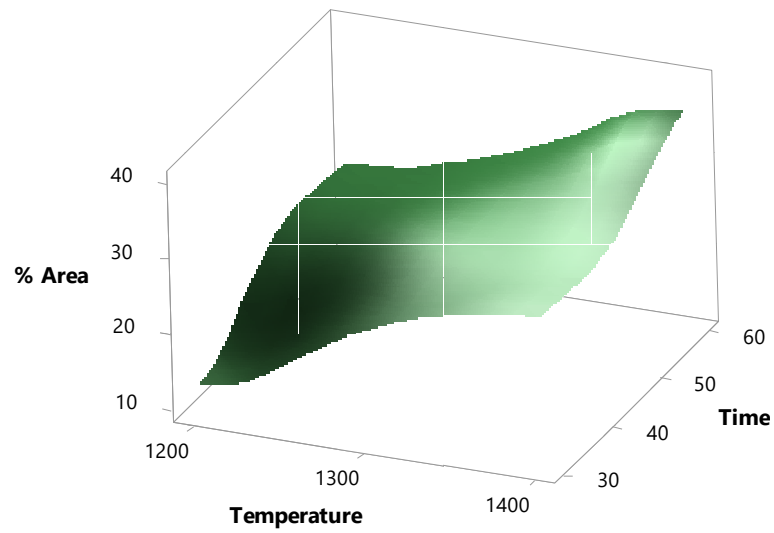
Figure 6-30: Surface plot of % Area vs time, temperature.

CHAPTER 7:

DISCUSSIONS

7. DISCUSSION

7.1. FURNACE LINER WEAR

The graphite furnace liner experiences high erosion. The erosion can be attributed to both physical and chemical wear.

The Vametco induction tube furnace is lined with 100 mm thick solid graphite. The liners are inserted as pipe sections on top of each other. The sections fit into each other with a male to female configuration.

The furnace is charged with raw briquettes from the top. The furnace is discharged from the bottom with mechanical valves. The briquettes move down the furnace due to gravity and due to the shrinkage of the lower pellets.

The physical wear on the liner is abrasive wear due to the movement of the briquettes down the furnace shaft. The physical wear can contribute to the progressive graphite loss from the surface of the solid graphite liner as a result of the relative movement of the briquettes past the liner. The hardness and sharpness of the conveyed materials' contact angle and contact pressure affects the extent of abrasive wear. It has been observed that this local progressive diameter increase causes a bowl effect in the graphite tube.

The significance of this bowl effect is not only the cost of liner replacement, but this effect is believed to contribute to the formation of plugs or bridging within the furnace. When the briquettes enter the bowled section of liner, briquettes fill the increased volume. As the lower briquettes move down the furnace, a gap is created between the end of the bowl, where the liner is less eroded, and the lower briquettes that is continues moving down. As with two lane traffic merging into one lane, the briquettes struggle to move past each other and essentially create a "traffic jam" within the furnace.

A further contributor to this traffic jam inside the furnace is the phenomenon of expanding briquettes as described in section 6.4. As the briquettes expand in volume, the already closely packed briquettes are forced in all directions. With limited space to move, the briquettes have nowhere to go and are forced into gridlock. The expanding briquettes also contribute to more aggressive furnace liner wear increasing the possibility of the bowl effect. Expanding briquettes also occur in the blast furnace [61]. The expansion can be explained by the ongoing changes in the crystal structure and gas evolution through the briquette producing cracks causing volume expansion.

The chemical erosion of the furnace liner can be attributed to the attack of the graphite by hydrogen and oxygen. Residual ammonia in the feed will undergo cracking in the shaft furnace which will yield free hydrogen and nitrogen. The hydrogen might react with the graphite to form hydrocarbons.

Although the nitrogen gas used for the reaction is relatively pure, minor amounts of oxygen enter the furnace with the nitrogen gas. From the post-mortem analysis, blow holes were observed on the liner edges where two liner join together. The theory is that gas escapes the furnace between the liner joints and form blow holes in the joints.

A sample of a white accumulation in the off-gas system of the laboratory induction furnace was analysed using XRD. The build-up consisted of $CaMg(CO_3)_2$, $Na_2Mg(CO_3)_2$, $NaCl$ and $Na_2(CO_3)$. The diffraction pattern is in Appendix D. This is proof that volatile alkalis exist within the furnace.

It is known that alkalis catalyse the Boudouard reaction [62]. The presence of alkalis in the shaft furnace will contribute to the chemical erosion and degradation of the graphite liner. NaV_6O_{15} was detected on the sampled liner indicating the presence of alkalis. The alkalis enter the furnace in the feed material and originate from the leaching process. The alkali compounds are volatile and tend to recirculate resulting in a build-up even if the concentration of the incoming briquettes is very low.

The alkali compounds volatilise in the hottest zones in the furnace and get carried upwards by the gas stream. At lower temperatures they condense onto the briquettes which then carry the alkali downwards into the hot zones. In this way the alkalis are trapped in the furnace and the concentration builds up.

7.2. SINTERING AND DIMENSIONAL CHANGES

When thermal energy is applied to a compacted powder, the powder densifies and the average grain size increases. This usually results in the shrinkage of the initial (green) volume [53][54].

In the experimental set using the induction furnace with a variable load, it was determined that the amount of spillage influences the shrinkage of the reacted pellets. Using a statistical model, spillage was determined to have a significant effect on the shrinkage of the pellets.

An increased amount of spillage decreased the overall shrinkage. Spillage contained already reacted products. From a test done in the coal ash fusibility furnace, it was observed that the reacted products did not shrink and only the unreacted material sintered and shrank during the reaction. With the addition of spillage, the amount of reacted products also increased which led to a decrease in the amount of materials that could potentially react and shrink.

The influence of temperature on shrinkage is statically significant according the statistical model. In general, an increase in temperature yielded an increase in the amount of shrinkage. An asymptote of maximum shrinkage exists at a temperature below the melting point.

From the sinter model in section 6.5, it was determined that temperature and time had a statistically significant effect on the sintering of pellets. An increase in temperature and retention time yielded an increase in sintering. The grains grew in size and the density of the pellets increased. This is in line with the findings of Kang [54] as to when thermal energy is applied to a compacted powder, the powder densifies and the average grain size increases. This usually results in the shrinkage of the initial (green) volume [53].

The driving force for sintering is the decrease of the total surface energy. The change in surface energy is due to densification and the change in surface area is due to grain coarsening. For solid state sintering, surface energy is related to the replacement of a solid/vapour surface by solid/solid interfaces [54].

From a visual inspection in the coal ash fusibility furnace, it was observed that both the laboratory pellets and industrial briquettes underwent expansion before shrinking.

At high reaction rates, gas may cause the pellet/briquette to expand. The exact mechanism of the expansion is unknown. This expansion will cause a reduction in the already limited space at the start of the reaction zone. Before the reaction zone, the briquettes experience a significant load due to the mass of briquettes in the upper section of the shaft furnace. A combination of the axial forces from above and the radial forces from the neighbouring, expanding briquettes may possibly key the mass in an effective bridge that can lead to plugging.

7.3.   FUSING (AGGLOMERATION) OF PELLETS

The fusion of pellets was observed in numerous experiments. Several factors, such as temperature, retention time, load and impurities affected the fusion of pellets. To quantify the fusion, a shear test was performed on the fused pellets.

In the induction furnace with a variable load experiments, none of the factors showed a statistically significant influence on the shear force. Load and temperature showed the highest probability of influence according the model.

The general trend of the model indicated that with increased load and temperature, the shear force needed to separate the pellets increased. The amount of spillage added did not have a notable influence in shear.

These results led to the conclusion that other factors may influence the fusion and the second induction furnace experiments were designed to eliminate unknown factors such as impurities and to keep the load constant. This experiment was done with a pure MVO. Sludge and barren were used to introduce impurities in a controlled way.

Induction furnace test runs with a constant load indicated that multiple factors had a statistically significant influence on the fusion of the pellets. The most significant factors influencing pellet fusion was found to be temperature and the presence of insoluble impurities. The degree of fusion increased as temperature and impurity levels increased. This was measured by the shear force required to separate the pellets.

It is however important to note that pellets without any impurities also fused, but to a lesser extent the pellets containing insoluble impurities.

Retention time had a statistically significant effect on the fusion strength of the reacted pellets. In comparison to the effects of temperature and insoluble impurities, the effect of retention time is small.

Soluble impurities, as a single factor, yielded no effect on the fusion strength between the pellets. The interaction of soluble impurities with other factors had an influence in accordance to the statistical model, but the contribution of the soluble impurities in the interaction effect is estimated to be small.

7.4. CHEMICAL

Vanadium carbonitride ($VC_{1-x}N_x$) is the solid solution of vanadium carbide and vanadium nitride which is completely miscible in each other [7]. Vanadium carbide and vanadium nitride are interstitial compounds with carbon or nitrogen atom vacancies resulting in unfilled nitrogen and carbon lattice sites in the vanadium carbonitride compound making it nonstoichiometric [43]. Vanadium carbonitride ($VC_{1-x}N_x$) might range from $VX_{0.75}$ to VX, where X is either nitrogen or carbon [1].

The chemical analysis on the pellets that was reacted in the induction furnace with a variable load showed a maximum nitrogen concentration at 1750 °C with a normalised stoichiometry of $VN_{0.78}C_{0.19}O_{0.03}$. The minimum nitrogen content was obtained at 1200 °C with a normalised stoichiometry of $VN_{0.30}C_{0.38}O_{0.32}$. This is observed in the nitrogen concentration vs temperature plot in Figure 6-14.

Nitrogen and vanadium concentrations showed a general increasing trend with an increase in temperature. Both carbon and oxygen concentrations decreased with increasing temperature.

The amount of spillage added to the pellets, influenced the chemistry of the reacted material. Increased amounts of spillage increased the nitrogen concentration and also increased the carbon concentration. Spillage is already reacted material. The available carbon is more than the available oxide in the standard Vametco mixture and will be left as free carbon in the pellet.

The applied load on the pellets had no influence on the chemistry of the reacted products. The load did not cause the pellets to compress in such a way that the porosity decreased to the point where nitrogen could not penetrate the centre of the pellets.

Due to the thermally activated reaction, the retention time had little influence on the chemical compositions at high temperatures. At low temperatures the reactions take place at a much slower reaction rate, therefore time is more important [52]. At 1200 °C, a longer retention time caused an increase in the vanadium and nitrogen concentrations and a decrease in carbon and oxygen concentrations. At higher temperatures the pellets were fully chemically reacted at the shortest retention time.

In the induction furnace with a constant load experiment, a normalised stoichiometry of $VN_{0.80}C_{0.18}O_{0.02}$ was obtained at a temperature of 1400 °C, retention time of 60 minutes and with no insoluble or soluble impurities. The lowest nitrogen content was recorded at a temperature of 1200 °C, retention time of 30 minutes with no insoluble or soluble impurities and had a normalised stoichiometry of $VN_{0.30}C_{0.37}O_{0.33}$.

Table 7-1: Time and temperature influence on stoichiometry.

Temperature (°C)	Time (min)	N	C	O
1200	30	0.30	0.37	0.33
1400	30	0.76	0.20	0.04
1200	60	0.42	0.33	0.25
1400	60	0.80	0.18	0.02

In Table 7-1 the normalised stoichiometric amounts of nitrogen, carbon and oxygen are given for 1200 °C and 1400 °C and 30 min and 60 min retention time. From this, it is evident that temperature and time have a significant influence on the chemistry. The degree of reaction is both temperature and time dependent. This is in line with research done by Ortega et.al. [48].

Although kinetic reaction data between metallic vanadium and nitrogen or ammonia is available, no data is available on the kinetics of carbonitride reduction of vanadium oxides. This can possibly be

explained by the complexity of the many intermediate reactions and the formation of carboxynitride carbonitride, oxycarbide, and oxynitride phases [52].

CHAPTER 8:

CONCLUSION

8.   CONCLUSION

A study has been conducted in the formation and sintering of vanadium carbonitride by heating a mixture of vanadium trioxide and carbon in a nitrogen atmosphere.

During the production of vanadium carbonitride, high erosion rates are observed on the graphite furnace liner and plugging occurs within the furnace that has a significant financial impact on Bushveld Vametco.

Evidence from a post-mortem study confirms the presence of alkali volatiles in the furnace which may cause chemical erosion of the liner. Although not confirmed due to the high oxidation states of the liner, ingress of oxygen is also likely to contribute to the erosion. Physical erosion of the liner can be speculated about, but no evidence of this was found in this study.

The Vametco briquettes undergo sintering during the heating process. In this study the extent of sintering was measured by the dimensional shrinkage of the pellets. It was found that the extent of sintering is dependent on the amount of already reacted material added to the mixture (spillage), reaction temperature, retention time and applied load. High amounts of spillage decrease the amount of sintering. With increased reaction temperature and time, an increase in sintering was observed. The amount of applied load to the pellets has shown an impact on the extent of shrinkage.

It is highly likely that cluster formation exacerbates plugging. Cluster formation is caused by reaction temperate, retention time, applied load and impurities. A shear testing was conducted to determine the extent of fusion between pellets. It was found that cluster formation is directly related to reaction temperature. Retention time, load and insoluble impurities have an influence on the bonding strength of the clusters. Laboratory pellets with no impurities formed clusters at 1200 °C with a retention time of 60 minutes and 1300 °C with a retention time of 30 minutes.

Another likely cause of plug formation in the furnace is the expansion of pellets and briquettes during the heating process. Expanding briquettes might cause a reduction in the already limited space in the furnace, causing a possible bridge to form or potentially a plug.

The optimal furnace operating temperature to avoid the formation of clusters is 1200 °C with a retention time of 30 minutes. Although this will be the ideal operating conditions to avoid cluster formation, it will have a significantly negative influence on the chemistry of the product.

Vanadium and nitrogen content increases with an increase in temperature and retention time.   To obtain a normalised stoichiometry of $VN_{0.80}C_{0.18}O_{0.02}$ a temperature of at least 1400 °C with a retention time of 60 minutes is needed. Although this is the optimum operation condition to ensure

a product that is high in both vanadium and nitrogen, the effect on cluster formation can be detrimental.

BIBLIOGRAPHY

[1]   J. H. Woodhead, "The Physical Metallurgy of Vanadium Steels," *Vanadium in High-Strength Steel*. pp. 3–10, 1979.

[2]   G. Bauer *et al.*, "Vanadium and Vanadium Compounds," *Ullmann's Encycl. Ind. Chem.*, pp. 1–22, Jun. 2000.

[3]   M. Gasik, "Chapter 13 – Technology of Vanadium Ferroalloys," in *Handbook of Ferroalloys*, 2013, pp. 397–409.

[4]   F. Cardarelli, "Less Common Nonferrous Metals," in *Materials Handbook*, vol. 8, no. 2, London: Springer London, 2000, pp. 338–343.

[5]   D. L. Harrod and R. E. Gold, "Mechanical properties of vanadium and vanadium-base alloys," *Int. Met. Rev.*, vol. 25, no. 4, pp. 163–221, 1980.

[6]   P. S. Mitchell, "The Use of Vanadium- A brief review," *Infacon 6*, vol. I, pp. 217–224, 1992.

[7]   C. K. Gupta and N. Krishnamurthy, *Extractive Metallurgy of Vanadium*. Amsterdam: Elsevier, 1992.

[8]   M. H. Kim and T. H. An, "A commercial V2O5-WO3/TiO2 catalyst used at an NH3-SCR deNOx process in an oil-fired power plant: cause of an increase in deNOxing and NH3 oxidation performances at low temperatures," *Res. Chem. Intermed.*, vol. 37, no. 9, pp. 1333–1344, 2011.

[9]   J. O. Nriagu, *Vanadium in the Environment, Part 1: Chemistry and Biochemistry*. John Wiley & Sons, Inc., 1998.

[10]   B. Rohrmann, "Vanadium in South Africa," *J. South African Inst. Min. Metall.*, vol. 85, no. 5, pp. 141–150, 1985.

[11]   U.S. Geological Survey, "Mineral Commodities Summaries 2017: U.S. Geological Survey," pp. 182–183, 2017.

[12]   R. P. Fischer, "Vanadium resources in titanoferous magnetite deposits," *U.S. Geol. Surv. Prof. Pap.*, vol. 926-B, 1975.

[13]   A. K. Suri, T. K. Mukherjee, and C. K. Gupta, "Aluminothermic process for the preparation of Ferromolybdenum and Ferrovanadium," pp. 200–209.

[14]   P. R. Taylor, S. A. Shuey, Edgar E. Vidal, W. Wang, and J. C. Gomez, "Extractive Metallurgy of Vanadium Containing Titaniferous Magnetite Ores : a Review," *2005 SME Annu. Meet.*, no. May, pp. 1–9, 2005.

[15]   C. D. Taylor, K. J. Schulz, J. L. Doebrich, G. J. Orris, P. D. Denning, and M. . Kirschbaum, "Bushveld_Igneous_Complex," *Geology and nonfuel mineral*

deposits of Africa and the Middle East, USGS Open-File Report, 2005. [Online].
Available:
https://commons.wikimedia.org/wiki/File:Bushveld_Igneous_Complex.png
#/media/File:Bushveld_Igneous_Complex.png. [Accessed: 28-Apr-2017].

[16] A. L. Guise-Brown and M. G. Atmore, "The recovery of vanadium pentoxide at Transvaal Vanadium (Pty) Ldt.," *J. South African Inst. Min. Metall.*, no. April, pp. 394–404, 1968.

[17] D. Chen, L. Zhao, Y. Liu, T. Qi, J. Wang, and L. Wang, "A novel process for recovery of iron, titanium, and vanadium from titanomagnetite concentrates: NaOH molten salt roasting and water leaching processes," *J. Hazard. Mater.*, vol. 244–245, pp. 588–595, 2013.

[18] W. S. Steinberg, W. Geyser, and J. Nell, "The history and development of the pyrometallurgical processes at Evraz Highveld Steel & Vanadium," in *Southern African Pyrometallurgy 2011*, 2011, no. March, pp. 63–76.

[19] X. J. X. S. Li, B. Xie, G. E. Wang, and X. J. X. S. Li, "Oxidation process of low-grade vanadium slag in presence of Na 2CO3," *Trans. Nonferrous Met. Soc. China (English Ed.*, vol. 21, no. 8, pp. 1860–1867, 2011.

[20] K.-J. Range, R. Zintl, and A. M. Heyns, "The Thermal Decomposition of Ammonium Metavanadate(V) in Open and Closed Systems," *Zeitschrift für Naturforsch. B*, vol. 43, no. 3, pp. 309–317, Jan. 1988.

[21] D. R. Lide, "CRC Handbook of Chemistry and Physics, 84th Edition, 2003-2004," *Handb. Chem. Phys.*, vol. 53, p. 4.93, 2003.

[22] E. F. Milan, "The Dissociation Pressure of Vanadium Pentoxide," *J. Phys. Chem.*, vol. 33, no. 4, pp. 498–508, Jan. 1928.

[23] R. J. H. Clark, *The chemistry of titanium and vanadium: An introduction to the chemistry of the early transition elements*, Volume 11. A,sterdam, sterdam: Elsevier Pub. Co., 1968.

[24] T. A. Mellan and R. Grau-Crespo, "Density functional theory study of rutile VO2 surfaces," *J. Chem. Phys.*, vol. 137, no. 15, p. 154706, Oct. 2012.

[25] "Timing nature's fastest optical shutter." [Online]. Available: https://phys.org/news/2005-04-natures-fastest-optical-shutter.html. [Accessed: 30-Apr-2017].

[26] J. B. Goodenough, "The two components of the crystallographic transition in VO2," *J. Solid State Chem.*, vol. 3, no. 4, pp. 490–500, 1971.

[27] N. Bahlawane and D. Lenoble, "Vanadium oxide compounds: Structure, properties, and growth from the gas phase," *Chem. Vap. Depos.*, vol. 20, no. 7–9, pp. 299–311, 2014.

[28] V. Ivanchenko and T. Pryadko, "Carbon – Iron – Vanadium," in *Landolt-Börnstein - Group IV Physical Chemistry*, vol. 11D2 (Iron, G. Effenberg and S. Ilyenko, Eds. Berlin, Heidelberg, Heidelberg: Springer Berlin Heidelberg, 2008, pp. 437–475.

[29] V. N. Lipatnikov, A. I. Gusev, P. Ettmayer, and W. Lengauer, "Phase transformations in non-stoichiometric vanadium carbide," *J. Phys. Condens. Matter*, vol. 11, no. 1, pp. 163–184, 1999.

[30] A. I. Gusev, "Phase equilibria, phases and compounds in the Ti-C system," *Russ. Chem. Rev.*, vol. 71, pp. 439–463, 2002.

[31] O. Carlson, A. Ghaneya, and J. Smith, "The C– V (Carbon-Vanadium) system," *Bull. Alloy Phase Diagrams*, vol. 6, no. 2, pp. 115–124, 1985.

[32] J. D. Venables, D. Kahn, and R. G. Lye, "Structure of the ordered compound V6C5," *Philos. Mag.*, vol. 18, no. 151, pp. 177–192, 1968.

[33] R. Pompe, "Some thermochemical properties of the system vanadium-nitrogen and vanadium-carbon-nitrogen in the temperature range 1000-1550°C," *Thermochim. Acta*, vol. 57, pp. 273–281, 1982.

[34] O. N. Carlson, J. F. Smith, and R. H. Nafziger, "The vanadium-nitrogen system: a review," *Metall. Mater. Trans. A*, vol. 17, no. 10, pp. 1647–1656, 1986.

[35] W. Lengauer and P. Ettmayer, "Physical and mechanical properties of cubic δ-VN1−x," *J. Less Common Met.*, vol. 109, no. 2, pp. 351–359, 1985.

[36] D. Potter and G. Altstetter, "Ordering of interstitial nitrogen in vanadium," *Acta Metall.*, vol. 19, no. 9, pp. 881–886, Sep. 1971.

[37] A. I. Gusev, A. A. Rempel, and A. J. Magerl, *Disorder and Order in Strongly Nonstoichiometric Compounds*, vol. 47. Berlin, Heidelberg: Springer Berlin Heidelberg, 2001.

[38] N. Kieda, N. Mizutani, and M. Kato, "Non-stoichiometry and phase equilibria of β-V2N and δ-VN," *J. Less Common Met.*, vol. 144, no. 2, pp. 293–299, Dec. 1988.

[39] P. K. Tripathy, "On the thermal decomposition of vanadium nitride," *J. Mater. Chem.*, vol. 11, pp. 1514–1518, 2001.

[40] P. K. Tripathy, A. Arya, and D. K. Bose, "Preparation of vanadium nitride and its subsequent metallization by thermal decomposition," *J. Alloys Compd.*, vol. 209, no. 1–2, pp. 175–180, 1994.

[41] Z. Zhao, Y. Liu, H. Cao, J. Ye, S. Gao, and M. Tu, "Synthesis of VN nanopowders by thermal nitridation of the precursor and their characterization," *J. Alloys Compd.*, vol. 464, no. 1–2, pp. 75–80, 2008.

[42]   B. Chicco, W. E. Borbidge, and E. Summerville, "Experimental study of vanadium carbide and carbonitride coatings," *Mater. Sci. Eng. A*, vol. 266, no. 1–2, pp. 62–72, 1999.

[43]   P. Cai, Z. Yang, C. Wang, P. Xia, and Y. Qian, "Synthesis of nanocrystalline VN via thermal liquid-solid reaction," *Mater. Lett.*, vol. 60, no. 3, pp. 410–413, 2006.

[44]   H. Ohtani and M. Hillert, "Calculation of V-C-N and Ti-C-N phase diagrams," *Calphad*, vol. 17, no. 1, pp. 93–99, 1993.

[45]   Bushveld Vametco Alloys, "Nitrovan MSDS," 2017.

[46]   R. Staśko, H. Adrian, and A. Adrian, "Effect of nitrogen and vanadium on austenite grain growth kinetics of a low alloy steel," *Mater. Charact.*, vol. 56, no. 4-5 SPEC. ISS., pp. 340–347, 2006.

[47]   D. L. Perry, *Handbook of inorganic compounds*, 2nd ed., vol. 33, no. 06. Boca Raton: Taylor & Francic Group, 1996.

[48]   A. Ortega, M. A. Roldan, and C. Real, "Carbothermal synthesis of vanadium nitride: Kinetics and mechanism," *Int. J. Chem. Kinet.*, vol. 38, no. 6, pp. 369–375, 2006.

[49]   P. Duwez and F. Odell, "Phase Relationships in the Binary Systems of Nitrides and Carbides of Zirconium, Columbium, Titanium, and Vanadium," *J. Electrochem. Soc.*, vol. 97, no. 10, pp. 299–304, 1950.

[50]   S. Yu, N. Fu, F. Gao, and Z. Sui, "Synthesis of Vanadium Nitride by a One Step Method," *J. Mater. Sci. Technol.*, vol. 23, no. 1, pp. 43–46, 2007.

[51]   J.-G. Choi, J. Ha, and J.-W. Hong, "Synthesis and catalytic properties of vanadium interstitial compounds," *Appl. Catal. A Gen.*, vol. 168, no. 1, pp. 47–56, 1998.

[52]   P. K. Tripathy, J. C. Sehra, and A. V. Kulkarni, "On the carbonitrothermic reduction of vanadium pentoxide," *J. Mater. Chem.*, vol. 11, no. 2, pp. 691–695, 2001.

[53]   H. O. Pierson, *Handbook of refractory carbides and nitrides : properties, characteristics, processing, and applications*. New Jersey: Noyes Publications, 1996.

[54]   S.-J. L. Kang, *Sintering : densification, grain growth, and microstructure*. Oxford: Elsevier Butterworth-Heinemann, 2015.

[55]   P. (Universität R. Drescher and H. (Universität R. Seitz, "Processability of an amorphous metal alloy powder by electron beam melting," *RTeJournal - Fachforum für Rapid Technol.*, no. 12, pp. 1–8, 2015.

[56] J. Zheng and J. S. Reed, "Effects of Particle Packing Characteristics on Solid-State Sintering," *J. Am. Ceram. Soc.*, vol. 72, no. 5, pp. 810–817, May 1989.

[57] D. C. Montgomery, *Design and Analysis of Experiments*, Eighth edi., vol. 2. John Wiley & Sons, Inc., 2012.

[58] J. B. Korright and A. C. Thompson, "X-Ray Emission Energies," in *X-Ray Data booklet*, 3rd ed., Berkeley: Lawrence Barkeley National Laboratory, Unioversity of California, 2009, pp. 1–9.

[59] C. T. . Rueden *et al.*, "ImageJ2: ImageJ for the next generation of scientific image data," *BMC Bioinformatics*, vol. 18, no. 1. BMC Bioinformatics, p. 529, 29-Dec-2017.

[60] W. G. (William G. Cochran and G. M. Cox, *Experimental designs*. Wiley, 1992.

[61] L. R. Lemos, S. H. F. S. Da Rocha, and L. F. A. De Castro, "Reduction disintegration mechanism of cold briquettes from blast furnace dust and sludge," *J. Mater. Res. Technol.*, vol. 4, no. 3, pp. 278–282, 2015.

[62] T. Lindstad, M. Syvertsen, R. J. Ishak, H. B. Arntzen, and P. O. Grøntvedt, "the Influence of Alkalis on the Boudouard Reaction," *Tenth Int. Ferroalloys Congr.*, no. February, pp. 261–271, 2004.

Appendix A

SAFETY DATA SHEET
ACCORDING TO EC-REGULATIONS 1907/2006 (REACH) & 1272/2008 (CLP)

BUSHVELD VAMETCO ALLOYS

Main Mothotlung Road,
Mothotlung, Brits
P O Box 595, Brits, 0250
T +27 (0) 12 318 3204
F +27 (0) 12 318 3201
e info@bushveldvametco.co.za

www.nitrovan.co.za

SECTION 1: IDENTIFICATION OF THE SUBSTANCE/MIXTURE AND OF THE COMPANY/UNDERTAKING

1.1	**Product identifier**	
	Chemical Name	Vanadium Carbide Nitride
	Trade name	NITROVAN®
	CAS No.	12069-91-9
	EINECS No.	Not listed
	REACH Registration No.	01-2119983497-18-0000
1.2	**Relevant identified uses of the substance or mixture and uses advised against**	
	Identified use(s)	A vanadium-nitrogen alloy used as a strengthener in the steelmaking process
	Uses advised against	No information available
1.3	**Details of the supplier of the safety data sheet**	
	Company Identification	Steptoe and Johnson L.L.P., Avenue Louise 489, B1050 Brussels, Belgium
	Telephone	+32 2626 0507
	E-Mail (competent person)	sds@steptoe.com
	Company Identification	BUSHVELD VAMETCO (Proprietary) Limited P. O. Box 595 Brits, 0250 South Africa
	Telephone	+27 12 318 3200
	E-Mail (competent person)	smtileni@bushveldvametco.co.za
1.4	**Emergency telephone number**	
	Emergency Phone No.	National Poisons Information Service +44 844 892 0111 or +44 8454 24 24 24
		Bushveld Vametco +27 12 318 3200 (M-F 07h00 – 16h00 only) Time Zone is GMT +2

SECTION 2: HAZARDS IDENTIFICATION

2.1	**Classification of the substance or mixture**	
2.1.1	**Regulation (EC) No. 1272/2008 (CLP).**	Not classified
2.1.2	**Directive 67/548/EEC & Directive 1999/45/EC**	Not classified
2.2	**Other hazards**	
2.2.1	**Label elements**	According to Regulation (EC¦ No. 1272/2008 (CLP).
	Hazard pictogram(s)	Not classified
	Signal word(s)	Not classified
	Hazard statement(s)	Not classified
	Precautionary statement(s)	Not classified
2.2.2	Label elements	According to Directive 67/548/EEC & Directive 1999/45/EC
	Hazard Symbol	Not classified
	Risk Phrases	Not classified
	Safety Phrases	Not classified
2.3	Other hazards	Chips may cause corneal injury. Handling of this substance may produce particles which could be considered a nuisance dust. Nuisance dust can cause unpleasant or uncomfortable deposits in the eyes, ears and nose, but does not cause any toxic effect or disease when exposures are kept in reasonable control, at or below the recommended exposure limits. Airborne concentrations of nuisance dusts in the workplace may also lead to reduced visibility.
2.4	Additional Information	None

SAFETY DATA SHEET
ACCORDING TO EC-REGULATIONS 1907/2006 (REACH) & 1272/2008 (CLP)

BUSHVELD
VAMETCO ALLOYS

SECTION 3: COMPOSITION/INFORMATION ON INGREDIENTS

3.1 Substances
EC Classification No. 1272/2008

Component	%W/W	CAS No.	REACH Registration No.	Hazard statement(s)
Vanadium Carbide Nitride	98 to 99%	12069-91-9	01-2119983497-18-0000	Not classified.

EC Classification No. 67/548/EEC

Component	%W/W	CAS No.	REACH Registration No.	EC Classification and Risk Phrases
Vanadium Carbide Nitride	98 to 99%	12069-91-9	01-2119983497-18-0000	Not classified.

3.2 Mixtures
Not applicable

3.3 Additional Information
For full text of H/P phrases see section 16.

SECTION 4: FIRST AID MEASURES

4.1 Description of first aid measures

Inhalation	Remove from exposure. Keep patient at rest and give oxygen if breathing difficult. If symptoms develop, obtain medical attention.
Skin Contact	After contact with skin, wash immediately with plenty of soap and water. If symptoms develop, obtain medical attention.
Eye Contact	Remove particles by irrigating with eye wash solution or clean water, holding the eyelids apart. If symptoms develop, obtain medical attention.
Ingestion	Unlikely to be hazardous if swallowed. Provided the patient is conscious, wash out mouth with water and give 200-300 ml (half a pint) of water to drink. Do not induce vomiting. If symptoms develop, obtain medical attention.

4.2 Most important symptoms and effects, both acute and delayed

Eye Contact: Dust may cause irritation. Chips may cause corneal injury.

Skin Contact: Repeated and/or prolonged contact may cause dermatitis.

Inhalation: Dust may cause irritation. (Coughing/Sneezing.) Extreme or repeated exposure may cause acute bronchitis like symptoms.

4.3 Indication of any immediate medical attention and special treatment needed

See Section: 4.1

SECTION 5: FIRE-FIGHTING MEASURES

5.1 Extinguishing media

Suitable Extinguishing Media	Non-flammable. Class D fire. Extinguishing media As appropriate for surrounding fire. Extinguish preferably with dry chemical, sand or carbon dioxide.
Unsuitable Extinguishing Media	Do not use water jet or water spray on burning material as it may generate hydrogen gas.

5.2 Special hazards arising from the substance or mixture — Oxidizes in air at temperatures above 150ºC with slow conversion to vanadium oxides.

5.3 Advice for fire-fighters — A self contained breathing apparatus and suitable protective clothing should be worn in fire conditions. Avoid generation of dust. Avoid release to the environment. Do not allow to enter drains, sewers or watercourses.

Appendices

SAFETY DATA SHEET
ACCORDING TO EC-REGULATIONS 1907/2006
(REACH) & 1272/2008 (CLP)

BUSHVELD
VAMETCO ALLOYS

Main Mothotlung Road,
Mothotlung, Brits
P O Box 595, Brits, 0250
T +27 (0) 12 318 3204
F +27 (0) 12 318 3201
e info@bushveldvametco.co.za

www.nitrovan.co.za

SECTION 6: ACCIDENTAL RELEASE MEASURES

6.1	Personal precautions, protective equipment and emergency procedures	Ensure suitable personal protection (including respiratory protection) during removal of spillages. Avoid generation of dust. Dust clouds are sensitive to ignition by electrostatic discharge.
6.2	Environmental precautions	Avoid release to the environment. Do not allow to enter drains, sewers or watercourses.
6.3	Methods and material for containment and cleaning up	Transfer the bulk of the spillage mechanically to a clean, suitably sized container such as an open-top steel drum with clamp-fitted lid. Mechanical transfer can be either manual (eg. shovel) or machine-aided in the case of larger spills (eg Bobcat FEL). Vacuum the undersize and add the contents to a separate clean drum. Avoid generating excessive dust (>1.0 mg / m3). The containers are to be sealed and disposal procedure discussed between supplier and customer, the prime issue being contamination of the material, and not by the material.
6.4	Reference to other sections	See Section: 13.
6.5	Additional Information	None

SECTION 7: HANDLING AND STORAGE

7.1	Precautions for safe handling	Handle in accordance with operating regulations. Where suitable engineering controls are not fitted or are inadequate, wear suitable protective equipment. Do not eat, drink or smoke at the work place. Wash hands before eating, drinking or smoking. Avoid dust generation. Avoid inhalation of dusts. Use of sweeping compounds may reduce dusting.
7.2	Conditions for safe storage, including any incompatibilities	Keep only in the original container. Keep container tightly closed, in a cool, well ventilated place. Keep away from heat and direct sunlight.
	Storage Temperature	< 150°C
	Storage Life	Stable under normal conditions.
	Incompatible materials	None
7.3	Specific end use(s)	Industrial use only.

SECTION 8: EXPOSURE CONTROLS/PERSONAL PROTECTION

8.1	Control parameters	
8.1.1	Occupational exposure limits	1 mg vanadium per m^3 for vanadium alloys (NIOSH) 5 mg per m^3 for Respirable Dust (PNOR)** (US OSHA) 15 mg per m^3 for Total Dust (PNOR)** (US OSHA) **PNOR = Particulates Not Otherwise Regulated
8.1.2	Biological limit value	No information available.
8.1.3	PNECs and DNELs	No information available.
8.2	Exposure controls	
8.2.1	Appropriate engineering controls	Provide adequate ventilation when using the material and follow the principles of good occupational hygiene to control personal exposures. Avoid dust generation. Avoid friction, sparks, or other means of ignition.
8.2.2	Personal protection equipment	
	Eye/face protection	Wear suitable eye/face protection.(EN 166).
	Skin protection (Hand protection/ Other)	Wear suitable gloves. Contaminated clothing should be thoroughly cleaned.

122

Appendices

Respiratory protection	Provide adequate ventilation, including appropriate local extraction if dusts, fumes or vapours are likely to be evolved. Wear suitable respiratory protective equipment if exposure to high levels of material are likely.
Thermal hazards	Dust is combustible. Pellets will burn slowly if heated to a high temperature in air. Oxidizes in air at temperatures above 150ºC with slow conversion to vanadium oxides.
8.2.3 **Environmental Exposure Controls**	Avoid release to the environment. Do not allow to enter drains, sewers or watercourses.

SECTION 9: PHYSICAL AND CHEMICAL PROPERTIES

9.1 Information on basic physical and chemical properties

Appearance	Solid. 35gm each)
Colour.	Dark. Grey. metallic
Odour	Slightly sulphurous
Odour threshold (ppm)	No information available.
pH (Value)	Not applicable.
Melting point (°C)	2427°C .
Boiling point/boiling range (°C):	No information available.
Flash point (°C)	Not applicable. Non-flammable.
Flammability (solid, gas)	Not applicable. Non-flammable.
Vapour pressure (Pascal)	**Essentially zero**
Vapour density (Air=1)	No information available.
Specific Gravity	No information available.
Bulk Density	1.6 g/cm³
Solubility (Water)	Insoluble
Fat solubility (g/l)	Insoluble
Partition coefficient (n-Octanol/water)	No information available.
Auto ignition point (°C)	Not applicable. Non-flammable.
Decomposition temperature (°C)	No information available.
Viscosity (mPa. s)	No information available.
Explosive properties	Dust is combustible. Pellets will burn slowly if heated to a high temperature in air.
Oxidising properties	Oxidizes in air at temperatures above 150ºC with slow conversion to vanadium oxides.
9.2 Other information	No information available.

SECTION 10: STABILITY AND REACTIVITY

10.1	**Reactivity**	No information available.
10.2	**Chemical stability**	Stable under normal conditions.
10.3	**Possibility of hazardous reactions**	Dust is combustible. Pellets will burn slowly if heated to a high temperature in air.
10.4	**Conditions to avoid**	Situations which cause dusting, fire and high temperatures
10.5	**Incompatible materials**	None.
10.6	**Hazardous Decomposition Product(s)**	Oxidizes in air at temperatures above 150ºC with slow conversion to vanadium oxides.

SECTION 11: TOXICOLOGICAL INFORMATION

11.1 Information on toxicological effects
11.1.1 Substances
Acute toxicity

Ingestion	Not classified. Unlikely to be hazardous if swallowed.

Appendices

SAFETY DATA SHEET
ACCORDING TO EC-REGULATIONS 1907/2006 (REACH) & 1272/2008 (CLP)

BUSHVELD VAMETCO ALLOYS

Main Mothotlung Road,
Mothotlung, Brits
P O Box 595, Brits, 0250
T +27 (0) 12 318 3204
F +27 (0) 12 318 3201
e info@bushveldvametco.co.za

www.nitrovan.co.za

Inhalation	Not classified. May cause irritation to the respiratory system.
Skin Contact	Not classified. Skin contact may cause contact dermatitis with itching and rash.
Eye Contact	Not classified. Dust may have irritant effect on eyes. Chips may cause corneal injury.
Serious eye damage/irritation	No information available.
respiratory or skin sensitization	No information available.
Mutagenicity	Not classified.
Carcinogenicity	Not classified.
Reproductive toxicity	Not classified.
STOT - single exposure	No information available.
STOT - repeated exposure	Inhalation: Extreme or repeated exposure may cause acute bronchitis like symptoms.
Aspiration hazard	No information available.
11.2 Other information	No information available.

SECTION 12: ECOLOGICAL INFORMATION

12.1	**Toxicity**	The substance is essentially insoluble in water. No environmental hazards have been reported or known.
12.2	**Persistence and degradability**	Will very slowly oxidize to vanadium oxide.
12.3	**Bio accumulative potential**	No information available.
12.4	**Mobility in soil**	No information available.
12.5	**Results of PBT and vPvB assessment**	Not classified as PBT or vPvB.
12.6	**Other adverse effects**	None identified

SECTION 13: DISPOSAL CONSIDERATIONS

This product does not possess characteristics which may qualify it as hazardous waste.

13.1	**Waste treatment methods**	Dispose surplus or waste materials in accordance with local or national regulatory guidelines. Normal disposal is via incineration operated by an accredited disposal contractor. Recover or recycle if possible.
13.2	**Additional Information**	Avoid release to the environment. Do not allow to enter drains, sewers or watercourses.

SECTION 14: TRANSPORT INFORMATION

14.1	**Land transport (ADR/RID)**	Not classified as dangerous for transport. Observe Local Regulations.
14.2	**Sea transport (IMDG)**	Not classified as dangerous for transport. Container shipments require a Container Packing Certificate
14.3	**Air transport (ICAO/IATA)**	Not classified as dangerous for transport. No limit on quantity
14.4	**Transport in bulk according to Annex II of MARPOL73/78 and the IBC Code**	No information available.

SECTION 15: REGULATORY INFORMATION

15.1	**Safety, health and environmental regulations/legislation specific for the substance or mixture**	
15.1.1	**EU regulations**	
	Authorisations and/or restrictions on use	None
15.1.2	**National regulations**	None
15.2	**Chemical Safety Assessment**	Not carried out

Appendices

SAFETY DATA SHEET
ACCORDING TO EC-REGULATIONS 1907/2006 (REACH) & 1272/2008 (CLP)

BUSHVELD
VAMETCO ALLOYS

SECTION 16: OTHER INFORMATION

The following sections contain revisions or new statements: 1-16.

LEGEND

LTEL	Long Term Exposure Limit
STEL	Short Term Exposure Limit
STOT	Specific Target Organ Toxicity
DNEL	Derived No Effect Level
PNEL	Predicted No Effect Concentration

References:

Regulation (EC) No. 1272/2008 (CLP).
(Directive 67/548/EEC & Directive 1999/45/EC)

Risk Phrases and Safety Phrases

Not classified.

Hazard statement(s) and Precautionary statement(s)

Not classified.

Training advice:

None required

Additional Information;

Information contained in this publication or as otherwise supplied to Users is believed to be accurate and is given in good faith, but it is for the Users to satisfy themselves of the suitability of the product for their own particular purpose. EVRAZ VAMETCO (Proprietary) Limited gives no warranty as to the fitness of the product for any particular purpose and any implied warranty or condition (statutory or otherwise) is excluded except to the extent that exclusion is prevented by law. EVRAZ VAMETCO (Proprietary) Limited accepts no liability for loss or damage (other than that arising from death or personal injury caused by defective product, if proved), resulting from reliance on this information. Freedom under Patents, Copyright and Designs cannot be assumed.

Appendices

Annex to the extended Safety Data Sheet (eSDS)

Identified use(s)

Manufacture			
Identified use(s) number	Identified use(s) name	Substance supplied to that use	Use descriptors
1	Manufacture of vanadium carbide nitride	No information available	**Process category [PROC]** PROC21 Low energy manipulation of substances bound in materials and/or articles PROC22 Potentially closed processing opera-ions with minerals/metals at elevated temperature Industrial setting **Environmental release categories [ERC]:** ERC1 Manufacture of substances

Industrial use			
Identified use(s) number	Identified use(s)name	Substance supplied to that use	Use descriptors
1	Industrial use of vanadium carbide nitrate in steel industry	as such / in a mixture	**Process category [PROC]** PROC21 Low energy manipulation of substances bound in materials and/or articles PROC22 Potentially closed processing opera-ions with minerals/metals at elevated temperature Industrial setting PROC23 Open processing and transfer operations with minerals/metals at elevated temperature **Chemical product category [PC] :** PC7 Base metals and alloys **Environmental release categories [ERC]:** ERC4 Industrial use of processing aids in processes and products, not becoming part of articles ERC5 Industrial use resulting in inclusion into or onto a matrix ERC6b Industrial use of reactive processing aids **Sectors of use [SU]:** SU14 Manufacture of basic metals, including alloys **Subsequent service life relevant for that use?:** Yes

Professional use			
Identified use(s) number	Identified use(s)name	Substance supplied to that use	Use descriptors
1	Professional use of vanadium carbide nitrate containing articles	as such / in a mixture	**Process category [PROC]** PROC21 Low energy manipulation of substances bound in materials and/or articles PROC24 High (mechanical) energy work-up of substances bound in materials and/or articles **Environmental release categories [ERC]:** ERC8c Wide dispersive indoor use resulting in inclusion into or onto a matrix ERC8f Wide dispersive outdoor use resulting in inclusion into or onto a matrix **Subsequent service life relevant for that use?:** Yes

Service life of substances in articles			
Identified use(s) number	Identified use(s)name	Substance supplied to that use	Use descriptors
1	Service life of vanadium carbide nitrate steel articles	-	**Article Categories [AC]** AC7 Metal articles **Environmental release categories [ERC]:** ERC10a Wide dispersive outdoor use of long-life articles and materials with low release ERC11a Wide dispersive indoor use of long-life articles and materials with low release

Appendix B

Job Number: 2015_W17

Sample Name Description	CORBON APRIL 2015		Date of Receipt Method	23/04/2015 GeoChemTraces_Powder

Z	Symbol	Element	Norm. Int.	Concentration		Abs. Error	
13	Al2O3	Aluminum	20.9657	0.07419	%	0.00087	%
14	SiO2	Silicon	21.4775	0.04084	%	0.00049	%
15	P2O5	Phosphorus	1.7942	< 0.00069	%	(0.0)	%
16	S	Sulfur	381.6362	653.1	µg/g	1.6	µg/g
17	Cl	Chlorine	0.0000	< 2.0	µg/g	(0.0)	µg/g
19	K2O	Potassium	79.1130	0.00167	%	0.00001	%
20	CaO	Calcium	787.7265	0.01406	%	0.00003	%
21	Sc	Scandium	4.1500	< 0.0010	%	(0.0)	%
22	TiO2	Titanium	411.1371	0.00369	%	0.00001	%
23	V2O5	Vanadium	206.9625	12.6	µg/g	0.1	µg/g
24	Cr2O3	Chromium	274.3972	8.4	µg/g	0.1	µg/g
25	MnO	Manganese	1063.0305	21.3	µg/g	0.1	µg/g
26	Fe2O3	Iron	20868.9131	0.3230	%	0.0003	%
27	CoO	Cobalt	7.8858	1.6	µg/g	0.3	µg/g
28	NiO	Nickel	47.8152	3.0	µg/g	0.1	µg/g
29	CuO	Copper	62.0462	3.6	µg/g	0.1	µg/g
30	ZnO	Zinc	1035.8362	38.1	µg/g	0.1	µg/g
31	Ga	Gallium	81.3032	1.5	µg/g	0.1	µg/g
32	Ge	Germanium	29.4151	0.7	µg/g	0.1	µg/g
33	As2O3	Arsenic	243.6401	5.6	µg/g	0.1	µg/g
34	Se	Selenium	23.2818	< 0.5	µg/g	(0.3)	µg/g
35	Br	Bromine	28.6834	0.4	µg/g	0.1	µg/g
37	Rb2O	Rubidium	14.9049	< 0.5	µg/g	(0.1)	µg/g
38	SrO	Strontium	194.1013	3.4	µg/g	0.1	µg/g
39	Y	Yttrium	112.2878	1.7	µg/g	0.1	µg/g
40	ZrO2	Zirconium	25.1985	5.6	µg/g	0.1	µg/g
41	Nb2O5	Niobium	8.7946	1.6	µg/g	0.1	µg/g
42	MoO	Molybdenum	25.1985	3.8	µg/g	0.1	µg/g
44	Ru	Ruthenium	0.0000	< 0.5	µg/g	(0.0)	µg/g
45	Rh	Rhodium	0.0000	< 0.5	µg/g	(0.0)	µg/g
46	Pd	Palladium	0.8354	< 0.5	µg/g	(0.0)	µg/g
47	Ag	Silver	32.0964	2.1	µg/g	0.1	µg/g
48	Cd	Cadmium	5.3287	1.1	µg/g	0.1	µg/g
49	In	Indium	12.9304	2.8	µg/g	0.1	µg/g
50	SnO2	Tin	75.7609	23.7	µg/g	0.2	µg/g
51	Sb2O5	Antimony	19.6552	4.6	µg/g	0.2	µg/g
52	Te	Tellurium	30.3390	3.5	µg/g	0.1	µg/g
53	I	Iodine	38.5089	5.8	µg/g	0.3	µg/g
55	Cs	Cesium	76.3442	21.6	µg/g	0.6	µg/g
56	BaO	Barium	101.4561	70.9	µg/g	1.7	µg/g
57	La2O3	Lanthanum	115.3650	90.2	µg/g	2.2	µg/g
58	Ce2O3	Cerium	134.0004	97.8	µg/g	2.2	µg/g
59	Pr	Praseodymium	138.0985	82.3	µg/g	2.1	µg/g
60	Nd	Neodymium	139.9952	106.7	µg/g	2.8	µg/g
62	Sm	Samarium	14.5445	< 8.1	µg/g	(0.0)	µg/g
72	Hf	Hafnium	8.5405	< 2.0	µg/g	(0.5)	µg/g
73	Ta2O5	Tantalum	9.3974	< 2.0	µg/g	(0.0)	µg/g
74	WO3	Tungsten	16.9366	1.0	µg/g	0.1	µg/g
79	Au	Gold	0.4718	< 0.3	µg/g	(0.1)	µg/g
80	Hg	Mercury	4.0151	< 0.7	µg/g	(0.0)	µg/g
81	Tl	Thallium	13.5377	< 0.7	µg/g	(0.3)	µg/g
82	Pb	Lead	37.6379	1.9	µg/g	0.1	µg/g
83	Bi	Bismuth	9.1952	0.2	µg/g	0.1	µg/g
90	Th	Thorium	6.0275	0.1	µg/g	0.1	µg/g

Date:23/04/2015   Page 1

Appendix C

SAFETY DATA SHEET FOR : CS 98 Y

PHYSICAL PROPERTIES		OTHER CHARACTERISTICS
COLOUR : Yellow Pre-cooked Maize		

HAZARDS/SYMPTOMS	PREVENTION	FIRST AID AND EMERGENCY TREATMENT
INHALATION:		
Coughing and throat irritations may occur	Adequate dust control & dust extraction systems. Personnel breathing protection e.g. masks.	Fresh air: Remove from high risk area
EYES : Nil		
INGESTION : Nil		
SKIN : Nil		
FIRE : Nil		
EXPLOSION : Nil		
SPILLAGE	**STORAGE**	**PACKAGING & LABELLING**
Sweep up spilled substances	Dry storage	25kg Polypropylene bags
NOTES:	Manufactured from natural maize - corn. It contains no colorants, preservatives or animal derivatives or additives.	

Appendix D

Counts

FerreiraJ_Furncae Build-up

Position [°2θ] (Cobalt (Co))

Peak List

Dolomite; C2 Ca1 Mg1 O6

Eitelite, syn; Na2 Mg (C O3)2

Halite; Na4.00 Cl4.00

Na2 (C O3)
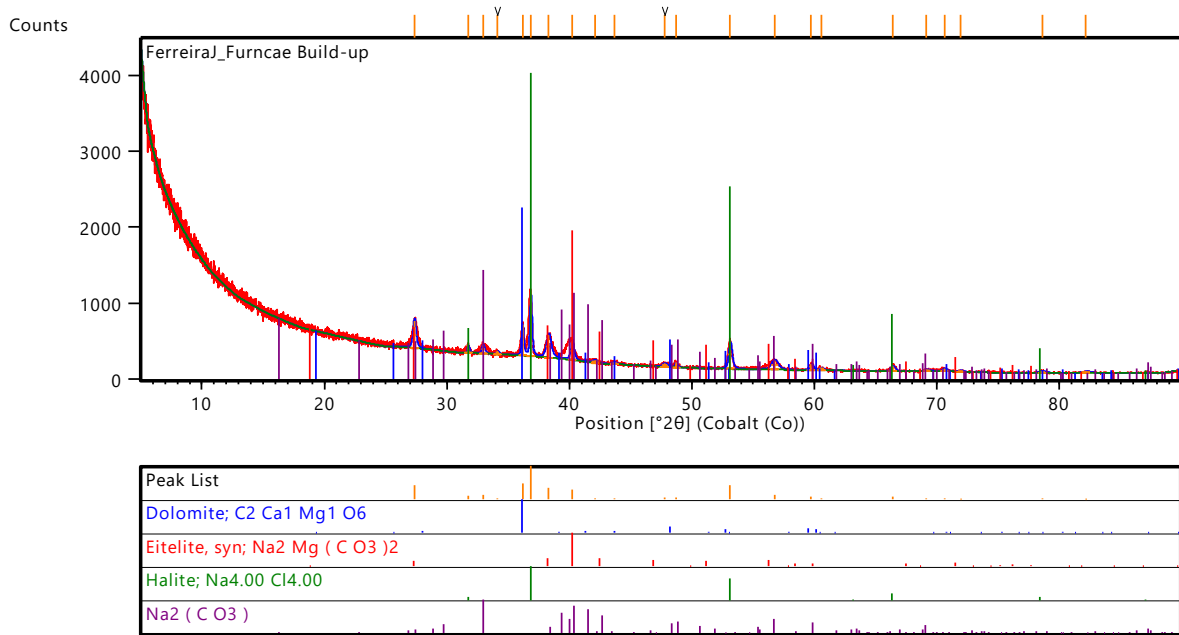
Figure D-1: Diffraction pattern of induction furnace off-gas accumulations.

Counts

FerreiraJ_graphite

Position [°2Theta] (Cobalt (Co))

Peak List

Graphite; C
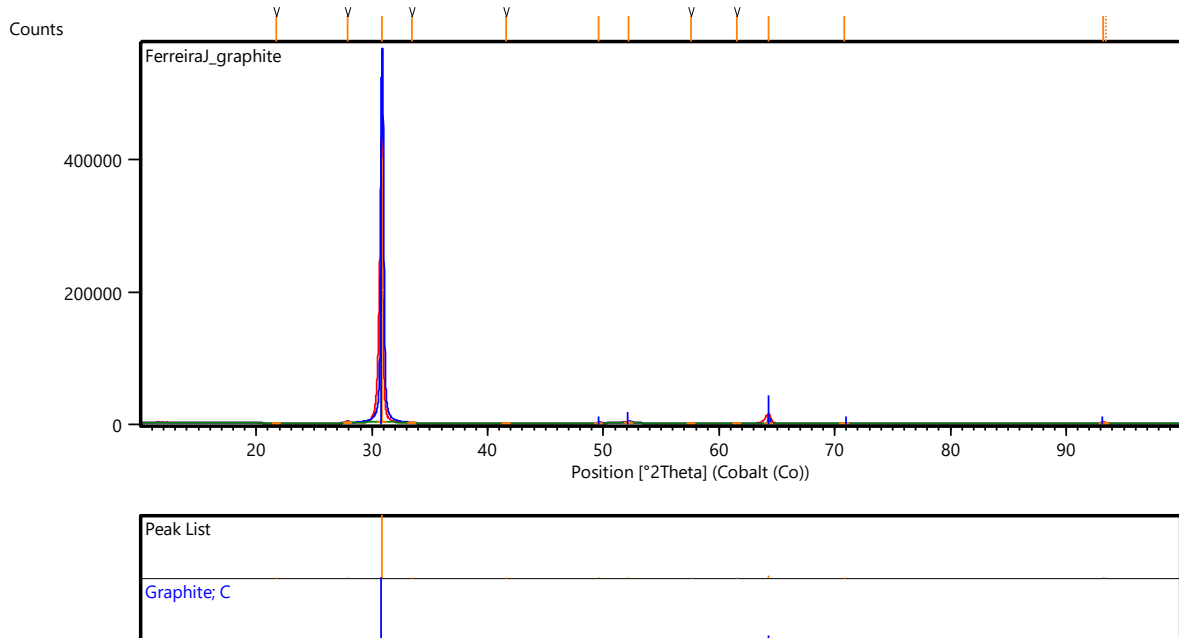
Figure D-2: Diffraction pattern of carbon used in all experiments in this study

Name and formula

Reference code:	01-074-0325

Mineral name:	Karelianite, syn
Compound name:	Vanadium Oxide
ICSD name:	Vanadium Oxide

Empirical formula:	O_3V_2
Chemical formula:	V_2O_3

Crystallographic parameters

Crystal system:	Rhombohedral
Space group:	R-3c
Space group number:	167

a (Å):	4.9520
b (Å):	4.9520
c (Å):	14.0020
Alpha (°):	90.0000
Beta (°):	90.0000
Gamma (°):	120.0000

Peak list

No.	h	k	l	d [Å]	2θ [°]	I [%]
1	0	1	2	3.65698	28.317	74.8
2	1	0	4	2.71181	38.520	100.0
3	1	1	0	2.47600	42.356	83.3
4	0	0	6	2.33367	45.077	6.4
5	1	1	3	2.18728	48.279	31.4
6	2	0	2	2.05027	51.734	6.4
7	0	2	4	1.82849	58.577	30.6
8	1	1	6	1.69824	63.569	83.6
9	0	1	8	1.62049	67.008	0.7
10	2	1	1	1.61017	67.495	0.3
11	1	2	2	1.57915	69.006	5.6

12	2	1	4	1.47088	74.911	21.7
13	3	0	0	1.42952	77.473	31.0
14	1	2	5	1.40287	79.230	0.2
15	2	0	8	1.35591	82.555	0.1
16	1	0	10	1.33105	84.448	11.4
17	1	1	9	1.31731	85.537	2.6

Name and formula

Reference code: 01-072-0977

Compound name: Vanadium Oxide
ICSD name: Vanadium Oxide

Empirical formula: O_5V_3
Chemical formula: V_3O_5

Crystallographic parameters

Crystal system: Monoclinic
Space group: P2/c
Space group number: 13

a (Å):   9.8590
b (Å):   5.0416
c (Å):   6.9910
Alpha (°):   90.0000
Beta (°):   109.4780
Gamma (°):   90.0000

Peak list

No.	h	k	l	d [Å]	2θ [°]	I [%]
1	1	0	0	9.29477	11.045	0.1
2	0	1	0	5.04160	20.440	0.2
3	2	0	0	4.64738	22.195	63.0
4	1	1	0	4.43165	23.290	19.7
5	0	1	1	4.00440	25.815	0.1
6	2	1	0	3.41707	30.351	0.3

7	0	0	2	3.29545	31.500	80.3
8	-2	0	2	3.24721	31.980	19.2
9	3	0	0	3.09826	33.562	0.2
10	-1	1	2	2.87211	36.293	77.8
11	3	1	0	2.63965	39.616	100.0
12	0	2	0	2.52080	41.568	41.3
13	1	1	2	2.46354	42.581	10.1
14	-3	1	2	2.42334	43.323	54.9
15	2	0	2	2.34452	44.857	11.3
16	4	0	0	2.32369	45.281	5.0
17	-4	0	2	2.29299	45.922	1.8
18	1	2	1	2.22029	47.516	18.9
19	2	2	0	2.21393	47.661	25.9
20	-2	2	1	2.20907	47.773	10.7
21	2	1	2	2.12589	49.766	0.1
22	-2	1	3	2.09653	50.512	12.3
23	0	1	3	2.01405	52.736	0.8
24	0	2	2	2.00220	53.072	23.9
25	-2	2	2	1.99123	53.388	3.9
26	3	2	0	1.95526	54.450	0.1
27	-5	0	2	1.91531	55.683	0.1
28	1	2	2	1.88045	56.808	0.1
29	-3	2	2	1.86239	57.410	0.1
30	1	1	3	1.85342	57.714	0.4
31	-5	1	1	1.83399	58.384	0.1
32	3	1	2	1.82296	58.772	1.2
33	-5	1	2	1.79046	59.946	0.1
34	3	2	1	1.77548	60.505	0.5
35	5	1	0	1.74417	61.708	25.5
36	2	2	2	1.71676	62.804	34.2
37	4	2	0	1.70854	63.141	5.5
38	-4	2	2	1.69622	63.653	0.9
39	0	3	0	1.68053	64.319	0.1
40	4	0	2	1.65664	65.361	0.6
41	1	3	0	1.65372	65.490	0.5
42	0	0	4	1.64773	65.759	0.3
43	-3	2	3	1.64232	66.003	0.7
44	-1	1	4	1.63148	66.498	32.6
45	-1	3	1	1.62618	66.743	23.8
46	-4	0	4	1.62361	66.862	12.6

47	-3	1	4	1.61964	67.048	7.6
48	1	3	1	1.58200	68.864	0.1
49	-2	3	1	1.57792	69.067	0.1
50	4	1	2	1.57385	69.271	0.1
51	5	1	1	1.56908	69.512	0.1
52	1	2	3	1.56405	69.768	0.1
53	-6	1	1	1.55465	70.252	0.1
54	6	0	0	1.54913	70.539	1.8
55	3	2	2	1.54465	70.774	1.0
56	1	0	4	1.53675	71.193	0.1
57	-5	2	2	1.52504	71.824	0.1
58	-1	3	2	1.51451	72.403	5.3
59	2	3	1	1.49877	73.286	0.2
60	5	2	0	1.49613	73.436	0.1
61	3	3	0	1.47722	74.534	10.2
62	1	1	4	1.46997	74.965	1.6
63	-5	1	4	1.44440	76.529	2.1
64	-2	2	4	1.43588	77.066	17.7
65	2	0	4	1.41180	78.631	3.2
66	3	3	1	1.39491	79.772	0.1
67	-6	0	4	1.38176	80.687	5.3
68	0	2	4	1.37922	80.866	3.1
69	5	1	2	1.37405	81.234	10.0
70	-6	2	1	1.37131	81.430	5.6
71	-6	2	2	1.36651	81.777	8.5
72	-4	2	4	1.36498	81.889	6.7
73	4	3	0	1.36173	82.126	3.5
74	-4	3	2	1.35534	82.598	0.8
75	-7	1	2	1.35309	82.765	0.7
76	0	3	3	1.33480	84.156	0.1
77	3	2	3	1.32838	84.657	0.5
78	6	2	0	1.31983	85.335	1.2
79	-4	1	5	1.31044	86.094	0.1
80	-7	1	3	1.30710	86.368	0.1
81	4	3	1	1.28404	88.315	0.3
82	0	1	5	1.27531	89.079	0.5

Name and formula

Reference code: 98-001-5889

Compound name: Vanadium(IV) Oxide
Common name: Vanadium(IV) Oxide

Chemical formula: O_2V_1

Crystallographic parameters

Crystal system: Monoclinic
Space group: P 1 21/c 1
Space group number: 14

a (Å):   5.3480
b (Å):   4.5170
c (Å):   5.3750
Alpha (°):   90.0000
Beta (°):   115.2350
Gamma (°):   90.0000

Peak list

No.	h	k	l	d [Å]	2θ [°]	I [%]
1	1	0	0	4.83762	21.311	0.6
2	0	1	1	3.30927	31.365	1.5
3	1	1	0	3.30153	31.440	2.8
4	1	1	-1	3.19777	32.488	100.0
5	1	0	-2	2.67802	39.026	4.0
6	0	0	2	2.43102	43.179	10.7
7	1	1	1	2.42325	43.324	23.6
8	2	0	0	2.41881	43.408	14.3
9	1	1	-2	2.30359	45.699	1.0
10	2	1	-1	2.29578	45.863	0.2
11	2	0	-2	2.26384	46.548	2.9
12	0	2	0	2.25850	46.664	3.2
13	0	1	-2	2.14068	49.399	5.6
14	2	1	0	2.13233	49.606	8.7
15	0	2	-1	2.04830	51.788	0.8
16	1	2	0	2.04646	51.838	0.0

17	2	1	-2	2.02388	52.460	1.7
18	1	2	-1	2.02102	52.540	2.1
19	1	0	2	1.87501	56.988	1.8
20	1	2	1	1.77519	60.516	0.1
21	1	1	2	1.73174	62.200	0.2
22	2	1	1	1.72841	62.333	1.3
23	1	2	-2	1.72649	62.410	1.5
24	3	0	-2	1.72447	62.492	0.5
25	2	2	-1	1.72320	62.543	1.6
26	1	1	-3	1.65815	65.294	10.7
27	0	2	-2	1.65463	65.450	5.7
28	2	2	0	1.65077	65.622	12.4
29	3	1	-1	1.65040	65.639	14.2
30	2	1	-3	1.61555	67.240	2.8
31	3	0	0	1.61254	67.383	0.1
32	3	1	-2	1.61105	67.453	0.1
33	2	2	-2	1.59888	68.036	16.1
34	0	1	-3	1.52546	71.801	1.3
35	3	1	0	1.51867	72.173	0.3
36	1	2	2	1.44264	76.639	1.3
37	2	2	1	1.44072	76.760	0.4
38	0	3	-1	1.43828	76.914	0.2
39	1	3	0	1.43764	76.954	1.6
40	2	0	2	1.43572	77.077	6.3
41	3	1	-3	1.43144	77.350	3.6
42	1	3	-1	1.42874	77.523	3.6
43	1	2	-3	1.39926	79.475	0.7
44	3	2	-1	1.39459	79.794	0.2
45	2	2	-3	1.37338	81.282	0.4
46	3	2	-2	1.37061	81.481	0.2
47	2	1	2	1.36826	81.650	0.1
48	2	0	-4	1.33901	83.831	3.2
49	1	3	1	1.33346	84.260	7.7
50	4	0	-2	1.33288	84.305	4.3
51	1	0	-4	1.31927	85.380	1.1
52	0	2	-3	1.31674	85.583	0.2
53	1	3	-2	1.31245	85.930	0.5
54	3	2	0	1.31236	85.937	0.1
55	1	1	3	1.31169	85.992	3.0
56	2	3	-1	1.31100	86.048	0.1

57	3	1	1	1.30784	86.307	4.0
58	2	1	-4	1.28379	88.337	0.2

Name and formula

Reference code: 01-073-2362

Compound name: Vanadium Oxide
ICSD name: Vanadium Oxide

Empirical formula: O_2V
Chemical formula: VO_2

Crystallographic parameters

Crystal system: Tetragonal
Space group: P42/mnm
Space group number: 136

a (Å):   4.5170
b (Å):   4.5170
c (Å):   2.8720
Alpha (°):   90.0000
Beta (°):   90.0000
Gamma (°):   90.0000

Peak list

No.	h	k	l	d [Å]	2θ [°]	I [%]
1	1	1	0	3.19400	32.527	100.0
2	1	0	1	2.42359	43.318	45.8
3	2	0	0	2.25850	46.664	6.7
4	1	1	1	2.13561	49.524	15.1
5	2	1	0	2.02006	52.567	4.5
6	2	1	1	1.65228	65.555	43.1
7	2	2	0	1.59700	68.128	13.4
8	0	0	2	1.43600	77.059	5.3
9	3	1	0	1.42840	77.545	6.5

10	2	2	1	1.39573	79.716	0.3
11	3	0	1	1.33352	84.255	12.6
12	1	1	2	1.30972	86.153	6.3
13	3	1	1	1.27895	88.759	0.9

Name and formula

Reference code: 01-089-0611

Compound name: Vanadium Oxide
ICSD name: Vanadium Oxide

Empirical formula: O_5V_2
Chemical formula: V_2O_5

Crystallographic parameters

Crystal system: Orthorhombic
Space group: Pmn21
Space group number: 31

a (Å):   11.5440
b (Å):   4.3830
c (Å):   3.5710
Alpha (°):   90.0000
Beta (°):   90.0000
Gamma (°):   90.0000

Peak list

No.	h	k	l	d [Å]	2θ [°]	I [%]
1	2	0	0	5.77200	17.830	43.6
2	0	1	0	4.38300	23.552	100.0
3	1	1	0	4.09759	25.218	31.1
4	2	1	0	3.49066	29.696	4.5

5	1	0	1	3.41150	30.402	71.5
6	3	1	0	2.88600	36.112	48.5
7	0	1	1	2.76847	37.702	26.0
8	1	1	1	2.69213	38.813	8.9
9	3	0	1	2.61753	39.965	26.6
10	2	1	1	2.49619	41.998	3.1
11	4	1	0	2.41040	43.567	2.5
12	3	1	1	2.24729	46.911	0.7
13	0	2	0	2.19150	48.180	11.7
14	1	2	0	2.15305	49.097	6.4
15	2	2	0	2.04880	51.774	0.6
16	5	1	0	2.04272	51.940	0.4
17	4	1	1	1.99786	53.196	11.6
18	5	0	1	1.93886	54.949	0.7
19	6	0	0	1.92400	55.410	15.2
20	3	2	0	1.90432	56.033	10.5
21	0	2	1	1.86782	57.228	10.4
22	1	2	1	1.84384	58.042	2.5
23	0	0	2	1.78550	60.130	16.9
24	2	2	1	1.77709	60.444	2.5
25	5	1	1	1.77312	60.594	1.4
26	6	1	0	1.76174	61.027	7.2
27	4	2	0	1.74533	61.663	1.0
28	2	0	2	1.70575	63.256	1.6
29	3	2	1	1.68032	64.328	0.1
30	0	1	2	1.65356	65.498	7.7
31	1	1	2	1.63685	66.252	2.7
32	2	1	2	1.58962	68.488	0.7
33	6	1	1	1.57993	68.967	3.9
34	4	2	1	1.56806	69.564	7.1
35	7	1	0	1.54350	70.835	2.8
36	3	1	2	1.51840	72.188	8.9
37	7	0	1	1.49720	73.375	10.6
38	0	3	0	1.46100	75.506	0.2
39	1	3	0	1.44944	76.215	2.0
40	6	2	0	1.44585	76.438	3.3
41	8	0	0	1.44300	76.617	1.5
42	4	1	2	1.43475	77.138	1.3
43	7	1	1	1.41682	78.299	3.9
44	0	2	2	1.38423	80.513	2.6

45	1	2	2	1.37439	81.210	2.2
46	8	1	0	1.37063	81.479	1.2
47	3	3	0	1.36586	81.825	3.5
48	0	3	1	1.35221	82.831	3.6
49	2	2	2	1.34607	83.293	0.4
50	5	1	2	1.34302	83.524	1.3
51	6	2	1	1.34017	83.742	3.7
52	7	2	0	1.31772	85.504	2.5
53	6	0	2	1.30877	86.231	5.1
54	4	3	0	1.30252	86.747	4.9
55	8	1	1	1.27961	88.701	0.5
56	3	3	1	1.27573	89.042	5.3

Appendix E
Induction furnace setup

Main

//Test number #

close all

//Step variables
TempTarget! = 1400   //Temperature set point
StepTime! = 5   //Step time depends on ramp rates & temperatures

close all

create filename showdialog

setmasterdir lastdialog

select network

//Print header and info
print filename date "\t"
print filename time "\t"
print filename (ticks) "\r"

define inputs# "1/1/1/1 1/1/1/4"
define outputs# "1/1/1/3"

print filename "INPUT CHANNELS"
print filename "\r CHANNEL \t 1/1/1/1 \t 1/1/1/4"
print filename "\r NAME \t"
table inputs# general user_name filename \t \r

139

Appendices

```
print filename "DISTANCE \t"
table inputs# general units_label filename \t \r
print filename "SENSOR \t"
table inputs# hardware sensor filename \t \r
print filename "WIRING \t"
table inputs# hardware wiring filename \t \r
print filename "RANGE \t"
table inputs# hardware range filename \t \r
print filename "LOW PASS \t"
table inputs# hardware low_pass filename \t \r
print filename "SCALE \t"
table inputs# mapping scale filename \t \r
print filename "OFFSET \t"
table inputs# mapping offset filename \t \r


print filename "\r OUTPUT CHANNELS"
print filename "\r CHANNEL \t 1/1/1/3"
print filename "\r NAME \t"
table outputs# general user_name filename \t \r
print filename "UNITS \t"
table outputs# general units_label filename \t \r
print filename "SCALE \t"
table outputs# mapping scale filename \t \r
print filename "OFFSET \t"
table outputs# mapping offset filename \t \r

print filename "\r

//Print column headers
print filename "\r Step \t Status \t Time \t TickTime"
print filename " \t SetPoint \t Reactor_Temp \t Smooth_Temp"
print filename " \t Delta \t P \t I \t D \t Power \t Power_Set \t Distance"



Eexit! = 0
SetRead! = 0
Status$ = 0

delete pages
newpage Display
select Display

open rampup masterdir
execute RampUp
close RampUp
if (Eexit! == 1) then goto Crash

open AtTemp masterdir
execute AtTemp
close AtTemp
if (Eexit! == 1) then goto Crash

open CoolDown masterdir
execute CoolDown
close CoolDown
if (Eexit! == 1) then goto Crash

TickTime! = ticks - StartTick!

Print filename "\r" time "\t" TickTime! "\t Normal process ending"
goto Normstop

Crash:
        Print filename "\r" time "\t" TickTime! "\t Abnormal process ending"
        Print Display "\r" time "\t" TickTime! "\t Abnormal process ending"
// Go to safe mode
        Power! = 0

        Print filename "\r" time "\t" TickTime! "\t Safe"
```

```
            close all

            goto finish


Normstop:
            Print filename "\r" time "\t" TickTime! "\t Normal process ending"
            Print Display "\r" time "\t" TickTime! "\t Normal process ending"

// Go to safe mode
            Power! = 0

            Print filename "\r" time "\t" TickTime! "\t Safe"

close all


Finish:
end
```

Appendices

Rump-up

```
//Test

close all

//Step variables
TempTarget! = 1400                    //Temperature set point
StepTime! = 5                                  //Step time depends on ramp rates & temperatures

close all

create filename showdialog

setmasterdir lastdialog

select network

//Print header and info
print filename date "\t"
print filename time "\t"
print filename (ticks) "\r"

define inputs# "1/1/1/1 1/1/1/4"
define outputs# "1/1/1/3"

print filename "INPUT CHANNELS"
print filename "\r CHANNEL \t 1/1/1/1 \t 1/1/1/4"
print filename "\r NAME \t"
table inputs# general user_name filename \t \r
print filename "DISTANCE \t"
table inputs# general units_label filename \t \r
print filename "SENSOR \t"
table inputs# hardware sensor filename \t \r
print filename "WIRING \t"
table inputs# hardware wiring filename \t \r
print filename "RANGE \t"
table inputs# hardware range filename \t \r
print filename "LOW PASS \t"
table inputs# hardware low_pass filename \t \r
print filename "SCALE \t"
table inputs# mapping scale filename \t \r
print filename "OFFSET \t"
table inputs# mapping offset filename \t \r


print filename "\r OUTPUT CHANNELS"
print filename "\r CHANNEL \t 1/1/1/3"
print filename "\r NAME \t"
table outputs# general user_name filename \t \r
print filename "UNITS \t"
table outputs# general units_label filename \t \r
print filename "SCALE \t"
table outputs# mapping scale filename \t \r
print filename "OFFSET \t"
table outputs# mapping offset filename \t \r

print filename "\r

//Print column headers
print filename "\r Step \t Status \t Time \t TickTime"
print filename " \t SetPoint \t Reactor_Temp \t Smooth_Temp"
print filename " \t Delta \t P \t I \t D \t Power \t Power_Set \t Distance"
```

```
Eexit! = 0
SetRead! = 0
Status$ = 0

delete pages
newpage Display
select Display

open rampup masterdir
execute RampUp
close RampUp
if (Eexit! == 1) then goto Crash

open AtTemp masterdir
execute AtTemp
close AtTemp
if (Eexit! == 1) then goto Crash

open CoolDown masterdir
execute CoolDown
close CoolDown
if (Eexit! == 1) then goto Crash

TickTime! = ticks - StartTick!

Print filename "\r" time "\t" TickTime! "\t Normal process ending"
goto Normstop

Crash:
        Print filename "\r" time "\t" TickTime! "\t Abnormal process ending"
        Print Display "\r" time "\t" TickTime! "\t Abnormal process ending"
// Go to safe mode
        Power! = 0

        Print filename "\r" time "\t" TickTime! "\t Safe"

        close all

        goto finish


Normstop:
        Print filename "\r" time "\t" TickTime! "\t Normal process ending"
        Print Display "\r" time "\t" TickTime! "\t Normal process ending"

// Go to safe mode
        Power! = 0

        Print filename "\r" time "\t" TickTime! "\t Safe"

close all


Finish:
end
```

Appendices

At Temp

```
//Measure shrinkage at fixed temperature
Step! = 2


SetPoint! = TempTarget!


//Unused analogue channels
Ch9_Vout! = 0                              //Dead channel
Ch24_Vout! = 0                             //Unused channel



//Constants
CycleRate! = 2
                                           //Number of control loops per second
ReadRate! = 2
                                           //Time betwee write cycles
StableTime! = 5
                                           //End of ramp stabilization time in minutes
SmoothT! = 0.1
                                           //Temperature smoothing factor
Smooth! = 0.2
                                           //Delta & D! smoothing factor
MaxPower! = 4.5
TempMinLim! = (TempTarget! - 15)                      //Lower cutoff temperature
TempMaxLim! = (TempTarget! + 15)                      //Upper cutoff temperature



if (SetRead! == 1) then goto Finish


//Measure displacement at constant temperature

StartSecs! = secssincelaunch
Secs! = secssincelaunch
StopSecs! = (secssincelaunch + (60*StepTime!))

Status$ = "Measure"

while (Secs! < StopSecs!)


        Secs! = secssincelaunch

        loop 4, 0.5
                if (mouseb == 1) then goto Estop
                SmoothTemp! = ((SmoothT!*Reactor_Temp!)+((1-SmoothT!)*SmoothTemp!))
                                        //Smoothed temperature reading
                Delta! = (((Smooth! * (Setpoint! - SmoothTemp!)) + ((1-Smooth!) * Delta!)))
//smoothed error term
                if (Reactor_Temp! < TempMinLim!) then goto TempStop
                                                        // test for TC open error
                if (Reactor_Temp! > TempMaxLim!) then goto TempStop
                                                        // test for max temperature error


                P! = (PGain! * Delta!)
                                                                    //proportional control term


                if (Power! >= MaxPower!)
                //integral control term with anti windup limiting
                                I! = I!
                        elseif (Power! <= MinPower!)
                                I! = I!
```

```
                            else
                                    I! = (I! + ((IGain! * Delta!) * ElapseTime!))
                    endif

                    D! = ((((Smooth! * DGain!)*(1/ElapseTime!))* (OldTemp! - SmoothTemp!)) + ((1-Smooth!)* D!))
            //derivative control term
                    OldTemp! = SmoothTemp!


                    if ((((P! + I!) + D!) + B!) >= MaxPower!)
                            Power! = MaxPower!
                    elseif ((((P! + I!) + D!) + B!) <= MinPower!)
                            Power! = MinPower!
                    else
                            Power! = (((P! + I!) + D!) + B!)
                    endif

                    Power_Set! = ((0.1*Power!)+(0.9*Power_Set!))

            endloop

            TickTime! = ((ticks - StartTick!)/1000)
            print filename "\r" Step! "\t" Status$ "\t" time "\t" TickTime!
            print filename "\t" SetPoint! "\t" Reactor_Temp! "\t" SmoothTemp!
            print filename "\t" Delta! "\t" P! "\t" I! "\t" D! "\t" Power! "\t" Power_Set!
            print filename " \t" Distance!

            clear pages

            print Display "\r Step" Step! "\t" Status$
            print Display "\r time: " time "\t Tick Time: " %1.3f:TickTime!
            print Display "\r Set Point: \t" %1.3f:SetPoint! "\t Reactor Temp: \t" %1.3f:Reactor_Temp! "\t Smooth Temp: \t"
%1.3f:SmoothTemp!
            print Display "\r Power: \t" %1.3f:Power_Set!
            print Display "\r Distance: \t" %1.3f:Distance!

endwhile

goto Finish

TempStop:                       //System shut down due to temperature excursion


        if (Reactor_Temp! < TempMinLim!) then Status$ = "Minimum process temperature error"              //Test for TC
open error
        if (Reactor_Temp! > TempMaxLim!) then Status$ = "Maximum process temperature error"              //Test for max
temperature error

        print filename "\r" time "\t" TickTime! "\t Abnormal exit: Temperature error at step :" Step! ". " Status$
        Eexit! = 1

// Go to safe mode
        Power_Set! = 0

        goto finish

Estop:                                  //System shut down due to mouse press (E-Stop)
        print filename "\r" time "\t" TickTime! "\t Abnormal exit: MouseB = 1 at step" Step!
        Eexit! = 1

// Go to safe mode
        Power_Set! = 0



Finish:

end
```

Appendices

Cool down

```
//Step 3: Cool down
Step! = 3

//Step variables
TempTarget! = 400                          //Temperature set point
StepTime! = 0                              //Step time depends on ramp rates & temperatures

//Unused analog channels
Ch9_Vout! = 0                              //Dead channel
Ch24_Vout! = 0                             //Unused channel


RampRate! = -25                            //Ramp rate C per minute. Must convert to C per second
CycleRate! = 2                             //Number of control loops per second
ReadRate! = 10                             //Time betwee write cycles
SmoothT! = 0.1                             //Temperature smoothing factor
Smooth! = 0.2                              //Delta & D! smoothing factor
MaxPower! = 3.0                            //Maximum power while temperature ramps down

TempMinLim! = (TempTarget! - 15)           //Lower cutoff temperature
TempMaxLim! = (SmoothTemp! + 15)           //Upper cutoff temperature


//Initialize variables
RampRate! = (RampRate!/60)
OldTemp! = Reactor_Temp!
AveTemp! = Reactor_Temp!
SmoothTemp! = Reactor_Temp!
Setpoint! = SmoothTemp!
StartSecs! = secsincelaunch
Secs! = secsincelaunch


if (SetRead! == 1) then goto Finish


// Ramp to target with P control

Status$ = "Cooldown"

ElapseTime! = 0.5
                //initialise elapsetime
CycleTick! = ticks

PGain! = 0.1
                //fixed Pgain for cool down
IGain! = 0
                //use only proportional
DGain! = 0
                //use only proportional

while (SetPoint! >= TempTarget!)
        synchronize (ReadRate!)

        if (Reactor_Temp! < TempMinLim!) then goto TempStop          // test for TC open error
        if (Reactor_Temp! > TempMaxLim!) then goto TempStop          // test for max temperature error



        loop 20, (1/CycleRate!)
                if (mouseb == 1) then goto estop                     //Emergency stop
                ElapseTime! = ((ticks - CycleTick!)/1000)
                CycleTick! = ticks
                SetPoint! = (SetPoint! + (RampRate!*ElapseTime!))
                SmoothTemp! = ((SmoothT!*Reactor_Temp!)+((1-SmoothT!)*SmoothTemp!))
        //Smoothed temperature reading
                Delta! = (((Smooth! * (Setpoint! - SmoothTemp!)) + ((1-Smooth!)* Delta!)))     //smoothed error term
```

```
                        P! = (PGain! * Delta!)
                                                        //proportional control term
                        OldTemp! = SmoothTemp!

                        if (P! >= MaxPower!)
                                    Power! = MaxPower!
                        elseif (P! <= 0)
                                    Power! = 0
                        else
                                    Power! = (P!)
                        endif
                        Power_Set! = ((0.3*Power!)+(0.7*Power_Set!))

        endloop

        TickTime! = ((ticks - StartTick!)/1000)

        print filename "\r" Step! "\t" Status$ "\t" time "\t" TickTime!
        print filename "\t" SetPoint! "\t" Reactor_Temp! "\t" SmoothTemp!
        print filename "\t" Delta! "\t" P! "\t" I! "\t" D! "\t" Power! "\t" Power_Set!
        print filename " \t" Distance!

        clear pages

        print Display "\r Step" Step! "\t" Status$
        print Display "\r time: " time "\t Tick Time: " %1.3f:TickTime!
        print Display "\r Set Point: \t" %1.3f:SetPoint! "\t Reactor Temp: \t" %1.3f:Reactor_Temp! "\t Smooth Temp: \t"
%1.3f:SmoothTemp!
        print Display "\r Power: \t" %1.3f:Power_Set!
        print Display "\r Distance: \t" %1.3f:Distance!


endwhile

SetPoint! = TempTarget!

goto Finish

TempStop:                       //System shut down due to temperature excursion

        if (Reactor_Temp! < TempMinLim!) then Status$ = "Minimum process temperature error"//Test for TC open error
        if (Reactor_Temp! > TempMaxLim!) then Status$ = "Maximum process temperature error"//Test for max temperature error

        print filename "\r" time "\t" TickTime! "\t Abnormal exit: Temperature error at step :" Step! ". " Status$

        Eexit! = 1
// Go to safe mode
        Power_Set! = 0

        goto Finish


Estop:                                  //System shut down due to mouse press (E-Stop)
        print filename "\r" time "\t" TickTime! "\t Abnormal exit: MouseB = 1 at step" Step!
        Eexit! = 1
// Go to safe mode
        Power_Set! = 0


Finish:

// Go to safe mode
        Power_Set! = 0


END
```

Appendix F

Table F-1: Porosity and density data of Vametco briquettes.

Pellet	M_1	M_2	Fluid	p_{fuid}	Void volume	Porosity	M_3	M_4	M_5	V_{fluid}	$V_{mesured}$	$V_{briquette}$	P_{dry}
	(g)	(g)		(g/cm^3)	(cm^3)	(%)	(g)	(g)	(g)	(cm^3)	(cm^3)	(cm^3)	(g/cm^3)
1	49.703	52.786	water	0.997	3.093	15.017	5.326	58.112	137.250	79.402	100.000	20.598	2.413
2	66.348	74.438	water	0.997	8.117	25.144	5.358	79.796	147.289	67.718	100.000	32.282	2.055
3	61.050	69.383	water	0.997	8.361	29.717	5.336	74.719	146.345	71.865	100.000	28.135	2.170
4	64.350	70.317	Paraffin	0.740	8.063	27.163	5.536	75.853	127.887	70.316	100.000	29.684	2.168
5	54.505	59.409	Paraffin	0.740	6.628	25.864	5.336	64.746	119.784	74.376	100.000	25.624	2.127
6	60.798	65.662	Paraffin	0.740	6.573	23.243	5.332	70.994	124.066	71.720	100.000	28.280	2.150
7	60.195	64.827	Paraffin	0.740	6.260	22.482	5.333	70.161	123.556	72.156	100.000	27.844	2.162
8	62.328	67.268	Paraffin	0.740	6.676	22.992	5.332	72.600	125.115	70.966	100.000	29.034	2.147
9	53.527	58.344	Paraffin	0.740	6.509	26.349	5.333	63.676	119.396	75.297	100.000	24.703	2.167

Total average porosity	Avg.	Std.	Var.		Total average density	Avg.	Std.	Var.
Average porosity using water	23.293	6.142	37.725		Average density using water	2.213	0.149	0.022
Average porosity using paraffin	24.682	1.830	3.350		Average density using paraffin	2.153	0.014	0.000

M1   Dry Briquette V_{water} Volume of water

M2   Wet Briquette $V_{briquette}$ volume of briquette

M3   Flask

M4   Flask + Wet Briquette

M5   Flask + Wet Briquette + fluid

Appendices

Table F-2: Induction furnace with variable load data.

Temperature	Load	Spillage	Measured Shrinkage	LVDT Shrinkage	Shear	V	N	C	O
1475	1.40	25	7.60	7.31	0.02	74.56	13.70	5.66	3.65
1475	1.40	0	8.90	7.15	0.31	76.37	16.40	3.69	1.06
1475	1.40	25	7.10	6.83	0.04	76.38	16.13	3.83	0.95
1200	1.40	25	1.95	1.91	0.00	68.30	8.35	10.64	8.85
1475	0.10	25	4.90	3.50	0.03	76.76	16.83	3.60	1.16
1640	2.00	10	10.60	9.19	0.02	77.74	13.03	4.91	0.78
1640	0.17	10	5.20	2.95	0.00	77.38	13.10	5.52	0.66
1310	0.17	10	3.60	3.19	0.01	71.48	13.53	7.67	3.53
1475	1.40	50	6.00	6.04	0.29	76.49	16.78	3.65	0.98
1640	0.17	40	5.70	5.25	0.03	75.56	14.45	4.74	2.31
1640	2.00	40	3.80	3.20	0.00	76.24	13.70	5.37	2.49
1750	1.40	25	10.60	10.15	0.44	78.05	15.90	3.91	0.56
1475	1.40	25	8.90	8.86	0.49	76.52	16.50	3.86	1.15
1310	2.00	10	8.70	8.62	0.06	74.45	14.50	6.29	2.21
1310	2.00	40	5.90	5.50	0.04	70.80	12.38	6.96	5.48
1475	3.00	25	5.80	5.40	0.56	75.95	17.03	3.31	1.50
1310	0.17	40	3.80	3.47	0.00	70.38	12.30	7.48	6.42
1475	1.40	25	8.60	8.34	0.33	76.53	16.15	4.02	1.30

Appendices

Table F-3: Induction furnace with constant load data.

Temperature	Time	Insoluble Impurities	Soluble Impurities	Weight	Shear	V	C	N	O	S	Si	Al	Fe	Cr	P	Mn	Cu	Ca	Na	Mo	Mg	K	Ti	As
1200	30	0	0	10.6064	0	63.35	11.23	8.99	9.81	0.06	0.199	0.082	0.305	0.009	0.007	0.003	0.001	0.05	0.097	0.003	0.021	0.029	0.017	0.001
1400	30	0	0	33.6024	2.331708	78.31	4.15	15.8	0.92	0.07	0.156	0.059	0.39	0.011	0.006	0.004	0	0.06	0.124	0.003	0.019	0.027	0.035	0.002
1200	60	0	0	13.2184	0	66.115	9.54	11.9	7.07	0.05	0.133	0.045	0.198	0.008	0.005	0.002	0	0.036	0.085	0.002	0.021	0.027	0.007	0.002
1400	60	0	0	19.1165	2.635312	78.71	3.73	16.7	0.38	0.03	0.116	0.048	0.356	0.011	0.007	0.003	0	0.074	0.081	0.003	0.021	0.025	0.031	0.002
1200	30	1	0	13.9591	0	67.08	8.41	11.8	7.73	0.08	0.441	0.248	1.331	0.011	0.005	0.013	0	0.128	0.31	0.002	0.044	0.029	0.162	0.001
1400	30	1	0	19.2703	2.717795	77.31	3.45	15.8	1.01	0.08	0.452	0.249	1.384	0.014	0.008	0.011	0	0.151	0.182	0.005	0.042	0.04	0.189	0.002
1200	60	1	0	17.3755	0	72.625	5.43	14.9	2.82	0.07	0.453	0.283	1.428	0.013	0.006	0.014	0	0.137	0.39	0.003	0.049	0.035	0.171	0.002
1400	60	1	0	19.2251	2.483255	77.05	3.41	16.3	0.79	0.06	0.44	0.22	1.412	0.014	0.008	0.01	0	0.158	0.146	0.004	0.035	0.034	0.199	0.002
1200	30	0	1	18.5258	0	74.08	6.16	13.7	4.46	0.19	0.101	0.036	0.278	0.007	0.005	0.003	0	0.048	0.18	0.001	0.029	0.023	0.016	0.001
1400	30	0	1	20.4516	0.403632	78.23	3.38	16.7	0.91	0.13	0.091	0.041	0.323	0.01	0.006	0.003	0	0.058	0.126	0.003	0.031	0.014	0.022	0.002
1200	60	0	1	17.3755	0.129337	77.92	3.52	17.7	0.8	0.16	0.111	0.035	0.302	0.01	0.008	0.003	0	0.07	0.117	0.002	0.026	0.043	0.012	0.002
1400	60	0	1	20.3792	0.287354	77.5	4.35	15.5	1.07	0.11	0.059	0.044	0.217	0.011	0.003	0.001	0	0.046	0.05	0.002	0.019	0.014	0.006	0.002
1200	30	1	1	18.6125	0.233481	72.78	5.5	13.6	3.65	0.36	0.542	0.312	1.577	0.013	0.007	0.016	0	0.184	0.63	0.004	0.057	0.055	0.207	0.002
1400	30	1	1	19.4658	3.000827	77.04	3.46	16.1	0.67	0.23	0.466	0.286	1.499	0.014	0.008	0.013	0	0.172	0.194	0.004	0.048	0.047	0.212	0.002
1200	60	1	1	18.9475	2.382311	74.65	3.98	15.9	2.35	0.28	0.559	0.342	1.57	0.015	0.007	0.016	0.001	0.221	0.791	0.004	0.106	0.04	0.196	0.002
1400	60	1	1	19.3624	3.709937	77.24	2.92	16.6	0.87	0.17	0.342	0.207	1.277	0.021	0.016	0.013	0.001	0.177	0.181	0.004	0.053	0.048	0.156	0.002
1300	45	0.5	0.5	19.2508	1.188121	77.41	3.12	16.4	0.9	0.13	0.579	0.328	1.013	0.02	0.011	0.009	0.002	0.128	0.163	0.004	0.051	0.019	0.1	0.002
1300	45	0.5	0.5	18.9449	0.608369	76.01	4.04	16.1	2.17	0.15	0.319	0.169	0.957	0.011	0.006	0.009	0	0.091	0.165	0.002	0.035	0.025	0.105	0.001
1300	45	0.5	0.5	19.1781	0.964541	77.42	3.59	17.1	1.1	0.12	0.277	0.161	0.826	0.013	0.009	0.008	0	0.1	0.202	0.004	0.036	0.05	0.099	0.002
1300	45	0.5	0.5	18.37	0.871099	77.28	3.5	16.9	0.75	0.16	0.328	0.191	1.007	0.016	0.011	0.01	0.001	0.134	0.196	0.004	0.043	0.047	0.122	0.002
1300	45	0.5	0.5	19.3395	0.739324	77.47	3.44	16.5	1.13	0.15	0.318	0.165	0.923	0.013	0.009	0.009	0	0.113	0.155	0.004	0.036	0.035	0.115	0.002

Appendix G

Table G-1: Tube furnace data.

Temperature	Time	Insoluble Impurities	Soluble Impurities	Image	Count	Total Area	Average size	% Area	Mean
1200	60	0	0	08165445.JPG	3024	274362	90.728	22.328	255
1200	30	1	0	08140950.JPG	3221	173591	53.894	14.127	255
1200	30	1	1	08170338.JPG	2632	198580	75.448	16.16	255
1400	30	0	0	08165931.JPG	2606	347892	133.497	28.312	255
1400	60	0	0	08141645.JPG	2194	391599	178.486	31.868	255
1400	30	0	1	08165931.JPG	2606	347892	133.497	28.312	255
1400	30	1	1	Pellet disintegrated					
1200	60	1	0	08142036.JPG	3659	286565	78.318	23.321	255
1200	30	0	1	08140725.JPG	2235	143262	64.099	11.659	255
1400	30	1	0	08141144.JPG	2912	370017	127.066	30.112	255
1300	45	0.5	0.5	08165744.JPG	2593	337724	130.245	27.484	255
1400	60	1	0	Pellet disintegrated					
1400	60	0	1	08134156.JPG	2425	490498	202.267	39.917	255
1200	30	0	0	08134033.JPG	3002	124132	41.35	10.102	255
1300	45	0.5	0.5	08170242.JPG	3298	342399	103.82	27.865	255
1200	60	1	1	08141420.JPG	2934	296733	101.136	24.148	255
1300	45	0.5	0.5	08140424.JPG	1893	320685	169.406	26.097	255
1300	45	0.5	0.5	08170447.JPG	2822	347682	123.204	28.294	255
1400	60	1	1	08141307.JPG	3873	486312	125.565	39.576	255
1200	60	0	1	08170108.JPG	2430	273407	112.513	22.25	255
1300	45	0.5	0.5	08165559.JPG	2860	309537	108.23	25.19	255

Appendix H
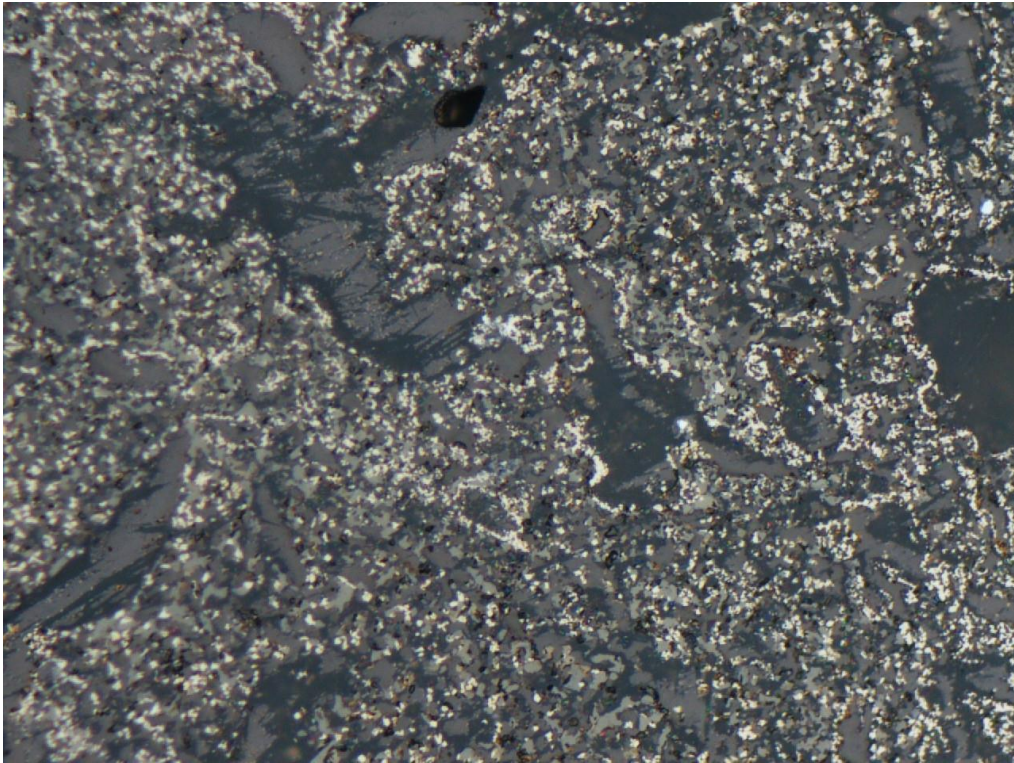
Figure H-1: Sinter model image 08165445.JPG.
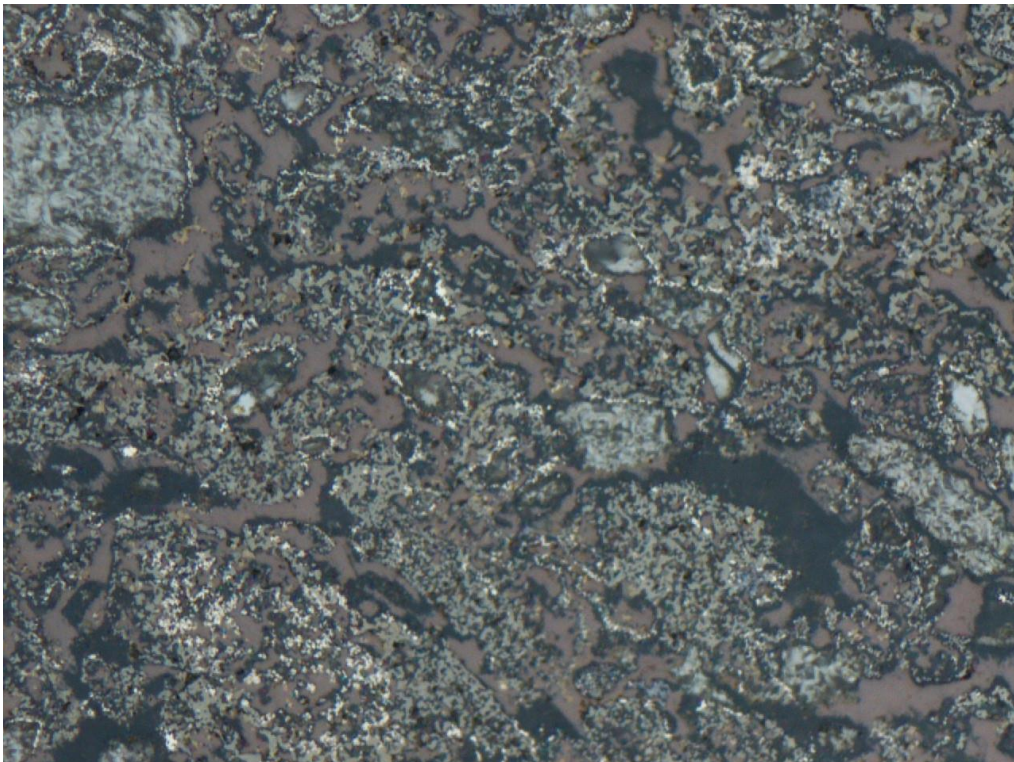
Figure H-2: Sinter model image 08140950.JPG.
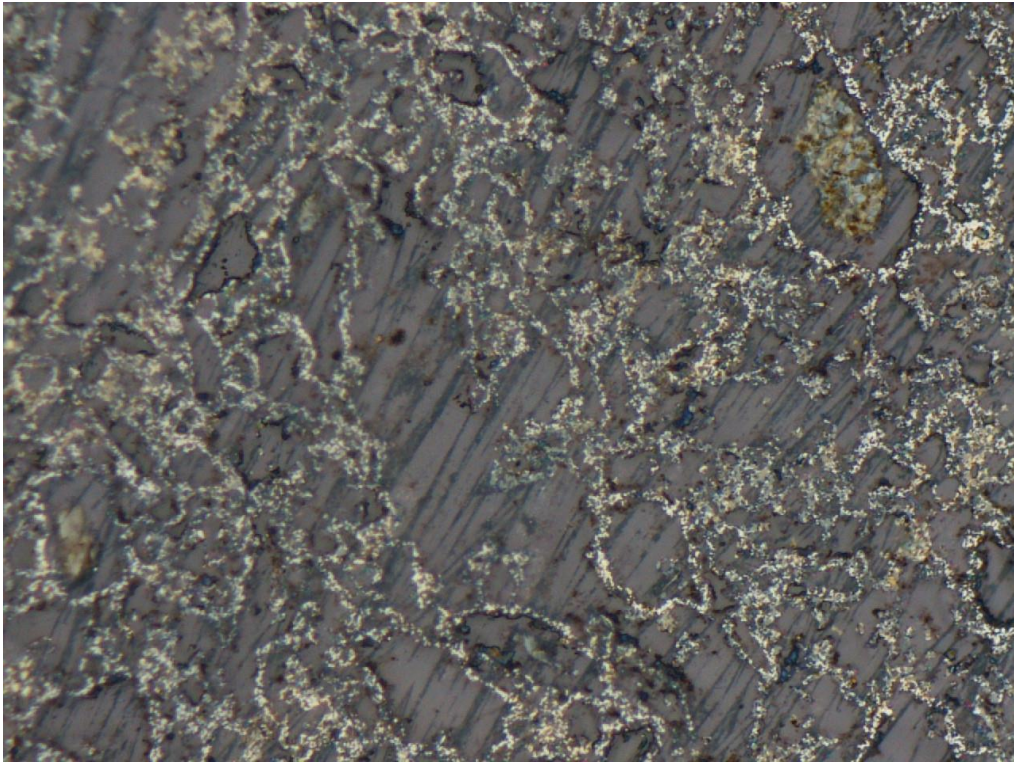
Figure H-3:Sinter model image 08170338.JPG.

Figure H-4:Sinter model image 08165931.JPG.
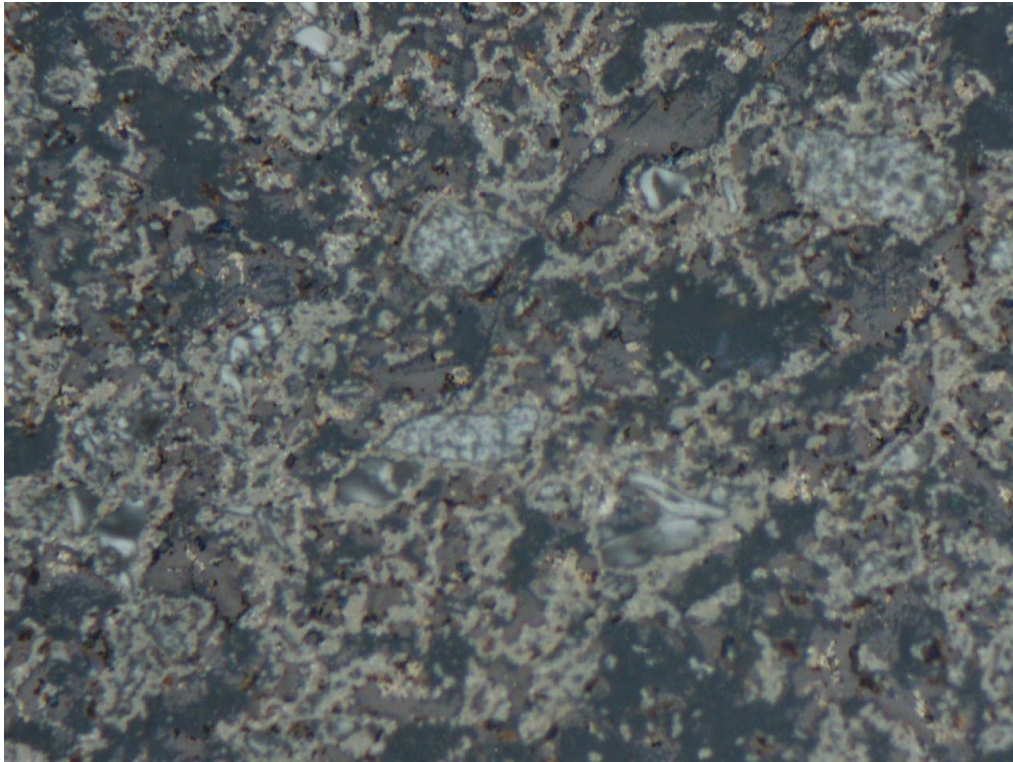
Figure H-5: Sinter model image 08141645.JPG.
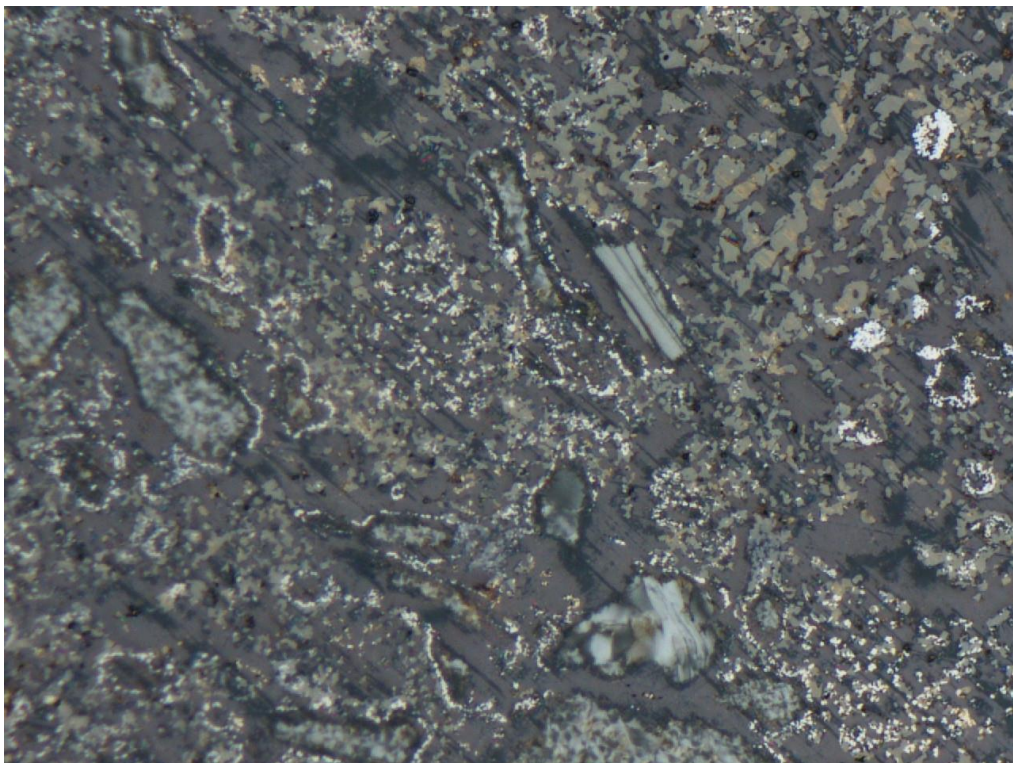
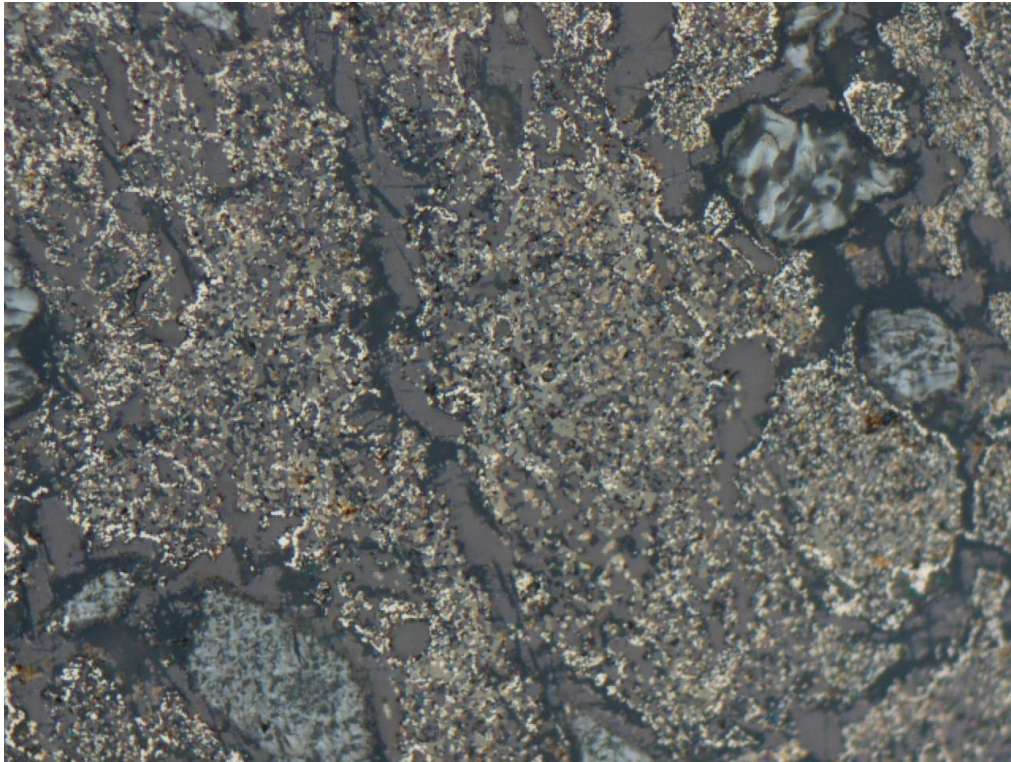*Figure H-6: Sinter model image 08165931.JPG.*
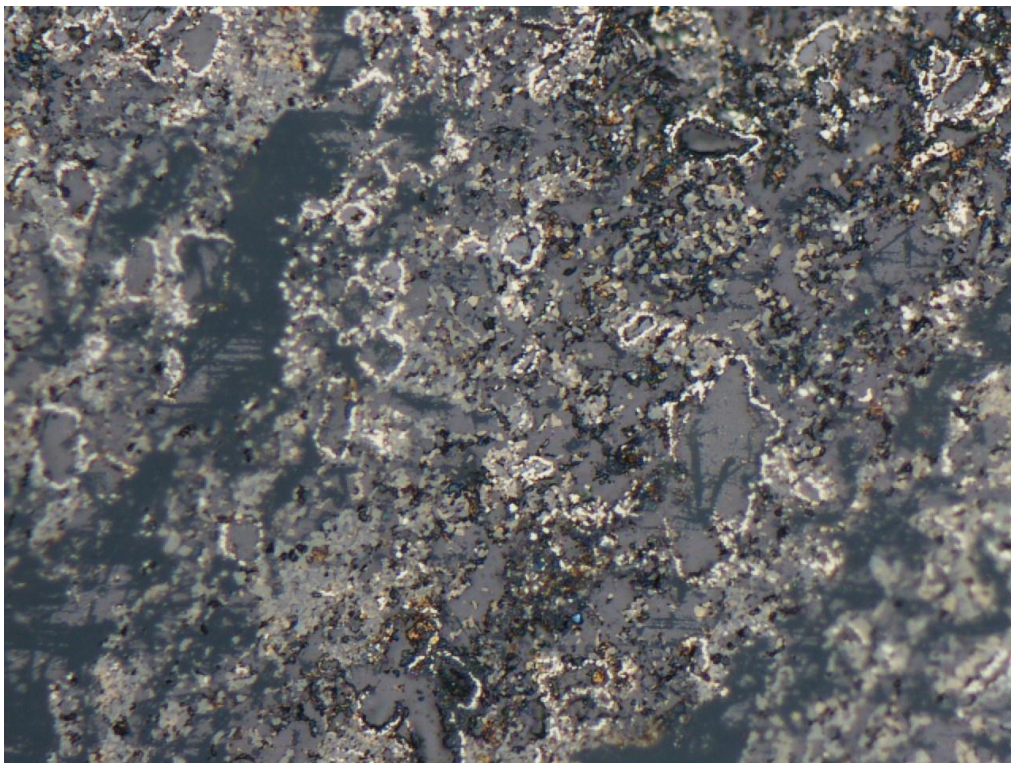
Figure H-7: Sinter model image 08142036.JPG.
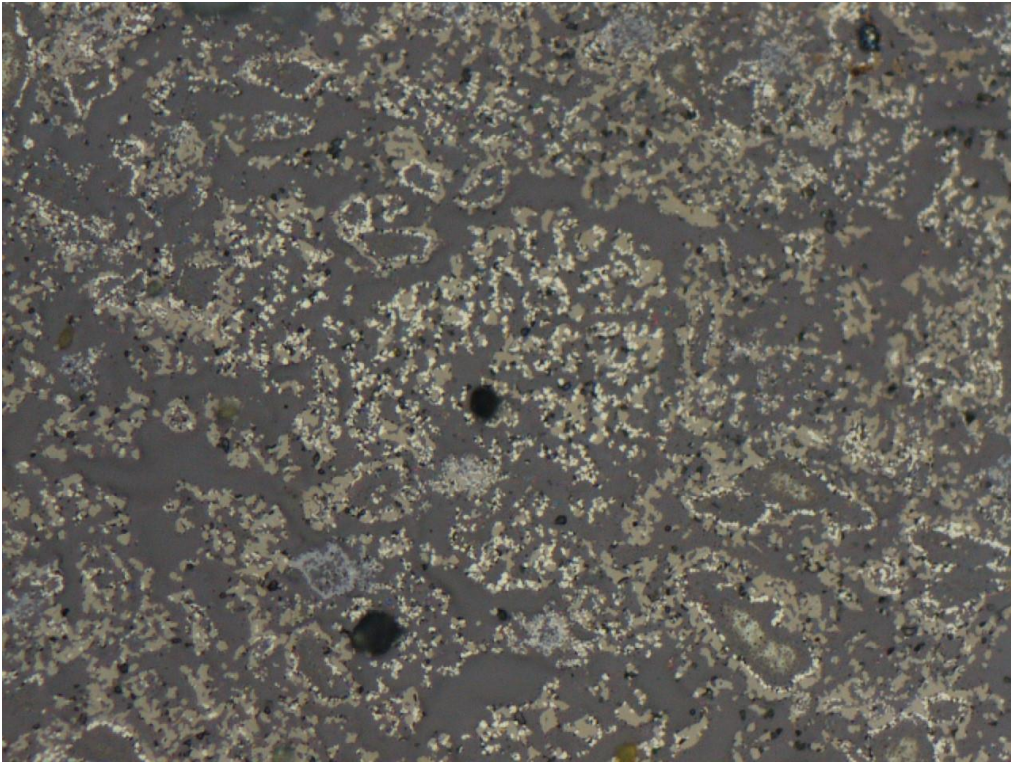

Figure H-8: Sinter model image 08140725.JPG.
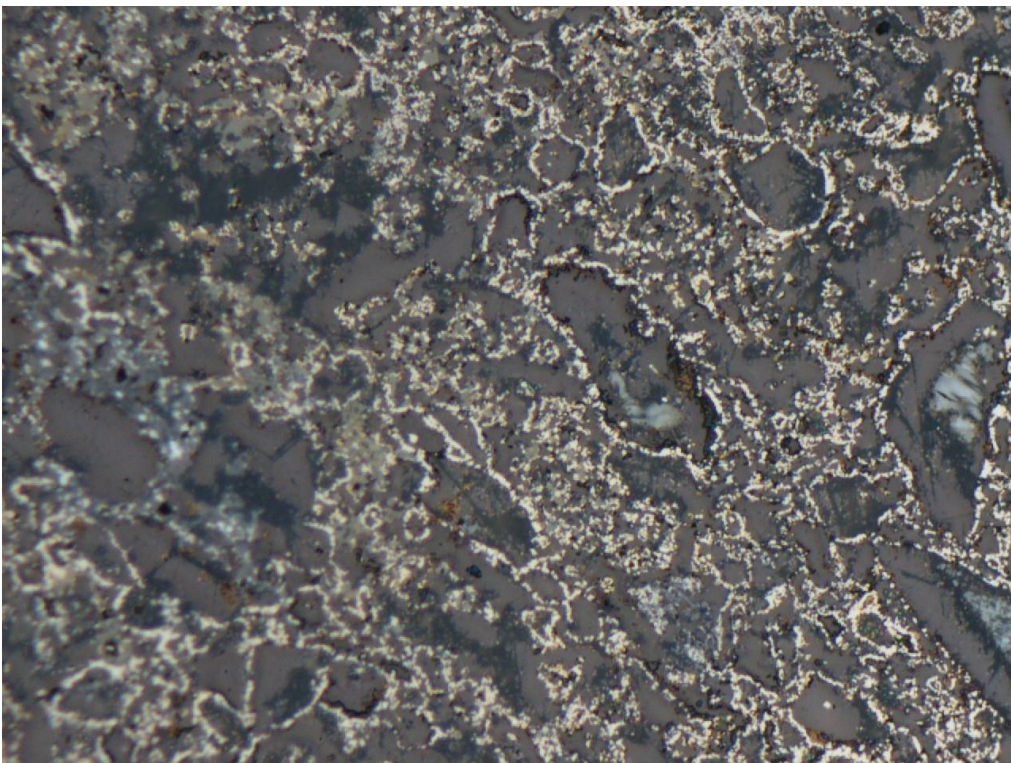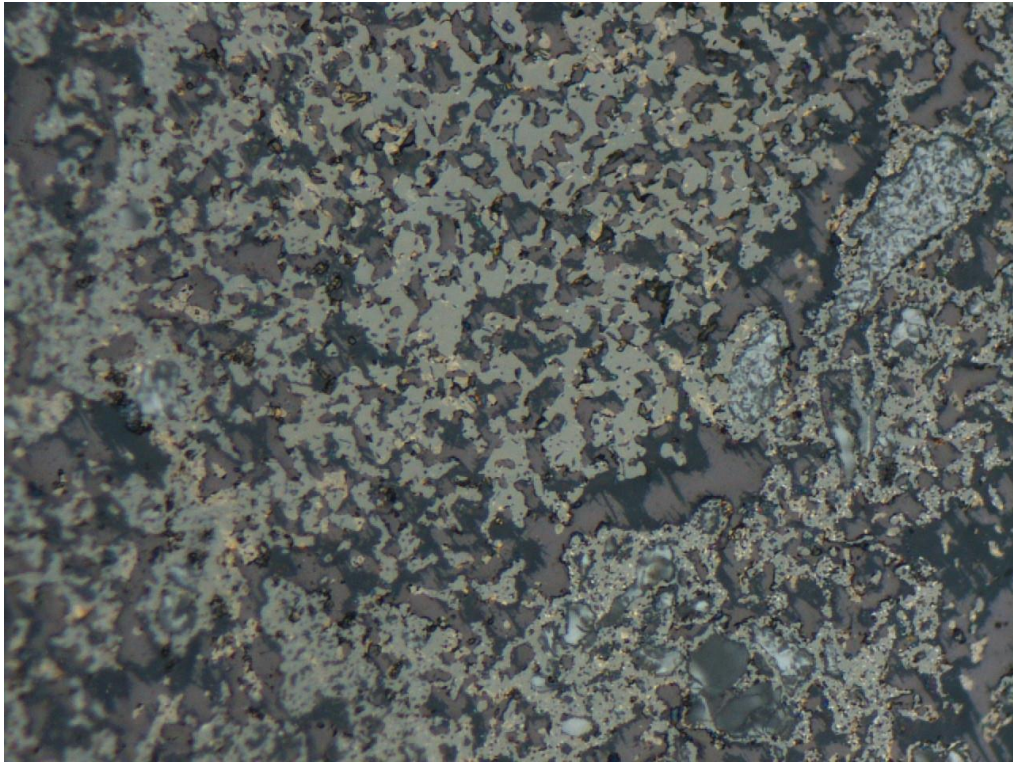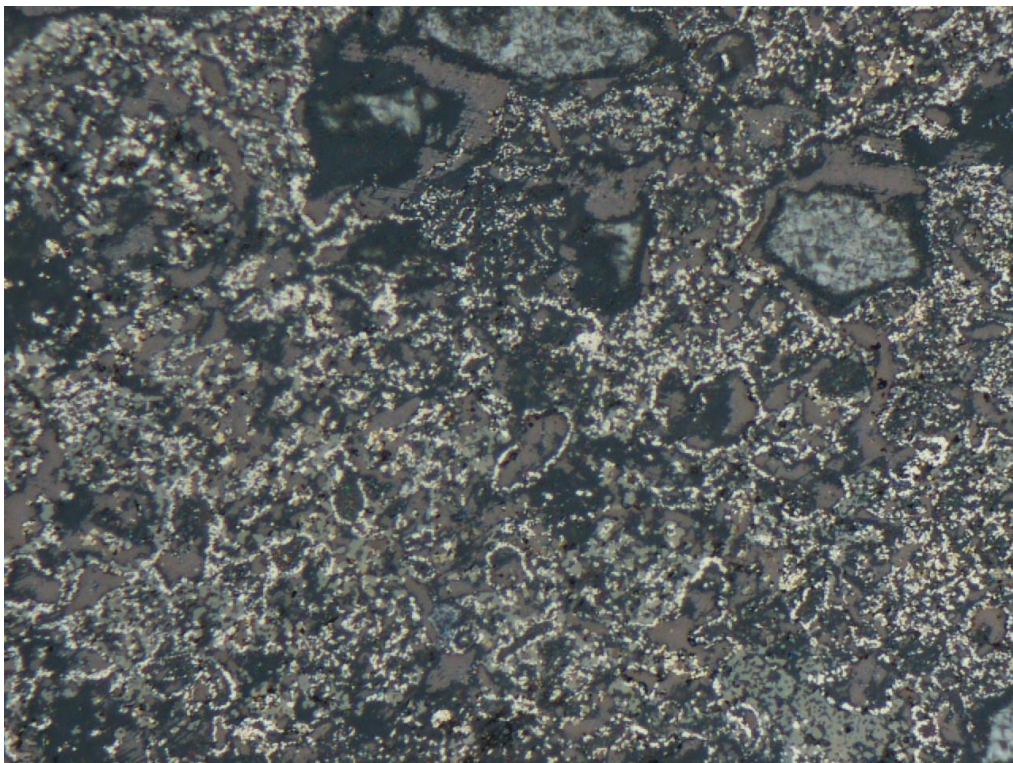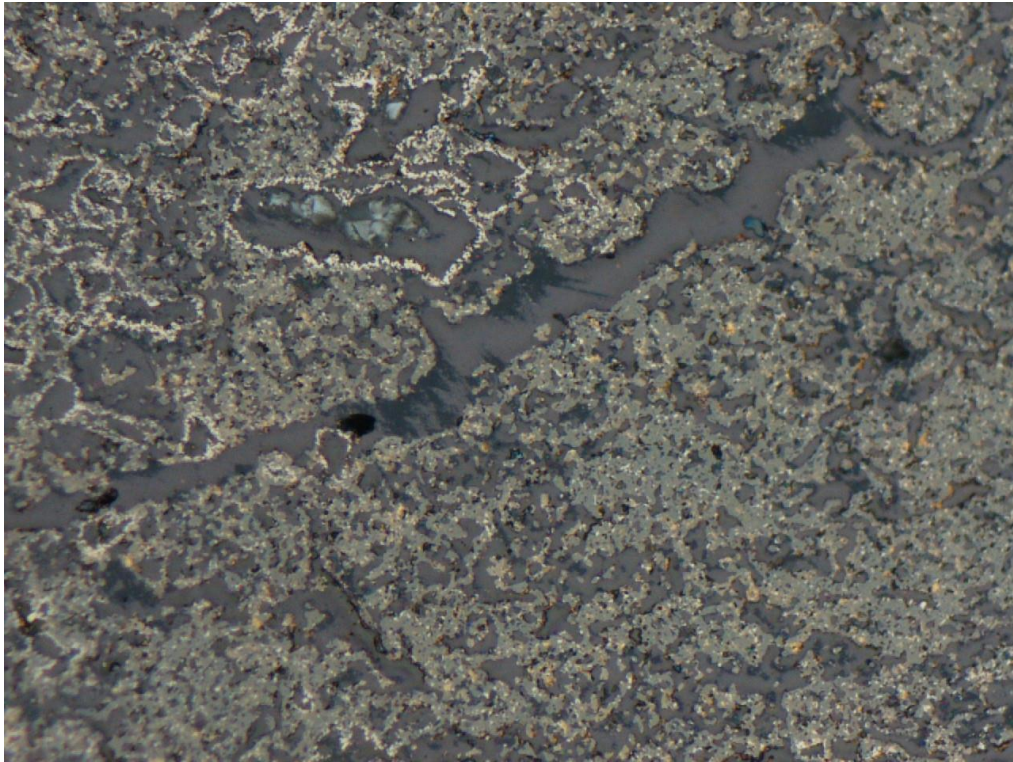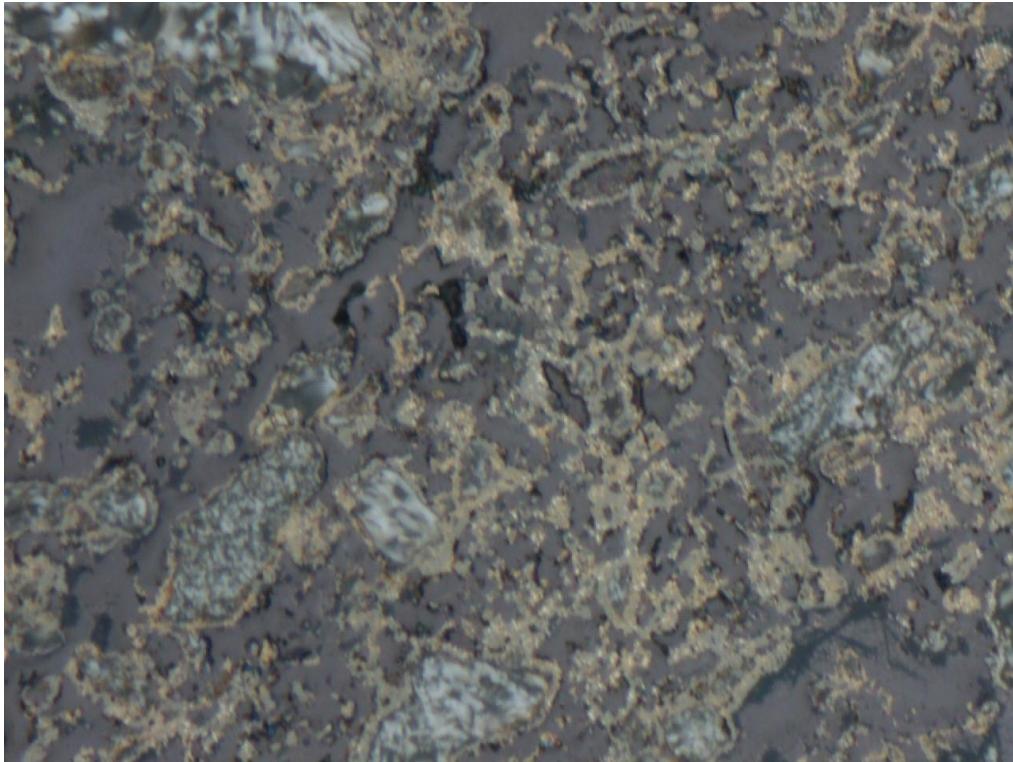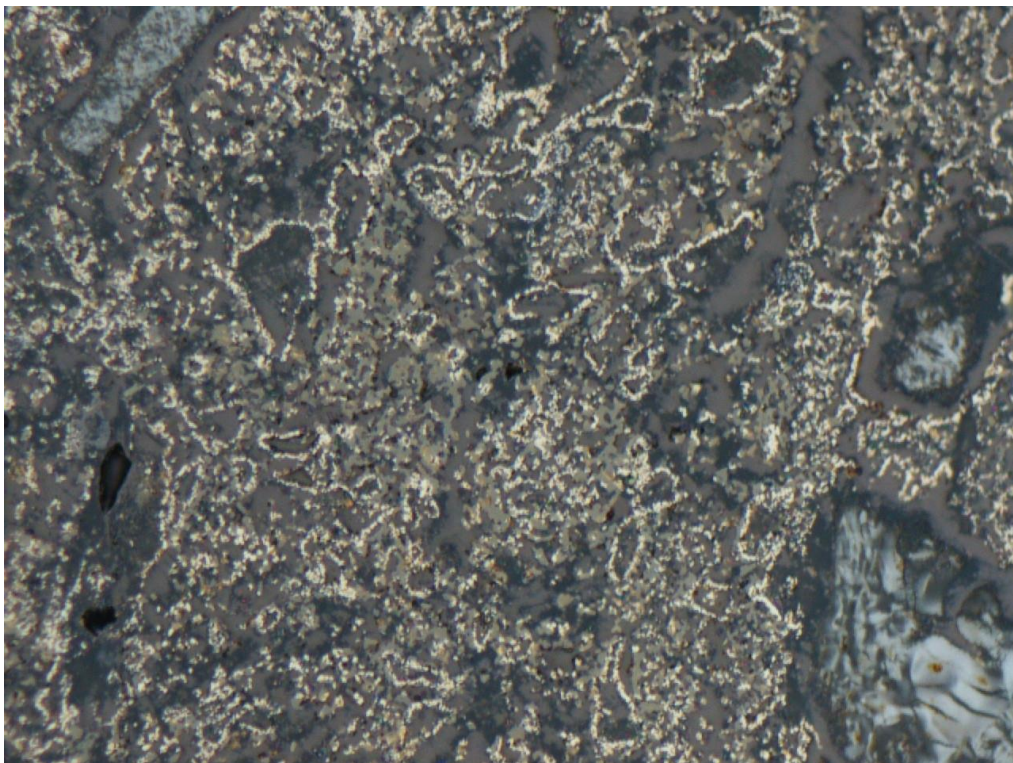
Figure H-9: Sinter model image 08141144.JPG.

Figure H-10: Sinter model image 08165744.JPG.

Figure H-11: Sinter model image 08134156.JPG.

Figure H-12: Sinter model image 08134033.JPG.

Figure H-13: Sinter model image 08170242.JPG.

Figure H-14: Sinter model image 08141420.JPG.

Figure H-15: Sinter model image 08140424.JPG.
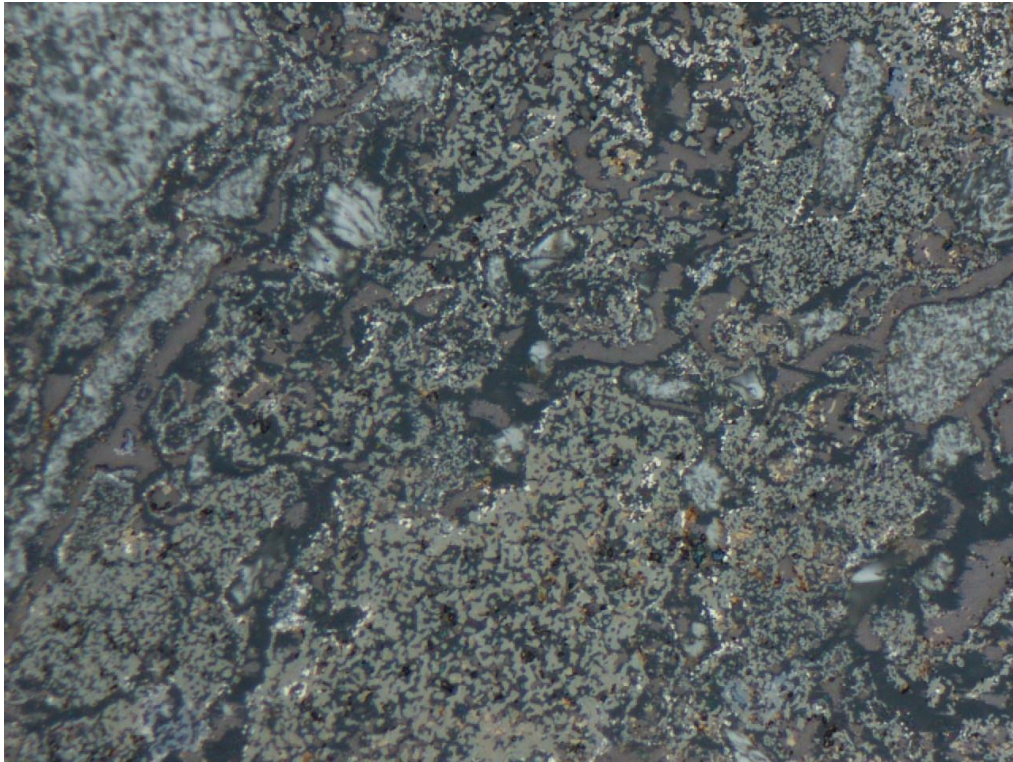

Figure H-16: Sinter model image 08170447.JPG.

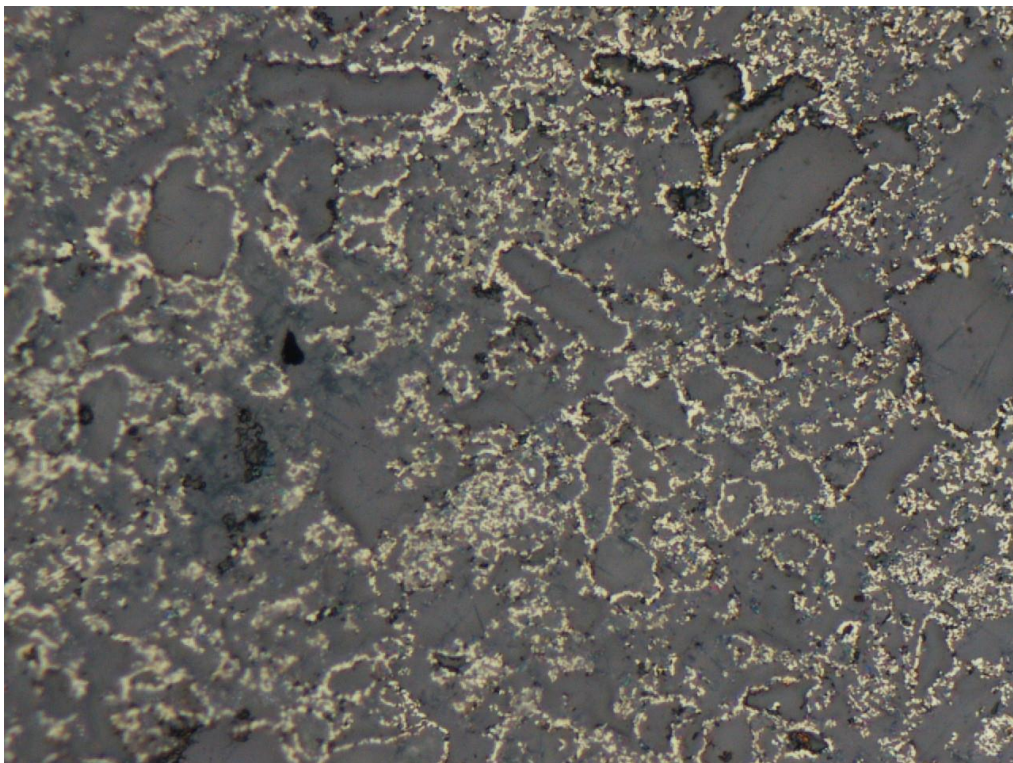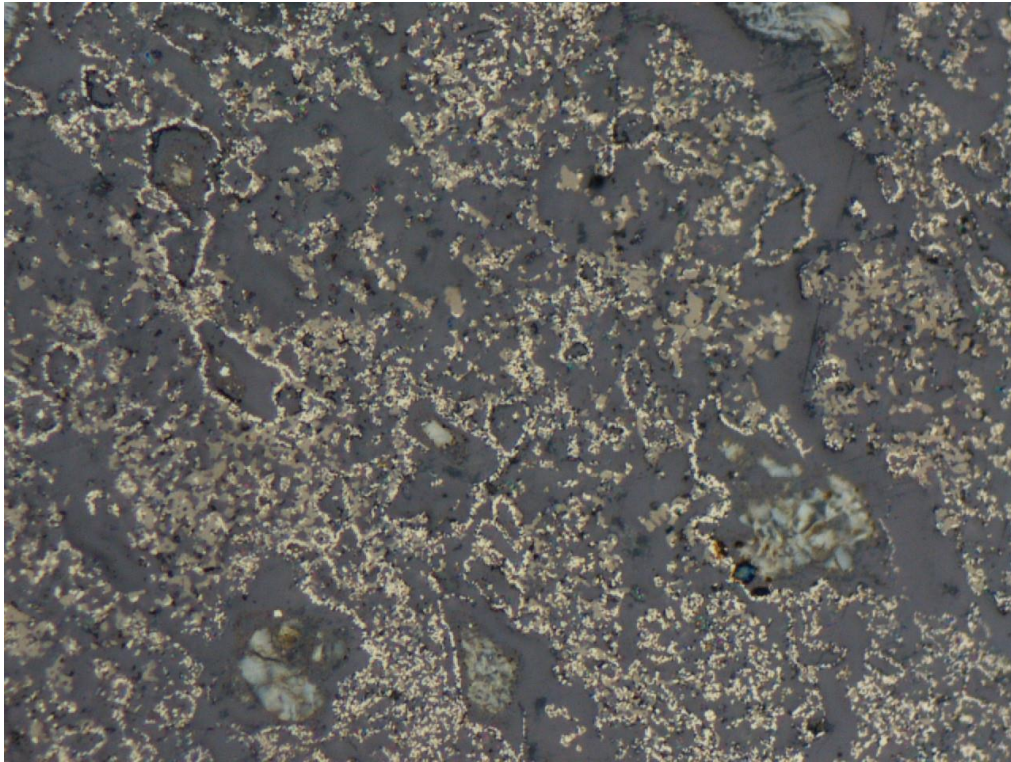*Figure H-17: Sinter model image 08141307.JPG.*

Figure H-18: Sinter model image 08170108.JPG.

Figure H-19: Sinter model image 08165559.JPG.